

Knowing is not enough;
We must apply.
Willing is not enough;
We must do.

Von Goethe

University of Alberta

Catalytic NO_x Reduction in
Lean Burn Engine Exhaust

by



Anant Pandya

A thesis submitted to the Faculty of Graduate Studies and Research in
partial fulfilment of the requirements for the Degree of Master of Science

in

Chemical Engineering

Department of Chemical and Materials Engineering

Edmonton, Alberta

Fall 2006



Library and
Archives Canada

Bibliothèque et
Archives Canada

Published Heritage
Branch

Direction du
Patrimoine de l'édition

395 Wellington Street
Ottawa ON K1A 0N4
Canada

395, rue Wellington
Ottawa ON K1A 0N4
Canada

Your file *Votre référence*
ISBN: 978-0-494-22340-6
Our file *Notre référence*
ISBN: 978-0-494-22340-6

NOTICE:

The author has granted a non-exclusive license allowing Library and Archives Canada to reproduce, publish, archive, preserve, conserve, communicate to the public by telecommunication or on the Internet, loan, distribute and sell theses worldwide, for commercial or non-commercial purposes, in microform, paper, electronic and/or any other formats.

The author retains copyright ownership and moral rights in this thesis. Neither the thesis nor substantial extracts from it may be printed or otherwise reproduced without the author's permission.

AVIS:

L'auteur a accordé une licence non exclusive permettant à la Bibliothèque et Archives Canada de reproduire, publier, archiver, sauvegarder, conserver, transmettre au public par télécommunication ou par l'Internet, prêter, distribuer et vendre des thèses partout dans le monde, à des fins commerciales ou autres, sur support microforme, papier, électronique et/ou autres formats.

L'auteur conserve la propriété du droit d'auteur et des droits moraux qui protègent cette thèse. Ni la thèse ni des extraits substantiels de celle-ci ne doivent être imprimés ou autrement reproduits sans son autorisation.

In compliance with the Canadian Privacy Act some supporting forms may have been removed from this thesis.

Conformément à la loi canadienne sur la protection de la vie privée, quelques formulaires secondaires ont été enlevés de cette thèse.

While these forms may be included in the document page count, their removal does not represent any loss of content from the thesis.

Bien que ces formulaires aient inclus dans la pagination, il n'y aura aucun contenu manquant.


Canada

University of Alberta

Library Release Form

Name of the Author : Anant Pandya
Title of Thesis : Catalytic NOx reduction from Lean Burn Engine Exhaust
Degree : Master of Science
Year This Degree Granted : 2006

Permission is hereby granted to the University of Alberta Library to reproduce single copies of this thesis and lend to or sell copies for private, scholarly, or scientific research purposes only.

The author reserves the publication and any other copyrights in the thesis, and except as herein before provided, neither the thesis nor any substantial portion thereof may be printed or otherwise reproduced in any material form whatsoever without the written permission of the author.

.....k.....

Mr. Anant Pandya
Department of Chemical Engineering
University of Alberta
Edmonton, AB,
Canada, T6G 2G8

Date : July 25, 2006.

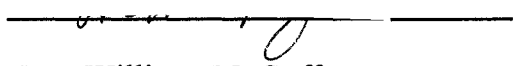
University of Alberta

Faculty of Graduate Studies and Research

The undersigned certify that they have read, and recommend to the Faculty of Graduate Studies and Research for acceptance, a thesis entitled **Catalytic NO_x Reduction From Lean Burn Engine Exhaust** submitted by Anant Pandya in partial fulfillment of the requirements for the degree of Master of Science.


Dr. Robert E. Hayes

Dr. David Chekel


Dr. William McCaffrey

Date :

April 12 2006

Abstract

NO_x emissions from automotive engines a major concern, especially from lean burn engines fuelled by diesel or natural gas. These engines are more fuel efficient than gasoline engines, however, catalytic NO_x removal from these engines is difficult because of the high oxygen content.

This work describes the development of kinetic models for the description of SCR using propene as a reductant. The models proposed are based on literature models for oxidation of CO and hydrocarbons, and the reduction of NO_x. A single channel monolith reactor model is coupled to a general pattern search optimizer to validate the proposed models using experimental data. A reasonable fit was obtained for the proposed models.

An experimental program was performed to evaluate the emission characteristics of a single cylinder compressed natural gas engine, and the efficiency of a NO_x absorber catalyst placed in the exhaust. Hydrogen was used to regenerate the catalyst.

Acknowledgements

I would like to acknowledge here the organizations and the people, without whom, this project would not have been possible.

- My M.Sc. Supervisors, Dr. Robert E. Hayes and Dr. David M. Checkel both provided a challenging opportunity for me to explore, discover, learn and become a good researcher. Through their knowledge, support, and efforts. I thank Dr. Hayes and Dr. Checkel for their time, patience, wisdom and encouragement to me.
- I am thankful to NSERC for funding.
- I am grateful to Umicore for funding and providing data and catalyst samples.
- Many thanks to my colleagues, Joe Mmbaga, Benlin Liu, Rajab Litto, Hemant More, Vahid Hosseini, and Xiang Shu, who were wonderful to work with and greatly helped me along the way. A special thanks to Joe Mmbaga who helped me with computer code and simulation runs during my research work as well as giving me his building keys for the department, so that I can work on my thesis during the Christmas holidays.
- A special Thanks to Dr. William McCaffrey who as graduate admissions coordinator and Ms. Ann Marie Brereton as a graduate admissions secretary, helped my admission into the M.Sc. Programme offered by the department of Chemical Engineering, at the University of Alberta.
- Dr. K. Nandakumar and Dr. Tony A. Yeung for helping me understand tough courses of Numerical Methods and Transport Phenomena, respectively.
- Bob Barton and Jack Gibeau for their computer and network support during my work.

Dedication

I dedicate this work to my *Dad*, (who passed away while this work was in the final stages of preparation) my *Mom*, my Wife and our two little girls named Vinisha and Kritika

Their love, support and patience for me, is invaluable.

Table of Contents

1	Introduction	1
1.1	Green House Gases	2
1.1.1	Canada's Contribution to Global GHG emissions	3
1.1.2	Long term GHG emissions trends for Canada	4
1.2	Automotive NO _x emissions regulation	12
1.3	Pollution from Automobiles and Initiatives taken by Canadian Automotive Industry	16
1.3.1	Formation of Pollutants in the Internal Combustion Engine	17
1.3.2	Steps taken by Automotive Industry	18
1.4	Types of NO _x from Combustion Processes	22
2	Methods of Controlling NO_x	24
2.1	Primary Methods	24
2.1.1	Stoichiometry based combustion control	24
2.1.2	Using lean combustion mode	25
2.1.3	Exhaust Gas Recirculation EGR	25
2.1.4	HCCI	27
2.2	Secondary Methods	28
2.2.1	Selective non catalytic reduction	28
2.2.2	Problems associated with SNCR	29
2.2.3	Three way catalytic converters – TWCC	30
2.2.4	SCR with Ammonia	32
2.2.5	SCR with NO _x using Hydrocarbons	34
3	Selective Catalytic NO_x Reduction with Hydrocarbons	35
3.1	Pioneering work in direct de-composition of NO	35
3.1.1	Performance of Cu- ZSM-5	36
3.1.2	Future challenges in Technology Development	37
3.2	SCR of NO _x using Methane	38

3.2.1	Performance of Co-ZSM-5	38
3.3	SCR of NO _x on Zeolites and Metal Oxides	40
3.3.1	Platinum containing zeolites	40
3.3.2	SCR of NO _x on supported metal oxide catalyst	41
3.3.3	Future challenges for developing supported noble metal oxide catalysts	43
3.4	SCR of NO _x on metal catalyst using other Hydrocarbons	44
3.5	SCR of NO _x on basic metal oxide catalysts	45
3.6	NO _x storage catalyst	46
3.7	Direction for future research	47
4	Modelling a Monolith Reactor for NO_x Reduction	48
4.1	Modelling the monolith reactor	48
4.1.1	Single channel monolith model	49
4.1.2	Model dimensionality	50
4.1.3	Choosing the model	51
4.2	Axial dispersion model	52
4.3	Tanks in series model	55
4.4	Software for solution of SCM	58
4.5	Generalized Pattern Search-GPS optimizer	60
4.6	Testing and validation of software	60
4.7	Summary for validation	67
5	Model Development for SCR of NO Using Hydrocarbons	68
5.1	Literature model for SCR using hydrocarbon	68
5.2	Modelling of engine exhaust from CNG engine	72
5.2.1	Experimental results	72
5.2.2	Modelling results	75
5.3	Experiments with synthesis gas mixture	79
5.3.1	Model development	79
5.3.2	Experimental methods for synthetic exhaust gas data	82

5.3.3	Simulation results for the synthetic exhaust data	83
5.4	Summary	95
6	Testing of NO_x Absorber Catalyst on CNG Engine	96
6.1	Experimental system and procedure	96
6.2	Experimentation strategy	105
6.3	Engine performance in SI lean combustion using CNG	106
6.4	Performance of the NO _x absorber catalyst	111
6.5	Summary of catalyst performance	117
7	Conclusion and Recommendations	118
	References	119

List of Tables

1.1	Canada's GHG emissions by Gas & Sector	5
1.2	Canada's GHG emissions long term trends	9
1.3	EU emission standards for Passenger Cars	14
1.4	EU emission standards for Light Commercial Vehicles	15
4.1	Inlet concentrations and GHSV for nine experiments	62
4.2	Optimal parameters for CO light off curves	67
5.1	Experimental data provided by Umicore	82
5.2	Best parameters for CO light off curves for fig. 5.9	84
5.3	Best fit parameter values for runs 1 to 4 and all runs	87
6.1	CNG lean burn test engine specifications	97
6.2	Engine system schematic label descriptions	99
6.3	Engine fuelling and hydrogen injection system schematic label description	102
6.4	Engine performance NO and THC	104

List of Figures

1.1	Canada's GHG Emissions by Gas (1990 & 2002)	4
2.1	Honeycomb type three way catalytic converter	31
4.1	Different shapes of monoliths for automotive exhaust	49
4.2	Solution scheme for 1D model	59
4.3	Experimental and predicted light off curves for run 6474 for GHSV of 25000 h ⁻¹ with excess O ₂	62
4.4	Experimental and predicted light off curves for run 6476 for GHSV of 25000 h ⁻¹ with stoichiometric O ₂	63
4.5	Experimental and predicted light off curves for run 6478 for GHSV of 25000 h ⁻¹ with excess CO	63
4.6	Experimental and predicted light off curves for run 6481 for GHSV of 50000 h ⁻¹ with excess O ₂	64
4.7	Experimental and predicted light off curves for run 6483 for GHSV of 50000 h ⁻¹ with stoichiometric O ₂	64
4.8	Experimental and predicted light off curves for run 6485 for GHSV of 50000 h ⁻¹ with excess CO	65
4.9	Experimental and predicted light off curves for run 6488 for GHSV of 100000 h ⁻¹ with excess O ₂	65
4.10	Experimental and predicted light off curves for run 6490 for GHSV of 100000 h ⁻¹ with stoichiometric O ₂	66
4.11	Experimental and predicted light off curves for run 6492 for GHSV of 100000 h ⁻¹ with excess CO	66
5.1	Experimental conversion curves for propene and NO _x	69
5.2	Comparison of predicted curves to experiment For the data of Ansell et. al	71
5.3	Experimental system used by AFS	73
5.4	Catalyst activity with age	74

5.5	Effect of HC / NO ratio on the NO conversion	75
5.6	Comparison of predicted and experimental conversions, NO _x and Propane, data for 13 experiments	77
5.7	Comparison of predicted and experimental conversions, NO _x and Propane, data for 24 experiments	78
5.8	Comparison of the simulation and experimental results When all four of the CO light curves optimized simultaneously	85
5.9	Comparison of the simulation and experimental results when all four of the CO light curves optimized individually	85
5.10	Simulated and experimental conversions for inlet conc. of 100 ppm CO, 350 ppm propene and 150 ppm NO GHSV 50000 h ⁻¹	88
5.11	Simulated and experimental conversions for inlet conc. of 300 ppm CO, 350 ppm propene and 150 ppm NO GHSV 50000 h ⁻¹	88
5.12	Simulated and experimental conversions for inlet conc. of 1000 ppm CO, 350 ppm propene and 150 ppm NO GHSV 50000 h ⁻¹	89
5.13	Simulated and experimental conversions for inlet conc. of 3000 ppm CO, 350 ppm propene and 150 ppm NO GHSV 50000 h ⁻¹	89
5.14	Simulated and experimental conversions for inlet conc. of 100 ppm CO, 350 ppm propene and 150 ppm NO Common parameters, GHSV 50000 h ⁻¹	90
5.15	Simulated and experimental conversions for inlet conc. of 300 ppm CO, 350 ppm propene and 150 ppm NO Common parameters, GHSV 50000 h ⁻¹	90
5.16	Simulated and experimental conversions for inlet conc. Of 1000 ppm CO, 350 ppm propene and 150 ppm NO Common parameters, GHSV 50000 h ⁻¹	91
5.17	Simulated and experimental conversions for inlet conc. of 3000 ppm CO, 350 ppm propene and 150 ppm NO Common parameters, GHSV 50000 h ⁻¹	91

5.18	Simulated and experimental conversions for inlet conc. of 1000 ppm CO, 350 ppm propene and 150 ppm NO Common parameters, GHSV 25000 h ⁻¹	93
5.19	Simulated and experimental conversions for inlet conc. of 1000 ppm CO, 350 ppm propene and 150 ppm NO parameters from experiment 3, GHSV 25000 h ⁻¹	93
5.20	Simulated and experimental conversions for inlet conc. of 1000 ppm CO, 350 ppm propene and 150 ppm NO parameters from experiment 3, GHSV 50000 h ⁻¹	94
5.21	Simulated and experimental conversions for inlet conc. of 1000 ppm CO, 350 ppm propene and 150 ppm NO Common parameters, GHSV 50000 h ⁻¹	94
6.1	Engine schematic arrangement	98
6.2	Engine fuelling and hydrogen injection system	101
6.3	Effect of Engine speed on exhaust gas temperature	107
6.4	Effect of engine speed on the NO exhaust concentration	107
6.5	Effect of Engine speed on hydrocarbon emissions	108
6.6	Effect of Engine speed on the mass flow rate of feed	108
6.7	Effect of Engine torque on exhaust gas temperature	109
6.8	Effect of Engine torque on NO exhaust conc.	109
6.9	Effect of Engine torque on hydrocarbon emissions	110
6.10	Effect of Engine torque on the mass flow rate of feed	110
6.11	Steady state NO _x emissions upstream and downstream of the reactor, with and without hydrogen injection	111
6.12	Transient NO _x concentration in the reactor effluent, following the switch of hydrogen into and out of the reactor feed	112
6.13	Steady state THC emissions upstream and downstream of the reactor, with and without hydrogen injection	113

6.14	Transient THC concentration in the reactor effluent, following the switch of hydrogen into and out of the reactor feed.	113
6.15	Steady state CO emissions upstream and downstream of the reactor, with and without hydrogen injection	115
6.16	Transient CO concentration in the reactor effluent, following the switch of hydrogen into and out of the reactor feed.	115
6.17	Steady state maximum reactor temperature, with and without hydrogen injection	116
6.18	Transient maximum reactor temperature, following the switch of hydrogen into and out of the reactor feed	116

List of Symbols

Symbol	Units	Description
a_j	-	Constant in Galerkin approximate solution.
A_w	m^2	Wall cross sectional area
C_f	Mol/M^3	Fluid Concentration
C_j	Mol/M^3	Concentration of component j
C_p	$J/Kg \cdot K$	Constant pressure heat capacity
C_{pf}	$J/Kg \cdot K$	Constant pressure heat capacity of the fluid
C_{pw}	$J/Kg \cdot K$	Constant pressure heat capacity of the wall
C_{Tf}	Mol/M^3	Total molar density of fluid
C_{Ts}	Mol/M^3	Total molar density of solid
D_{AB}	m^2/sec	Molecular diffusion coefficient of A in B
$D_{a,eff}$	m^2/sec	Effective axial dispersion coefficient
D_H	m	Hydraulic diameter
D_I	m^2/sec	Axial dispersion coefficient
D_{wc}	m	Channel outside diameter
h	$W /m^2 K$	Heat transfer coefficient
ΔH_R	J/Mol	Heat of reaction, component j
k_m	m/s	Mass transfer coefficient
k_w	$W /m K$	Thermal conductivity of reactor wall
k_f	$W /m K$	Thermal conductivity of fluid
L	m	Length
n	-	Number of tanks in series
Pe	-	Peclet number - Dimensionless
R	m	Radius of the tubular passage way
$(-R_j)_s$	$mol/m^2 \cdot sec$	Rate of disappearance of species j
T	K or $^{\circ}C$	Temperature, unit in consistent with other parameters in an expression
T_o	K or $^{\circ}C$	Temperature at inlet
T_f	K or $^{\circ}C$	Fluid temperature
T_s	K or $^{\circ}C$	Solid surface temperature
T_{fo}	K or $^{\circ}C$	Temperature of fluid at inlet
t	sec	Time

Symbol	Units	Description
u_0	m/s	fluid velocity at inlet
u	m/s	fluid velocity in the channel
u_m	m/s	Mean mass average velocity
W_p	m	Wetted perimeter
w_t	m	Washcoat thickness
Y_{jf}	-	Mol fraction of species j in fluid
Y_{js}	-	Mol fraction of species j in solid
z	m	Axial co ordinate in cyllindrical system
Greek symbols		
Symbol	Units	Description
α	m^2/sec	Thermal diffusivity
α_i	m^2/sec	Effective thermal diffusivity
δ_w	m	Reactor wall thickness
η	-	Effectiveness factor, dimensionless
η_i	-	Effectiveness factor species i , dimensionless
θ_j	-	Dimensionless temperature
ρ	Kg /m^3	Mass density of fluid
ρ_w	Kg /m^3	Mass density of solid (weighted average of washcoat + substrate)

Chapter 1

Introduction

Concern over the pollutants in the exhaust gases from automobiles and the resulting environmental regulations has led to much research into methods for the reduction of these emissions.

Engine exhaust gases contain oxides of nitrogen, generally nitric oxide (NO) and nitrogen dioxide (NO₂), which are collectively known as NO_x. NO_x are considered a major pollutant because they consume oxygen from the environment and can cause acidic rain (nitrous acid). NO_x is a known occupational and health hazard. Numerous studies on the effects of NO_x suggested that NO_x increases susceptibility to bacterial lung infections and viral infections. It can also cause alterations to lung metabolism, structure and function, which can result in increased susceptibility to pulmonary disorders.

Nitrogen dioxide has several harmful effects. It absorbs visible solar radiation, thus contributing to impaired atmospheric visibility. It is a significant green house gas. It is, along with NO, a chief regulator of the oxidizing capacity of the free troposphere by controlling the build-up and fate of radical species, including hydroxyl radicals. Finally, it plays a critical role in determining ozone (O₃) concentrations in the troposphere because the photolysis of nitrogen dioxide is the only key initiator of the photochemical formation of ozone, whether in polluted or unpolluted atmospheres [1, 2].

This research work focuses on the reduction of NO_x emissions from the exhaust gases generated by lean burn engines. Because lean burn engine have an excess of oxygen, NO_x removal presents a challenge. Of the

available control technologies, the process of Selective Catalytic Reduction (SCR) of NO_x by hydrocarbon is studied.

The remainder of Chapter 1 gives an overview of the problem and some background to this work. Chapter 2 compares the technologies available for reduction of NO_x. The advantages of SCR of NO_x by hydrocarbons, compared to other methods are discussed. Chapter 3 gives a literature review of the research on the SCR technology, including catalysts and methods for SCR of NO_x using hydrocarbons. Chapter 4 deals with modelling, reaction mechanism, kinetics and rate expression for NO_x reduction in the lean burn engine exhaust and how they are applied to model experimental data. In Chapter 5, experimental data are used to test a kinetic model for SCR of NO_x using hydrocarbons in lean exhaust. Some modelling insights and how this technique is useful for selective catalytic reduction of NO_x Chapter 6 shows the results from engine tests and performance parameters for a NO_x absorber catalyst. Chapter 7 contains the summary, conclusion and recommendations.

1.1 Green House Gases

The earth is warmed by radiant energy from the sun. Over time, the amount of energy transmitted to the Earth's surface is equal to the amount of energy re-radiated back into space, and the temperature of the Earth's surface stays roughly constant; however, the temperature of the Earth is strongly influenced by the existence, density, and composition of its atmosphere. Many gases in the Earth's atmosphere absorb infrared radiation re-radiated from the surface, trapping heat in the lower atmosphere. Without the natural greenhouse effect, it is likely that the average temperature of the Earth's surface would be on the order of -19° Celsius, rather than the +14° Celsius actually observed. The gases that help trap the sun's heat close to the earth's surface are referred to as greenhouse gases (GHG). All GHG absorb infrared radiation

(heat) at particular wavelengths. The following are classified as GHG by Environment Canada.

Direct GHGs :

Carbon dioxide	-	CO ₂
Methane	-	CH ₄
Nitrous oxide	-	N ₂ O
Sulphur hexafluoride	-	SF ₆
Hydro fluoro carbons	-	HFCs
Per fluoro carbons	-	PFCs

Indirect GHGs :

Sulphur oxides	-	SO _x
Nitrogen oxides	-	NO _x
Carbon monoxide	-	CO
Non methane volatile organic compounds.	-	NMVOCs

Direct GHG is the name given to emissions from sources that are owned or controlled by an emissions reporting company. Indirect GHG emissions are emissions that are a consequence of the operations of the reporting company, but occur from sources owned or controlled by another company, e.g., as a consequence of the import of electricity, heat, or steam.

1.1.1 Canada's Contribution to Global GHG emissions

Although Canada only contributes about 2% of global GHG emissions, it is one of the highest per capita emitters, mainly due to its size and energy demands that result from its cold climate and the resource based economy. In 1990 Canadians emitted 22.0 tons of GHG per capita. By 2002 emissions had increased to 23.3 tons per capita. Figure 1.1 shows Canada's GHG emissions for the years 1990 and 2002 [3].

Canada's GHG emission by Gas - 1990

Canada's GHG emission by Gas - 2002

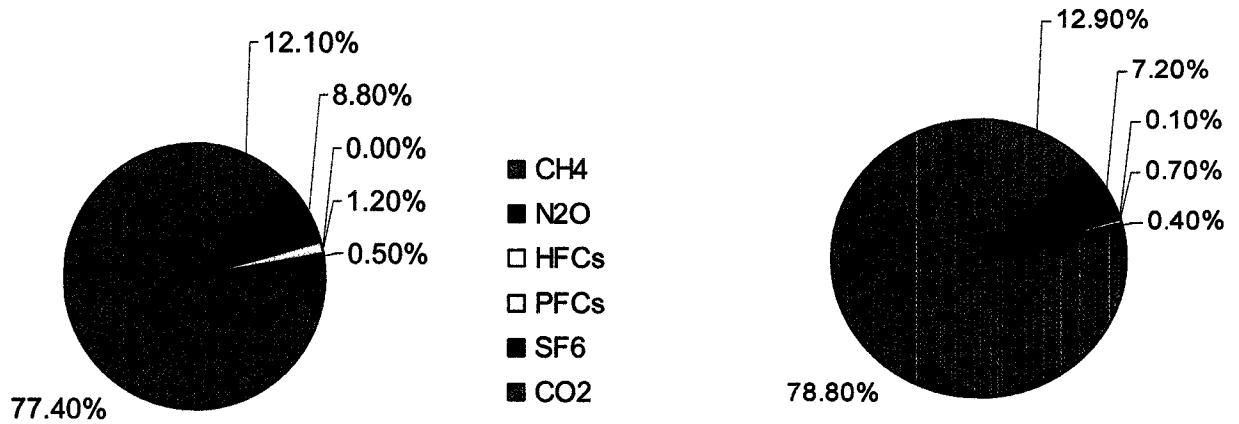


Figure 1.1 - Canada's GHG emissions for the years 1990 and 2002[3]

Table 1.1 gives the GHG emissions for Canada by gas and sectors for the year 2002. Although data from 1990 onwards are available, only 2002 numbers are given in the Table 1.1 to give an idea of GHG emissions. [source: environment Canada GHG inventory 1990-02].

1.1.2 Long term GHG emission trends for Canada (1990-2002)

The 1990-2002 data (Table 1.2) on Canada's GHG emissions show that progress has been made in reducing emissions in many sectors and also indicates areas where efforts are still needed. GHG emissions in 2002 were approximately 20 % above the 1990 level of 609 metric tonnes of CO₂ equivalent. Although emissions have been rising since 1990, annual emission growth peaked at 5.7 % in 1994. This growth in emission is mainly due to increased energy exports and fossil fuel consumption for heating in the residential and commercial sectors, resulting from lower

TABLE 1.1 Canada's GHG Emissions by Gas and Sector, 2002

Global Warming Potential Unit	CO2 kt	CH4 kt	CH4 kt CO2 eq	N2O kt	N2O kt CO2 eq	HFCs kt CO2 eq	PFCs kt CO2 eq	SF6 kt CO2 eq	Total kt CO2 eq
TOTAL	576,000	4,500	94,000	170	53,000	900	5,000	2,700	731,000
ENERGY	537,000	2,100	44,000	37	11,000	-	-	-	592,000
a. Stationary Combustion Sources	341,000	220	4,600	7.8	2,400	-	-	-	348,000
Electricity and Heat Generation	128,000	4.7	98	2.4	750	-	-	-	129,000
Fossil Fuel Industries	70,500	120	2,500	1.5	460	-	-	-	73,400
Petroleum Refining	34,000	0.5	10	0.4	110	-	-	-	34,100
Fossil Fuel Production	36,500	120	2,500	1.1	340	-	-	-	39,300
Mining	11,700	0.2	5	0.3	86	-	-	-	11,800
Manufacturing Industries	49,500	1.7	36	1.2	360	-	-	-	49,900
Iron and Steel	6,370	0.2	5	0.2	57	-	-	-	6,430
Non-Ferrous Metals	3,290	0.1	1.5	0.1	16	-	-	-	3,300
Chemical	6,390	0.1	2.7	0.1	35	-	-	-	6,430
Pulp and Paper	8,860	0.8	17	0.4	120	-	-	-	9,000
Cement	3,470	0.1	1.7	0.1	16	-	-	-	3,490
Other Manufacturing	21,100	0.4	8.5	0.4	120	-	-	-	21,200
Construction	1,230	0	0.5	0	9	-	-	-	1,240
Commercial & Institutional	35,600	1.2	24	0.7	230	-	-	-	35,800
Residential	41,800	94	2,000	1.7	530	-	-	-	44,300
Agriculture & Forestry	2,090	0	0.7	0.1	17	-	-	-	2,110
b. Transportation Combustion Sources	181,000	30	640	29	8,900	-	-	-	190,000
Domestic Aviation	12,800	0.6	13	1.3	390	-	-	-	13,200
Road Transportation	131,000	14	290	19	5,900	-	-	-	137,000
Gasoline Automobiles	47,800	4.7	99	7.5	2,300	-	-	-	50,200
Light Duty Gasoline Trucks	37,800	5	100	9.8	3,000	-	-	-	40,900
Heavy Duty Gasoline Vehicles	3,900	0.6	12	0.6	180	-	-	-	4,090
Motorcycles	268	0.2	4.5	0	2	-	-	-	274
Diesel Automobiles	662	0	0.4	0	15	-	-	-	677

Table 1.1.1 contd.

Global Warming Potential	CO2	CH4	CH4 kt CO2 eq	N2O	N2O kt CO2 eq	HFCs kt CO2 eq	PFCs kt CO2 eq	SF6 kt CO2 eq	Total kt CO2 eq
Unit	kt	kt	eq	kt	eq	eq	eq	eq	eq
Light Duty Diesel Trucks	738	0	0.4	0.1	17	-	-	-	755
Heavy Duty Diesel Vehicles	39,200	1.9	40	1.1	360	-	-	-	39,600
Propane and Natural Gas Vehicles	821	1.3	26	0	5	-	-	-	853
Railways	5,280	0.3	6.1	2.1	660	-	-	-	5,950
Domestic marine	5,150	0.4	8.1	1.1	330	-	-	-	5,490
Others	26,400	16	330	5.2	1,600	-	-	-	28,400
Off - Road	15,900	4.9	100	5	1,500	-	-	-	17,500
Pipelines	10,600	11	220	0.3	86	-	-	-	10,900
c. Fugitive emissions	16,000	1,900	39,000	-	-	-	-	-	55,000
Coal Mining	-	47	990	-	-	-	-	-	990
Oil & Natural Gas	16,000	1,800	38,000	-	-	-	-	-	54,000
Oil	77	640	13,000	-	-	-	-	-	13,000
Natural Gas	29	1,100	24,000	-	-	-	-	-	24,000
Venting	8,100	-	-	-	-	-	-	-	8,100
Flaring	7,400	31	660	-	-	-	-	-	8,100
INDUSTRIAL PROCESSES	39,000	-	-	7	2,100	900	5,000	2,700	50,000
a. Mineral Production	8,730	-	-	-	-	-	-	-	8,730
Cement	6,740	-	-	-	-	-	-	-	6,740
Lime	1,660	-	-	-	-	-	-	-	1,660
Limestone and Soda Ash Use	335	-	-	-	-	-	-	-	335

Table 1.1.1 contd.

Global Warming Potential	CO2	CH4	CH4 kt CO2 eq	N2O	N2O kt CO2 eq	HFCs kt CO2 eq	PFCs kt CO2 eq	SF6 kt CO2 eq	Total kt CO2 eq
Unit	kt	kt		kt					
b. Chemical Industry	6,240	-	-	7	2,100	-	-	-	8,300
Ammonia Production	6,240	-	-	-	-	-	-	-	6,240
Nitric Acid Production	-	-	-	2.6	810	-	-	-	813
Adipic Acid Production	-	-	-	4	1,200	-	-	-	1,250
c. Metal Production	11,500	-	-	-	-	-	5,000	2,700	19,000
Iron and Steel Production	7,120	-	-	-	-	-	-	-	7,120
Aluminium Production	4,360	-	-	-	-	-	5,000	-	9,210
SF6 Used in Magnesium Smelters	-	-	-	-	-	-	-	2,700	2,700
d. Consumption of Halocarbons	-	-	-	-	-	900	20	-	900
e. Other & Undifferentiated Products	13,000	-	-	-	-	-	-	-	13,000
SOLVENT & OTHER PRODUCT USE	-	-	-	1.5	470	-	-	-	470
AGRICULTURE	-500	1,200	24,000	110	34,800	-	-	-	59,000
a. Entric Fermentation	-	900	19,000	-	-	-	-	-	19,000
b. Manure management	-	270	5,600	15	4,600	-	-	-	10,000
c. Agricultural Soils	-500	-	-	100	30,000	-	-	-	30,000
Direct Sources	-500	-	-	70	20,000	-	-	-	20,000
Indirect Sources	-	-	-	20	7,000	-	-	-	7,000

Table 1.1.1 contd.

	CO2	CH4	CH4 kt CO2 eq	N2O	N2O kt CO2 eq	HFCs kt CO2 eq	PFCs kt CO2 eq	SF6 kt CO2 eq	Total kt CO2 eq
LAND USE CHANGE & FORESTRY	-	100	3,000	10	3,000	-	-	-	6,000
Global Warming Potential	kt	kt	kt CO2 eq	kt	kt CO2 eq	kt CO2 eq	kt CO2 eq	kt CO2 eq	kt CO2 eq
Unit									
a. Prescribed Burns	-	20	300	0.6	200	-	-	-	500
b. wild fires in the wood production forest	-	100	3,000	10	3,000	-	-	-	5,000
WASTE	290	1,100	22,000	3.4	1,000	-	-	-	24,000
a. Solid Waste Disposal on Land	-	1,000	22,000	-	-	-	-	-	22,000
b. Wastewater Handling	-	19	400	3.2	980	-	-	-	1,400
c. Waste Incineration	290	0.3	6.9	0.2	60	-	-	-	350
LAND USE CHANGE & FORESTRY	-20,000	-	-	-	-	-	-	-	-20,000
a. Changes in woody biomass stocks	-50,000	-	-	-	-	-	-	-	-50,000
b. Forest & Grassland Conversion	10,000	-	-	-	-	-	-	-	10,000
c. Abandonment of Managed Lands	-700	-	-	-	-	-	-	-	-700
d. CO2 emissions & removal from soil	10,000	-	-	-	-	-	-	-	10,000

Table 1.2

Canada's GHG emissions Long term trends (1990 - 2002) by sector

Green House Gas categories Mt CO2 eq.	1990	1995	2000	2001	2002
TOTAL	609,000	675,000	725,000	716,000	731,000
ENERGY	473,000	513,000	589,000	582,000	592,000
a. Stationary Combustion Sources	282,000	294,000	344,000	340,000	348,000
Electricity and Heat Generation	95,300	101,000	132,000	134,000	129,000
Fossil Fuel Industries	51,500	54,700	66,900	67,900	73,400
Petroleum Refining	26,100	28,400	27,800	29,700	34,100
Fossil Fuel Production	25,400	26,300	39,100	38,200	39,300
Mining	6,190	7,860	10,400	10,300	11,800
Manufacturing Industries	54,500	52,900	53,000	48,800	49,900
Iron and Steel	6,490	7,040	7,190	5,890	6,430
Non-Ferrous Metals	3,230	3,110	3,190	3,470	3,300
Chemical	7,100	8,460	7,860	6,760	6,430
Pulp and Paper	13,500	11,500	10,800	9,630	9,000
Cement	3,390	3,420	3,430	3,340	3,490
Other Manufacturing	20,800	19,400	20,500	19,700	21,200
Construction	1,880	1,180	1,080	1,010	1,240
Commercial & Institutional	25,800	29,000	33,200	33,200	35,800
Residential	44,000	44,900	45,000	41,900	44,300
Agriculture & Forestry	2,420	2,790	2,570	2,210	2,110
b. Transportation Combustion Sources	153,000	169,000	190,000	187,000	190,000
Domestic Aviation	10,700	10,900	13,700	12,100	13,200
Road Transportation	107,000	119,000	131,000	133,000	137,000
Gasoline Automobiles	53,700	51,300	48,300	49,300	50,200
Light Duty Gasoline Trucks	21,800	28,500	37,600	38,900	40,900
Heavy Duty Gasoline Vehicles	3,140	4,760	4,370	4,020	4,090

Motorcycles	230	214	239	238	274
Diesel Automobiles	672	594	605	640	677
Light Duty Diesel Trucks	591	416	645	681	755
Heavy Duty Diesel Vehicles	24,500	30,800	38,700	38,500	39,600
Propane and Natural Gas Vehicles	2,210	2,100	1,100	1,140	853
Railways	7,110	6,430	6,670	6,550	5,950
Domestic marine	5,050	4,380	5,110	5,510	5,490
Others	23,400	28,600	33,400	29,700	28,400
Off - Road	16,500	16,600	22,100	19,500	17,500
Pipelines	6,900	12,000	11,300	10,300	10,900
c. Fugitive emissions	38,000	50,000	54,000	55,000	55,000
Coal Mining	1,900	1,700	950	990	990
Oil & Natural Gas	36,000	48,000	53,000	54,000	54,000
Oil	8,600	13,000	14,000	14,000	13,000
Natural Gas	17,000	22,000	24,000	24,000	24,000
Venting	4,500	6,700	7,500	7,800	8,100
Flaring	5,800	6,800	7,800	8,000	8,100
INDUSTRIAL PROCESSES	53,000	57,000	49,000	48,000	50,000
a. Mineral Production	7,770	8,040	9,000	8,510	8,730
Cement	5,580	5,860	6,730	6,540	6,740
Lime	1,750	1,840	1,860	1,640	1,660
Limestone and Soda Ash Use	439	343	403	335	335
b. Chemical Industry	16,500	18,000	8,540	7,520	8,300
Ammonia Production	5,010	6,480	6,850	5,920	6,240
Nitric Acid Production	777	782	799	795	813
Adipic Acid Production	10,700	10,700	900	802	1,250
c. Metal Production	19,900	20,700	18,400	18,200	19,000
Iron and Steel Production	7,060	7,880	7,890	7,280	7,120
Aluminium Production	10,000	11,000	8,150	8,890	9,210
SF6 Used in Magnesium Smelters	2,900	1,900	2,300	2,000	2,700

d. Consumption of Halocarbons	-	500	900	900	900
e. Other & Undifferentiated Products	9,200	10,000	12,000	13,000	13,000
SOLVENT & OTHER PRODUCT USE	420	440	460	470	470
AGRICULTURE	59,000	61,000	61,000	60,000	59,000
a. Entric Fermentation	16,000	18,000	18,000	19,000	19,000
b. Manure management	8,300	9,200	9,400	10,000	10,000
c. Agricultural Soils	30,000	30,000	30,000	30,000	30,000
Direct Sources	30,000	30,000	30,000	20,000	20,000
Indirect Sources	5,000	6,000	7,000	7,000	7,000
LAND USE CHANGE & FORESTRY	3,000	20,000	2,000	2,000	6,000
a. Prescribed Burns	700	700	300	200	500
b. wild fires in the wood production forest	2,000	20,000	1,000	2,000	5,000
WASTE	20,000	22,000	24,000	24,000	24,000
a. Solid Waste Disposal on Land	19,000	20,000	23,000	22,000	22,000
b. Wastewater Handling	1,200	1,300	1,400	1,400	1,400
c. Waste Incineration	320	330	350	350	350
LAND USE CHANGE & FORESTRY	-200,000	100,000	-70,000	-80,000	-20,000
a. Changes in woody biomass stocks	-200,000	90,000	-100,000	-100,000	-50,000
b. Forest & Grassland Conversion	10,000	10,000	10,000	10,000	10,000
c. Abandonment of Managed Lands	-700	-700	-700	-700	-700
d. CO2 emissions & removal from soil	10,000	10,000	10,000	10,000	10,000

winter temperatures, as well as increases in transport, mining and manufacturing sectors. The average annual growth of GHG emissions over the 1990-2002 period was 1.7 %. In 2002 Canada's GHG emission increased by 15 Mt from 2001 level of 716 Mt. The energy sector was responsible for 10.4 Mt. of this change. Between 2001 and 2002 the transportation sector emissions increased for almost all modes of transportation. Domestic aviation emission rose by 9.2 %. Light duty gasoline trucks (LDGT : Minivans/SUVs / Panel Vans) increased by about 5.1% and heavy duty diesel vehicles (HDDV) by 2.7 % reflecting increased passenger travel and on road shipping. Emission in the off road sub sector decreased by 10.2 % between 2001 and 2002, reflecting a decrease in construction and agricultural activities. Long term trends (1990-2002) also showed some decrease in GHG emissions. Manufacturing Industry emissions declined by 4.6 Mt (-8.5 %). Emissions from light duty gasoline automobiles (LDGAs) continued to decline, showing a decrease of 3.0 Mt since 1990 (-6.7 %). However this decline has been more than offset by an increase in emissions from the light duty gasoline trucks category (LDGT : Minivans and SUV), which showed a continuous increase of over 19 Mt (88 %) since 1990. On average, LDGT emit 40 % more GHG per kilometre than cars. The long term GHG emissions increase associated with electricity and heat generation is mainly the result of the use of more GHG intensive fossil fuels and increased demand for electricity. (22 % increase in total electricity generation, the electricity sector is a significant and increasing contributor to Canada's GHG emissions (Statistics Canada 2002) [3].

1.2 Automotive NO_x emissions regulation

European Union emission regulations for new light duty vehicles (cars and light commercial vehicles) were specified in Directive 70/220/EEC. This regulation was amended a number of times; some of the most

important amendments include the Euro 1/2 standards, covered under directives 93/59/EC (EC93) and 96/69/EC (EC96). The most recent Euro 3/4 limits, covered by Directive 98/69/EC. The 2000/2005 standards were accompanied by the introduction of more stringent fuel quality rules that require minimum diesel cetane number of 51 (year 2000), maximum diesel sulphur content of 350 ppm in 2000 and 50 ppm in 2005, and maximum petrol (gasoline) sulphur content of 150 ppm in the year 2000 and 50 ppm in the year 2005 [4].

The emission test cycle for these regulations is the ECE 15 + EUDC procedure. Effective year 2000 (Euro 3), that test procedure was modified to eliminate the 40 s engine warm-up period before the beginning of emission sampling. All emission limits are expressed in g/km.

The Euro 2-4 standards are different for diesel and gasoline vehicles. Diesels have lower CO standards but are allowed higher NO_x. Gasoline vehicles are exempt from particulate matter (PM) standards. The standards for new cars are summarized in Table 1.3, the standards for light trucks in Table 1.4. The regulations additionally specify effective dates for first registration (entry into service), which in most cases is one year after the respective approval date. [4].

On December 17, 2002 Canada ratified the Kyoto Protocol to the United Nation's Framework convention on climate change (UNFCCC). The Kyoto Protocol, when it enters into force, commits Canada to a 6% reduction of 1990 GHG emissions and stipulates that progress in achieving this reduction commitment will be measured through the use of a set of internationally agreed norms for emissions measurement and reporting guidelines [3].

Table 1.3 EU emission Standards for Passenger Cars, gms / km

Tier	Year	CO	HC	HC + NOx	NOx	PM
Diesel						
Euro 1	1992.07	2.72 (3.16)	-	0.97 (1.13)	-	0.14 (0.18)
Euro 2, IDI	1996.01	1.00	-	0.70	-	0.08
Euro 2, DI	1996.01a	1.00	-	0.90	-	0.10
Euro 3	2000.01	0.64	-	0.56	0.50	0.05
Euro 4	2005.01	0.50	-	0.30	0.25	0.025
Petrol (Gasoline)						
Euro 1	1992.07	2.72 (3.16)	-	0.97 (1.13)	-	-
Euro 2	1996.01	2.20	-	0.50	-	-
Euro 3	2000.01	2.30	0.20	-	0.15	-
Euro 4	2005.01	1.00	0.10	-	0.08	-

Values in Bracket are Conformity of Production (COP) limits

a- Until 1999.09.30 (after that date DI engines must meet the IDI limits).

Table 1.4 EU emission standards for Light Commercial Vehicles, gm / km

Class	Tier	Year	CO	HC	HC + NOx	NOx	PM
Diesel							
N1, Class1 < 1305 Kg	Euro 1	1994.10	2.72	-	0.97	-	0.14
	Euro 2	1998.01	1.00	-	0.60	-	0.10
	Euro 3	2000.01	0.64	-	0.56	0.50	0.05
	Euro 4	2005.01	0.50	-	0.30	0.25	0.025
N1 Class II 1305 - 1760 Kg	Euro 1	1994.10	5.17	-	1.40	-	0.19
	Euro 2	1998.01	1.20	-	1.10	-	0.15
	Euro 3	2000.01	0.80	-	0.72	0.65	0.07
	Euro 4	2005.01	0.63	-	0.39	0.33	0.04
N1 Class III >1760 Kg	Euro 1	1994.10	6.90	-	1.70	-	0.25
	Euro 2	1998.01	1.35	-	1.30	-	0.20
	Euro 3	2000.01	0.95	-	0.86	0.78	0.10
	Euro 4	2005.01	0.74	-	0.46	0.39	0.06
Petrol							
(Gasoline)	Euro 1	1994.10	2.72	-	0.97	-	-
N1 Class I < 1350 Kg	Euro 2	1998.01	2.20	-	0.50	-	-
	Euro 3	2000.01	2.30	0.20	-	0.15	-
	Euro 4	2005.01	1.00	0.10	-	0.08	-
	N1 Class II 1305 - 1760 Kg	Euro 1	1994.10	5.17	-	1.40	-
Euro 2		1998.01	4.00	-	0.65	-	-
Euro 3		2000.01	4.17	0.25	-	0.18	-
Euro 4		2005.01	1.81	0.13	-	0.10	-
N1 Class III >1760 Kg	Euro 1	1994.10	6.90	-	1.70	-	-
	Euro 2	1998.01	5.00	-	0.80	-	-
	Euro 3	2000.01	5.22	0.29	-	0.21	-
	Euro 4	2005.01	2.27	0.16	-	0.11	-

For Euro 1/2 the weight class were: Class I <1250 Kg, Class II 1250-1700 Kg, Class III >1700 Kg

Notes :

* Useful vehicle life for the purpose of emission regulation is 80,000 km through euro 3 stage and 100,000 km beginning at the Euro 4 stage (2005)

* Requirement of On board emission diagnostic system (OBD) phased in between 2000 & 2005.

* Requirement of low temperature emission test (7 deg C) for gasoline vehicles effective 2002.

1.3 Pollution from automobiles and initiatives taken by the Canadian automotive industry

Spark ignition (SI) and compression ignition (CI) engines used by the automotive industry are a major source of urban air pollution. Spark ignition engines mainly use gasoline as a fuel and often run on stoichiometric or rich combustion mixtures, whereas compression ignition engines normally use diesel as a fuel and run in lean combustion mode. The concept of spark ignition lean burn internal combustion engines using natural gas as a fuel is increasing in popularity in the automotive industry owing to the latest environmental regulations.

The SI engine exhaust gases contain oxides of nitrogen, mostly NO but also small amounts of NO₂, carbon monoxide (CO) and hydrocarbons (HC). The relative concentrations of these emissions from an automotive engine depends on the engine design and operating conditions, but are of order of: NO_x; 500 to 1000 ppmv or 20 g/kg of fuel; CO; 1 to 2 % v/v or 200 g/kg of fuel and HC 3000 ppmv as C₁ or 25 g/kg of fuel [6]. In diesel engine exhaust, the concentration of NO_x is comparable to that from SI engines. Diesel hydrocarbon emissions (CI engine) are lower by a factor of 5 than typical SI gasoline engine levels. Diesel engines are also an important source of particulate emissions; between about 0.2 and 0.5 % w/w of the fuel mass is emitted as small particles (< 0.1 μm diameter). There is, however, only a small amount of CO formation in diesel engine due to lean combustion atmosphere. Gasoline and diesel contain significant amounts of sulphur, whereas natural gas contains only trace amounts. Gasoline may contain around ≤ 600 ppmw, whereas diesel contains about ≤ 0.5 % w/w of fuel. Sulphur in these fuels is oxidised during the combustion reaction to sulphur dioxide SO₂ and some part of this SO₂ can oxidized to sulphur trioxide SO₃, which combines with water to form sulphuric acid aerosol [6].

1.3.1 Formation of pollutants in the internal combustion engine

Emissions of CO, NO_x, CO₂, SO₂ and HC from engine depend on such variables as ignition timing, load, speed, fuel /air ratio and quality of fuel used, i.e. sulphur content of fuel, and octane numbers [7]. In spark ignition engines nitric oxide (NO) forms throughout the high temperature combustion reaction in the engine. Higher combustion temperatures near the flame zone give higher rates of NO formation. NO formation freezes during the expansion stroke, NO later oxidizes to form NO₂. Owing to the rich or stoichiometric combustion in SI engines, there is insufficient oxygen during the combustion process to burn all of carbon from the fuel completely to CO₂. As the burned gas temperature falls during the expansion stroke, oxidation of CO stops, leaving CO in exhaust. The HC emissions have several sources. During compression and combustion, the increasing cylinder pressure may force some of the gas in the cylinder into crevices, or narrow volumes, connected to the combustion chamber. Most of this gas is unburned fuel-air mixture, much of it escapes the primary combustion process because the entrance to these crevices is too narrow for the flame to enter. This gas which leaves these crevices later in the expansion and exhaust processes is one source of hydrocarbon, (HC) emissions. Another source of HC in engines is incomplete combustion owing to bulk quenching of the flame in that fraction of the engine cycles where combustion is slow. Such conditions are most likely to occur during transient engine operation when the air/fuel ratio, spark timing etc. may not be properly matched [6]. The unburnt HC exit the engine cylinder by being entrained in the bulk gas flow during blowdown and at the end of the exhaust stroke as the piston pushes gas scrapped off the wall out of the exhaust valve. Oxidation of this HC may occur during expansion and exhaust strokes of the engine cycle. The amount of HC oxidation depends on the temperature and oxygen concentration in the exhaust.

1.3.2 Steps taken by the automotive industry to reduce emissions

Canadian automotive industry and the oil industry have taken various measures to reduce the NO_x, CO, SO_x, and particulate emissions from the internal combustion engines used for automobiles. Measures taken include improving the quality of fuel used in automobiles as well as employing some innovative technologies for enhancing the engine performance, use of novel methods like Exhaust Gas Recirculation (EGR), three way catalytic converters for SI engines, particulate filters and traps etc. Some common measures are listed below.

➤ **Increasing the efficiency of fuel combustion in IC engines**

Increasing combustion efficiency reduces the amount of HC emitted from engine. A good combustion also reduces the coke deposition in the engine. This is mainly achieved by using multi point fuel injection system, and computerized control on engine feedback control system to control the air / fuel ratio so as to achieve the complete combustion of fuel. Most modern automobiles have multipoint fuel injection as well as being equipped with sophisticated engine control system.

➤ **Use of three way catalytic converters**

If an engine is operated with an air/fuel ratio close to stoichiometric, then both NO reduction and CO and HC oxidation can be done using a single catalyst, called the three way catalyst (TWC). The active catalyst is a combination of three noble metals viz: Platinum (Pt), Palladium (Pd), and Rhodium (Rh). Because the engine naturally oscillates around the stoichiometric point, leading to alternate lean and rich operation, ceria is added to retain oxygen during the lean combustion. The oxygen is subsequently released during rich operation. These active metal are dispersed in a porous support, which is usually coated onto the channels of a monolith substrate. The substrate is enclosed in a metal casing. A

three way catalyst can reduce the amount CO, HC, and NO_x in exhaust gases by over 90 %, if the air/fuel ratio is controlled close to stoichiometric. Diesel engines and CNG engines operate lean and therefore have excess oxygen in the exhaust, thus the TWC will not work. A diesel auto catalyst operates as an oxidation catalyst, cutting CO and HC emissions by more than 90 %, but having only a small effect on NO_x. For NO_x reduction in lean combustion, the subject of this dissertation, some innovative technologies are discussed in later chapters.

➤ Exhaust Gas Recirculation

Exhaust Gas Recirculation (EGR) is a novel approach to reduce the NO_x emissions from an engine. As seen earlier, the rate of NO_x formation increases with higher flame temperatures in combustion zone, therefore lowering the combustion temperature lowers the NO_x formation. One approach to reduce the flame temperature is to retard the ignition. This method is very effective because it reduces the engine peak pressure and temperature. However, it has an adverse effect on power output and engine economy. Another approach is to increase the concentration of residual gases (gas mixture remaining in the cylinder after the exhaust stroke) in the cylinder by EGR. EGR lowers the flame temperature and engine speed but gives significant NO_x reduction. Between 5 to 10 % EGR can reduce NO_x emissions by 50% [7]. However, EGR lowers the efficiency at full load. Further discussion on EGR is found in Chapter 2, which discusses some NO_x control strategies for automotive engines.

➤ Use of higher octane fuels

Knocking in engine reduces the complete combustion of HC and increases coke formation and HC emissions. Knocking is the ability of fuel to auto-ignite at a certain temperature. Knocking is characterized by spontaneous ignition and the resulting pressure rise giving an abnormal

audible sound, which is caused by resonance of combustion chamber walls. Use of cleaner fuel with higher auto ignition temperature solves this problem of knock in the engine. Fuel with higher octane number (Between 85 to 100) is normally used in SI gasoline engine to avoid knocking. The attraction of high octane fuel is that they enable high compression ratios to be used. Higher compression ratios give increased power output and improved engine performance [7]. Typically a compression ratio of 7.5 requires 85 octane fuel, while a compression ratio of 10 requires 100 octane fuel.

➤ Use of cleaner fuels

Along with using high octane fuel as mentioned above to reduce HC emissions and knocking, use of fuel with low sulphur content can significantly reduce the SO₂ emissions from engines. Currently used fuels contain sulphur in small proportions for example, gasoline contains around 500 ppmw and diesel contain about 0.01 to 0.03 wt% of sulphur. Canadian oil producers are aiming at reducing this fuel sulphur content further by application of fuel desulphurization methods at the crude refining stage. Natural gas as a clean fuel has trace amounts of sulphur and no fuel nitrogen. Some large utility vehicles already use CNG as a fuel. As natural gas combustion is in the lean combustion environment, reduction of NO_x poses a challenge in this excess oxygen present. Hence use of CNG vehicles at present is limited due to stringent emissions regulations as shown in Table 1.3 and 1.4.

➤ Use of alternative fuels

A significant amount of research has been carried out by car manufacturers for developing alcohol fuelled vehicles. Alcohols can also be blended with oil derived fuels. Alcohols can improve octane rating of oil derived fuels, owing to their high octane numbers. Also alcohols like

ethanol reduce the emission of CO₂ which is a GHG. Owing to its high octane ratings and high enthalpy of vaporisation it improves volumetric efficiency for an IC engine, but can cause starting problems. [7] For cold ambient conditions it may be necessary then to start engine with gasoline and then switch over to alcohol. This may require use of dual fuel engine and may raise initial cost of a vehicle. As an alternative to diesel fuel dimethyl ether (DME) which has a smaller molecular size and presence of oxygen atom (CH₃OCH₃) lead to a complete absence of particulates. Lower combustion temperatures than diesel may reduce the NO_x by around 50 %. DME is less expensive to produce than natural gas and easier to transport. Although use of DME may not require any engine modifications, the fuelling system elastomers need to be compatible with DME and the fuel injection system may need use of additives to compensate for the low lubricity of DME [7].

➤ Hybrid cars which run on fuel and electricity simultaneously

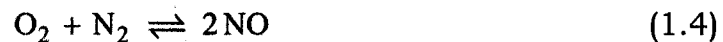
Hybrid cars use a combination of an engine and electric motors to give higher gas mileage than conventional gasoline cars. As a result, hybrid cars reduce GHG emissions significantly. A hybrid car has a fuel tank for engine, but also has a set of batteries that supply power to an electric motor. Both the engine and electric motor can turn the transmission at the same time. Typically, only one mode of power transmission is used at a given time, although the electric motors can be used to provide enhanced performance during engine operation. Whenever power from batteries is exhausted, power from the IC engine will be used to run the transmission as well as to charge the batteries at the same time. When the batteries are charged fully the transmission can then be switched to run with electric motor power. The Ford Escape 2005, for example, is a hybrid SUV that gives around 100 km on 8.8 litres of gas [9]. Another example is Honda Insight 2005.

1.4 Types of NO_x from combustion process

Three types of NO_x are produced during the combustion reaction of fuels: thermal NO_x, prompt NO_x and fuel NO_x. They are classified on the basis of method of their generation, for example thermal NO_x is generated from the nitrogen contained in the combustion air. However, from automotive engine exhaust point of consideration only the thermal and prompt NO_x are of importance and hence will be discussed briefly.

(a) Thermal NO_x :

Thermal NO_x is produced by the nitrogen in combustion air during combustion process. Air typically contains about 78% v/v nitrogen and 21% v/v Oxygen. At high combustion temperatures nitrogen and oxygen react to form NO_x compounds. Because this NO_x is generated by high temperature thermal oxidation of nitrogen, it is called thermal NO_x. Thermal NO_x forms via the extended Zeldovich mechanism [5]:



It is the primary source of NO_x emissions from fuels that do not contain organically bound nitrogen, for example natural gas.

(b) Prompt NO_x :

NO_x concentrations near the flame zone for hydrocarbon fuels demonstrate less temperature dependence than would be expected from the Zeldovich mechanism discussed above. For thermal NO_x, near the

flame zone, radicals such as O and OH enhance the rate of NO_x formation. Hence, some NO_x will still form despite aggressive controls on flame temperature and oxygen concentration. Prompt nitrogen oxides are formed in rich hydrocarbon flames via the interaction of hydrocarbon radicals with nitrogen molecule from combustion air. As demonstrated by the following reactions.



Unlike thermal NO_x, prompt nitrogen oxides are formed at temperature of 900 to 1100 °C. Prompt nitrogen oxides are formed more in rich combustion SI engines than in the lean combustion [8].

(c) Fuel NO_x:

Fuel NO_x is formed by oxidation of nitrogen containing compounds in the fuel. Some fuels contain nitrogen in the form of ammonia or organically bound nitrogen in hydrocarbon compounds. Nitrogen in the fuel reacts with oxygen from air supplied for combustion regardless of the flame temperature or excess oxygen concentration in the air. Carbon–nitrogen bonds are broken more easily than diatomic nitrogen bonds, so fuel- NO_x formation rates can be higher than thermal- NO_x. Combustion control techniques that aim at reducing thermal- NO_x formation by reducing flame temperature may not be effective for fuels that have higher nitrogen content. Automotive fuels such as gasoline, diesel and natural gas contain fuel bound nitrogen only in trace levels. Hence, discussion of fuel NO_x may not be of great importance for engine combustion.

Chapter 1 has focused on GHG and NO_x emissions, types of NO_x, and the initiatives taken by the Canadian automotive industry for their control. In Chapter 2, methods of controlling NO_x, particularly with respect to automotive engines, are discussed.

Chapter 2

Methods of controlling NO_x

The major contributors to the production of oxides of nitrogen are thermal NO_x and, if bound nitrogen is present in the fuel, fuel NO_x. For natural gas engines, contribution from fuel NO_x is minimal and thus is not a major concern. Thermal NO_x is the primary concern, while prompt NO_x formation is comparatively low, and primary methods used for thermal NO_x control are also applicable for control of prompt NO_x. This chapter reviews NO_x control methods for internal combustion engines.

2.1 Primary Methods

Primary methods involve control of NO_x generation during combustion by using various combustion technologies such as (i) keeping moderate peak flame temperature during combustion (ii) controlling air – fuel ratio. (iii) Lowering the temperature of combustion. (iv) Decreasing the residence time of gases in combustion chamber. (v) Exhaust gas recirculation (EGR) (vi) Modifications in fuel nozzle design and/or use of low NO_x burners. These primary measures are good for control of thermal NO_x. For fuel NO_x reduction, methods such as low oxygen combustion and staged combustion are applied.

2.1.1 Stoichiometry based combustion control

Stoichiometry based combustion control for NO_x reduction involves lowering the quantity of air in the initial combustion stage. This means supplying less than stoichiometric oxygen needed for the combustion. Reducing the burner stoichiometry means reducing the air-fuel ratio for combustion, which reduces the oxygen concentration in the primary combustion zone, hence creating a fuel rich combustion. This is a very

effective method for reducing fuel NO_x. Lower excess air operation can reduce NO_x levels by about 20 to 30 %.

2.1.2 Using the lean combustion mode

Spark ignition lean burn engines are increasing in popularity due to lower level of emissions. Diesel engines are always operated lean, as compared to SI gasoline engine, which usually operate with stoichiometric air to fuel ratio. Operating in the lean mode reduces the HC and CO emissions from an engine. The advantage of lean combustion over rich mode is a reduction in HC and CO levels by approximately 25 to 30 % v/v compared to the same capacity stoichiometric SI engine [6]. Another advantage of lean operation is the higher efficiency compared to the stoichiometric engine. Exhaust gas temperature in lean exhaust ranges from 200 to 600 °C. This is lower than the exhaust temperature of stoichiometric SI engine, which ranges from 300 to 900 °C. Application of catalytic pollutant reduction technology for the engine exhaust gases thus becomes more difficult in lean mode of combustion owing to the lower temperature[13]. The lean combustion diesel engine is, however, popular because of its higher efficiency and lower volumetric emissions of HC and CO.

2.1.3 Exhaust Gas Recirculation (EGR)

EGR involves recycling of exhaust gas into the combustion air or fuel prior to combustion. FGR reduces levels of thermal NO_x, by diluting local oxygen concentration, and reduces peak flame temperature by absorbing heat from the combustion product. EGR has little effect on fuel bound NO_x emissions. EGR is usually not more than 20 % v/v owing to flame stability considerations. NO_x reductions with EGR are typically in the 40 – 70 % range. It is the total burned fraction of the gas in the unburned fuel / air mixture in the cylinder which acts as a diluent. These burned

gases consist of both residual gas from the previous cycle and exhaust gas recycled to the intake. Mathematically, EGR is defined as the percentage of total intake mixture which is recycled exhaust.

$$\text{EGR}(\%) = \frac{m_{\text{EGR}}}{m_a + m_f} \quad (2.1)$$

For the spark ignition engines it has been observed that a 20 % EGR can reduce NO emissions from 2500 ppmv to 500 ppmv [6] The amount of EGR a particular combustion chamber will tolerate depends upon its combustion characteristics, the speed, load, and the equivalence ratio. Faster burning engine designs will tolerate more EGR than slower burning engine designs. The main effects EGR has on combustion are summarized as follows:

i) The dilution effect:

The dilution effect of EGR in lean combustion reduces the oxygen concentration in the charge by replacing the oxygen concentration with nitrogen, carbon dioxide (CO₂) and water vapour. Reduction in oxygen concentration result in reduced NO emissions and increased HC emissions and, in case of diesel engine increased particulate matter emission due to the significant increase in ignition delay [10].

ii) Thermal effect:

By introducing water vapour and CO₂ into the combustion chamber, the specific heat of the charge is increased. This results in lowered peak cylinder temperature, which in turn results in decreased NO_x.

iii) Chemical effect:

The chemical effect is a result of dissociation of CO₂, and water vapour. This highly endothermic process occurring at high temperature in the

combustion chamber absorbs the thermal energy of combustion reducing peak cylinder temperature. Among the three effects mentioned above, the dilution effect is the most significant.

EGR method of NO_x control has some disadvantages which include: It can lower the efficiency of engine at full load, it reduces the combustion rate which makes stable combustion more difficult to sustain [7]. HC emissions may increase with increasing EGR. It can also cause misfire in the combustion chamber. EGR has no significant effect on CO emission. In lean engines (equivalence ratio, $\phi > 1$) EGR of 20 % reduces NO levels by around 40 to 50 % [7]. However it increases the particulate matter emissions for the diesel fuel CI engine.

2.1.4 Homogeneous charge compression ignition

The basic concept of homogeneous charge compression ignition (HCCI) engine is that the ignition occurs at many points simultaneously within the cylinder with little requirement of flame propagation [14]. There is much interest in developing a better understanding of the HCCI concept because the conventional IC engine has limitations with respect to improving the combustion efficiency while reducing emissions. Combustion strategies that improve efficiency result in increased NO_x emissions. Combustion strategies that reduce the NO_x emissions result in increased HC and PM emissions from the engine, and conversely, strategies that reduce HC emissions almost always increase NO_x emissions [15]. The HCCI technique incorporates the best features of both spark ignition (SI) and compression ignition (CI) engines. The charge is pre-mixed, which minimizes the particulate matter emissions, like SI engine, and it is compression ignited like a CI engine, hence has no throttling losses. Since the homogeneously charged mixture reacts and burns in a very short time in the engine cylinder the losses due to finite combustion period are also minimized [15]. In addition the mixture is

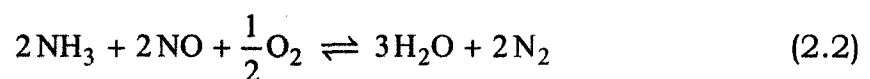
kept lean, which results in a lower combustion temperature (close to around 1000 °C) which in turn lowers the NO_x emission. In short, HCCI method of combustion promises the high efficiency of diesel engine and low emission of PM and NO_x like SI engine. HCCI in combination with techniques like EGR, use of VCR (variable compression ratio), and VVT (variable valve timing) can be applied to tune the engine performance as regard to obtaining higher efficiency and lower NO_x emissions. Stable HCCI operation can demonstrate the benefits of lower emissions from the engine. There are some barriers that remain to be resolved before HCCI concept can be practically applied to the engine design. The main barrier is controlling the auto ignition timing over a wide range of speeds and loads. Achieving cold start and limiting heat release at high load operation as well as providing the smooth operation during transient conditions encountered in actual road conditions [15].

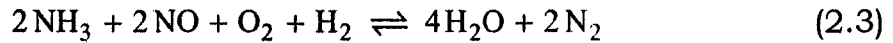
2.2 Secondary methods for NO_x reduction.

Dry methods for NO_x reduction involve processes such as selective non-catalytic reduction (SNCR) and selective catalytic reduction (SCR), where oxides of nitrogen are reduced to nitrogen and water vapor. The reagents used for these processes are NH₃ or urea injection in the exhaust gases. SCR can also be performed in a catalytic converter by adding hydrocarbons to the exhaust. This process of reduction is increasingly becoming popular for lean combustion in automotive engine NO_x control.

2.2.1 Selective Non catalytic reduction

Selective non catalytic reduction (SNCR) process uses ammonia (NH₃) or urea (NH₂ CO NH₂) to reduce NO_x to nitrogen and water. Overall reaction for a SNCR process is as follows [12].





No catalyst is required for this process; just good mixing of the reactants at the right temperature and adequate residence time of 1 s. The key to this process is operating within the narrow temperature window (900 to 1100 °C). Sufficient temperature is required to promote the reaction. At higher temperatures, ammonia oxidizes to form more NO, thereby wasting ammonia reagent and creating the pollutant that was intended to be removed. Above 1100 °C this reaction dominates.



In a typical application, SNCR produces about 30 to 50% NO_x reduction. Some facilities that require higher levels of NO_x reduction take advantage of the low capital cost of the SNCR system, then follow the SNCR section with an SCR system. Total capital costs may be lower than an SCR system alone because the catalyst bed for the SCR can be smaller due to the lower NO_x removal requirement for SCR after the SNCR system has removed a significant amount of NO_x.

2.2.2 Problems associated with SNCR

The ammonia slip is defined as the unreacted ammonia escaping from the catalyst along with the exhaust gases. Ammonia slip from SNCR systems occurs either from injection at temperatures too low for effective reaction with NO_x or from over-injection of reagent leading to uneven distribution. Controlling ammonia slip in SNCR systems is difficult because there is no opportunity for effective feedback to control reagent injection. The reagent injection system must be able to place the reagent where it is most effective within the combustion chamber because NO_x distribution varies within the cross section. An injection system that has too few injection control points or injects a uniform amount of ammonia across the entire section of the boiler will lead to a poor distribution ratio

and high ammonia slip. Distribution of the reagent can be especially difficult in larger coal-fired boilers because of the long injection distance required to cover the relatively large cross-section of the furnace. A potentially troublesome reaction is unreacted ammonia combining with SO_3 to form ammonium bisulphate. Ammonium bisulphate will precipitate at air heater operating temperatures and can ultimately lead to air heater fouling and plugging. Although no SO_2 is oxidised by the SNCR system, naturally occurring SO_3 concentrations are sometimes high enough (especially from higher sulphur coals) to be a concern with potentially high ammonia slip rates. An SNCR process can produce nitrous oxide (N_2O), which contributes to the greenhouse effect. N_2O formation resulting from SNCR depends upon the reagent used, the amount of reagent injected and the injection temperature. Hence, SNCR process alone is not an ideal solution to control NO_x emissions. The SCR process using ammonia as a reagent or hydrocarbon like methane (CH_4) or propane (C_3H_8) as a reducing agent for NO_x reduction is increasingly becoming popular for its low temperature operation and the wider temperature window as compared to the SNCR process [12].

2.2.3 Three way catalytic converters

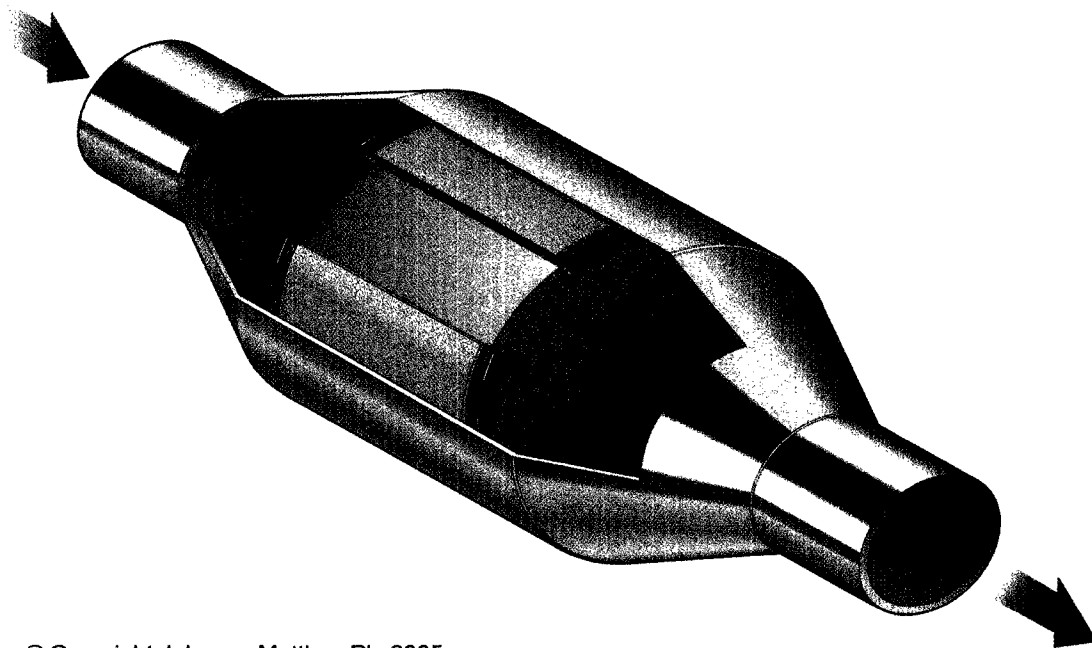
Three way catalytic converters were introduced in Chapter 1. As noted, for engines with stoichiometric fuel to air ratio, these converters can remove CO, HC and NO_x . Typically, these converters consist of a honeycomb type matrix, which has thousands of parallel channels of the order of 1 mm in size. This open porous structure is used to give a low pressure drop. The catalyst is deposited in a porous washcoat containing the catalyst. The substrate is made of cordierite (ceramic) or metal. The active catalyst is combinations of three noble metals: platinum (Pt), palladium (Pd) and rhodium (Rh), which are dispersed over the washcoat. Each noble metal is used for a specific purpose as highlighted below.

They are distributed such that they remain separate from each other on the wash coated substrate.

Pt is effective for CO, NO and HC removal at steady, near stoichiometric operation. However, it has poor high temperature stability [18]. Pt enhances the rate of O₂ uptake by ceria yet doesn't increase its oxygen storage capacity. It promotes the water gas shift reaction [19].

Pd possesses excellent light-off characteristics and high thermal durability. It increases oxygen storage ability [20] but is sensitive to poisoning by sulphur and lead compounds [18].

Rh is effective for reducing NO and oxidizing CO. Under stoichiometric conditions, however it offers better NO_x reduction in the presence of trace O₂, or SO₂ than Pt and Pd. It is especially good at promoting the water gas shift reaction [16] and is resistant to sintering [17] but is severely poisoned by lead compounds [18].



© Copyright Johnson Matthey Plc 2005

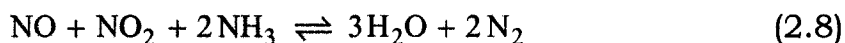
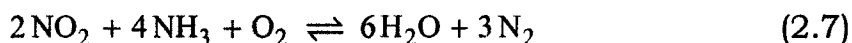
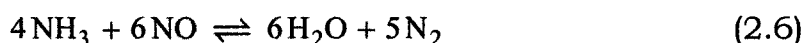
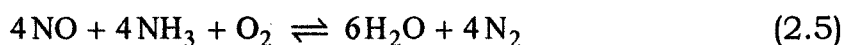
Figure 2.1 Honeycomb type three way catalytic converter used for automotive exhaust emission control. (figure courtesy of Johnson Matthey Catalysts Co.)

Ceria - CeO₂ in its oxidized state provides oxygen for CO and HC oxidation in a rich exhaust gas environment, and in the process is reduced. When the exhaust cycles to lean conditions, this reduced component can absorb O₂ or NO. (which removes NO directly or indirectly from the exhaust gases by reducing the O₂ concentration.) The oxidized component can in turn provide oxygen for CO and HC oxidation in the next rich cycle [16].

The three way catalytic converters are effective for NO_x reduction only with stoichiometric feed, and are not effective in a lean environment.

2.2.4 Selective Catalytic Reduction with Ammonia

There are two types of this selective catalytic reduction (SCR) process. One uses ammonia as a reducing agent and the other uses hydrocarbons such as methane (CH₄), propene (C₃H₆) or propane (C₃H₈). When ammonia is used, ammonia vapour is injected into the exhaust gas stream before passing over a catalyst. The optimum reaction temperature is 300 to 400 °C. The following reactions occur in the reactor [21]:



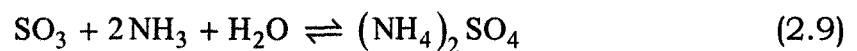
Different types of catalysts are used for SCR. Precious metals are used in the low temperature ranges of 175 to 285 °C. Vanadium pentoxide supported on titanium dioxide is a common catalyst for the temperature range of 260 to 425 °C. Zeolites, which are various alumino - silicates, are used as high temperature catalysts in the range of 450 to 600 °C. Reactor geometry may be a honeycomb monolith structure. In some

applications plate type structures are also used. Plate types generally have a higher resistance to deposition and erosion than honeycombs. SCR systems are capable of 70 to 90 % NO_x reduction. In the common power generation application of gas-fired turbines, less than 5 ppm NO_x at 15 % O₂ can be achieved in the exhaust gas.

Particulate matter and catalyst fouling can be a problem when there is a significant amount of particulate in the gas stream. Monoliths are advantages in this regard, because the large open area can allow the passage of particulate matter.

SCR operating considerations include ammonia storage and handling. Ammonia can be in either the anhydrous or aqueous form. A small amount of ammonia, about 5 to 20 ppm, will pass, or “slip,” through the catalyst, which creates an emission of a small amount of a hazardous air pollutant in exchange for reducing NO_x. Moreover this process has drawbacks for automotive exhaust because it involves ammonia injection. Storage of ammonia is a safety hazard in passenger vehicles.

Another catalyst issue is oxidation of SO₂ to SO₃ in exhaust gases from fuels that contain sulphur. SO₃ results in sulfuric acid mist emissions. Tungsten trioxide and molybdenum trioxide are catalysts that minimize sulfur oxidation. The SO₃ may combine with slipped ammonia and water vapors to form sulfates according to the following reactions. [21]



Ammonium sulphate is a powdery substance and contributes to the quantity of particulates in the exhaust gas. Ammonium bisulphate ((NH₄)₂SO₄) is a sticky compound that can be deposited on the catalyst layer and downstream equipment, when deposited into the catalyst layers ammonium bisulphate poisons the catalyst reducing the catalyst

activity. The higher the ammonia slippage and lower the temperature, the greater are the chances of forming the sulfates. Problem of sulphate deposition can be eliminated or minimized when natural gas or low sulphur oil is used as a combustion fuel, provided that the ammonia slippage is limited to < 10 ppm and the SO₃ content is < 5 ppm.

2.2.5 Selective catalytic reduction of NO_x, using hydrocarbon

The selective catalytic reduction (SCR) of NO_x by hydrocarbon is an attractive technique for NO_x reduction to N₂ in exhaust gas stream from both mobile and stationary sources. Hydrocarbons which can be used as a reducing agent are: methane (CH₄), propane (C₃H₈), butane (C₄H₁₀), propene (C₃H₆) or even hydrogen (H₂). Pioneering work in this field was carried out by Iwamoto [26] and Armour [32]. A reactor of similar geometry and design as the three way catalytic converter is used. Hydrocarbon is added to the lean engine exhaust before it enters the converter. Chapter 3 gives a literature review on SCR of NO_x.

Out of all the technologies mentioned in this chapter, the SCR of NO_x using hydrocarbon is a good choice for the following reasons.

- Primary methods of NO_x reduction are a good technique, but the problem associated with relying only on primary methods indicates that still there will be some NO_x in the exhaust gases from engine. Hence the best strategy would be to use the primary methods in combination with of any of the secondary methods for NO_x removal.
- Both SNCR and SCR of NO_x using ammonia / urea involves slippage of ammonia to the environment and storage of hazardous nature ammonia at the location of use for injection. For the same reason its use in automotive engine exhaust NO_x reduction, is not recommended. Moreover, SNCR technique can produce N₂O which is an indirect GHG.

In this work, the method focussed on is the SCR by hydrocarbons.

Chapter 3

Selective Catalytic NO_x Reduction with Hydrocarbons

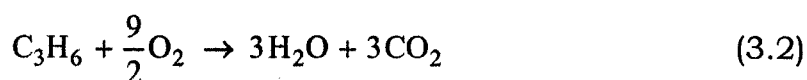
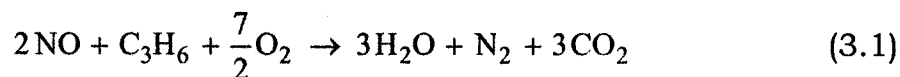
The three way catalyst was a major step in auto catalyst development, when the simultaneous removal of CO, HC, and NO_x became possible. As noted in Chapters 1 and 2, this technology is effective for stoichiometric engines. However, the desire for improved fuel economy and requirement of lower emissions of CO₂ and NO_x is projected to increase demand for diesel or natural gas fired vehicles through out the world. It is therefore of great importance to develop catalyst technologies that will allow NO_x reduction in lean exhaust environments of these type of engines. Although ammonia or urea injection is a possibility, the use of hydrocarbons as the reducing agent offers many advantages. This chapter gives a literature review of SCR using hydrocarbons.

3.1 Pioneering work in the direct de-composition of NO

The pioneering work by Iwamoto et al. [24, 26] led to a discovery in mid-1980s of a Cu-ZSM-5 catalyst for the direct decomposition of NO into N₂ and O₂ at 500 °C. They reported substantial conversion of NO (60 % to 85 %). Shortly thereafter they reported that the same catalyst was much more effective for selective catalytic reduction of NO_x using hydrocarbon as a reductant in the presence of excess O₂. They used different hydrocarbons, including C₂H₄, C₃H₆ and C₃H₈. They reported that oxygen enhanced the rate of NO-hydrocarbon reaction. The loss of activity at higher temperature which they reported was attributed to the onset of the oxidation of the hydrocarbon.

The discovery by [24, 26] created new momentum for research in the field of selective catalyst reduction of NO_x by hydrocarbon. Several groups reported interesting result on NO reduction in presence of excess oxygen with hydrocarbons such as propane, propene, and ethylene. Held, (1988)

[25] reported NO_x conversion of up to 66 % under lean conditions over catalyst based upon zeolites ion exchanged with various metals. Cu / modernite was found to be the best for this reaction. Different types of catalyst material were tried to obtain the best results. The reaction for NO reduction with propene (for example) under strongly oxidising condition can be written down as follows.



For good reduction of NO_x high selectivity for reaction (3.1) was needed. Reaction (3.2) is oxidation of hydrocarbon and is unwanted. The temperature at which the maximum rate of NO reduction obtained depends on the type of hydrocarbon used. For Cu-ZSM-5 catalyst maxima in activity were noticed at 523, 598 and 573 K for C₂H₄, C₃H₆ and C₄H₈ hydrocarbons, respectively [26]. The overall activity of Cu-ZSM-5 was found to depend on the exchange level of copper. The activity of the catalyst was maximum for NO reduction at a copper exchange level of 80-100 % on the zeolite. Low catalytic activity was observed for Cu exchange level of less than 40 %.

3.1.1 Performance of Cu - ZSM-5 catalyst

On Cu-ZSM-5 around 75 % conversion of NO to N₂ was observed when the O₂ level was 2 %, with C₃H₆ as a reducing HC. As the oxygen concentration increased, the conversion dropped below 50 % at 10 % oxygen in the engine exhaust gas [27]. NO conversion of around 70 % to 75 % was observed on Cu-ZSM-5 catalyst, between 450 to 500 °C exhaust gas temperature with C₃H₆ as a reductant. It was observed by [26] that NO conversion decreases in the presence of water. They observed that at 3.9 % v/v water in the feed and a temperature of 500 °C

the activity of Cu-ZSM- catalyst reduced from 75 % NO conversion to 45 % but this de-activation was completely reversible for exposure time up to 90 min. However, they reported irreversible deactivation of catalyst with higher water vapour percentage with gases and longer duration of catalyst exposure to such conditions [28]. Ansell et al. [29] reported that the activity of Cu-ZSM-5 monolith sample fell from 60 % to 17 % over the course of 70 hour at 485 °C under a simulated lean burn gas with 10 % H₂O flowing at a Gas Hourly Space Velocity (GHSV) of 30000 h⁻¹ [29]. The effect of thermal ageing on Cu-ZSM-5 catalyst was reported by Monroe [30]. They found that the NO conversion decreased from 41 % to 8 % following a 4 h ageing at 800 °C in 5 % H₂/N₂, and conversion dropped to 14 % following a 4 h ageing at the same temperature of 800 °C in 5 % O₂/N₂ and to 9 % following a 4 h ageing at 800 °C in a feed which switched between 5 % H₂/N₂ and 5 % O₂/N₂ every 10 s. This shows that Cu-ZSM catalyst can be rapidly deactivated by thermal ageing. Cu-ZSM-5 showed high catalytic activity for the reduction of NO_x using hydrocarbons in the presence of oxygen. It is the most effective catalyst for reduction of NO. However, it is difficult to accomplish high selectivity for conversion of NO to N₂ on Cu-ZSM if excess oxygen is present, which is the case with diesel or gas turbine exhaust. It was found active only for higher hydrocarbons like butane, propane, propene, ethylene. It is also very sensitive to the presence of water vapour at high temperatures for extended periods of time resulting in poor hydrothermal stability.

3.1.2 Future challenge in technology development

Cu-ZSM-5 was the starting catalyst in this research area, and remained popular until the shortcoming of this catalyst was recognized. It was a clear breakthrough in technology, but the challenge is to remove NO_x in oxygen rich combustion gases from diesel or natural gas engines. The catalyst must be optimized for high activity operation at the wider temperature window from lower operating temperatures of 350 °C to high

of 800 °C and must be able to operate in high water vapour environment for high space velocity. The use of hydrocarbons should ideally be the same as the on-board fuel, because any higher hydrocarbon will have to be stored and added separately to exhaust gases from lean combustion.

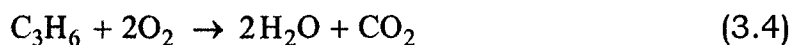
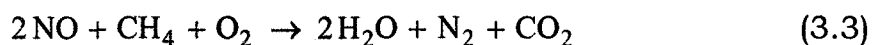
3.2 SCR of NO_x using Methane

Methane is a good candidate for a reductant. It is plentiful in supply, readily available and used as the fuel for stationary combustion engines in power plants as well as for mobile engines. Additionally methane does not pose storage and transportation hazard similar to ammonia. It would be easier to inject the onboard fuel (methane) for the SCR reaction in case of automotive engine if CNG is used as a fuel. Therefore, methane is a favourable choice for the NO_x reduction.

Li and Armor [31, 32] were the first to report that NO can be selectively reduced by methane in the presence of excess oxygen over Co-ZSM5 Cobalt exchanged zeolite catalyst. (Si/Al=14). This finding was another breakthrough in the selective catalytic reduction of NO_x with lower hydrocarbon like methane. Their work is summarised in the following.

3.2.1 Performance of Co-ZSM-5

Extensive research work by Li and Armor from 1992 to 1994 [31,32] for reduction of NO using methane as a reductant is a good reference for researchers in this field. They reported that a Co-metal exchanged zeolite catalyst Co-ZSM-5 can effectively reduce NO_x with CH₄ in the presence of excess O₂. NO was almost completely reduced to N₂ at 400 °C. The reactions taking place on the catalyst is [31]:



The activity of the catalyst was low in the absence of oxygen and increased significantly in the presence of excess oxygen. They achieved conversion of NO close to 100 % with 820 ppm of NO, 2.5 % v/v oxygen, at 7500 GHSV and 400 °C. They observed that Co-ZSM-5 is much more stable in wet environment and high temperatures for more than 24 h. Co-ZSM-5 was found to be a hydro thermally stable catalyst for the inlet conditions mentioned above. However, Co-ZSM-5 loses its activity rapidly at higher water vapour concentration. The effect of water vapour was studied in [31]. It was found that Co-ZSM-5 can withstand 2 to 7 % water vapour for more than 72 h without any change in performance. However, at 10 % v/v of H₂O the NO conversion to N₂ reduced from approximately 52 % to 12 % at the same temperature [32]. This effect is reversible i.e. removing water from the feed results in a return to the activity observed in the dry stream. Some of the inhibition caused by water can be regained by raising the reaction temperature [32]. Despite its better hydrothermal stability and better selectivity towards the reduction of NO by CH₄, Co-ZSM-5 was found not to be a good catalyst for commercial application, that is, for prolonged application under a wet environment and wide temperature window, because its activity deteriorates under prolonged exposure to 7 to 16 % water vapour. They later reported that Co-Ferrierite catalyst (Si/Al=8) showed a two fold increase in the activity compared to Co-ZSM-5. A quick comparison of the two catalyst is: Co-ZSM-5 used 38 % of the available methane for NO_x reduction and balance being used for CH₄ combustion. Co-ferrierite used 86 % of methane for NO_x reduction under the same operating conditions. The increased effectiveness of Co-ferrierite was due to availability of more sites for NO_x reduction reaction by CH₄. Ferrierite was also found to lose its activity reversibly when water vapour was present in the inlet gas. The Co-ZSM-and Co-ferrierite both were found to be better catalysts for NO reduction by CH₄, however, they were found to lose their activity under continuous operation in wet atmosphere. As

found in [31] both Co-ferrierite and Co-ZSM were about a factor of four too low in activity for commercial use in stationary engines [32].

3.3 SCR of NO_x on zeolites and metal oxide based catalyst using hydrocarbons

After the work by Iwamoto in Japan [26], Held [25] in Germany (1988-89), and by Li and Armor (1990-1994) [31, 32] from the U.S., many researchers worked on selective catalytic reduction of NO_x using a variety of hydrocarbons and catalysts. They reported promising results, but no researcher has yet arrived at an economical solution to the lean burn NO_x reduction using hydrocarbon, particularly methane. Hence application and commercialization of this innovative technology is awaiting a better hydro-thermally stable catalyst. Work done by other researchers is summarized below.

3.3.1 Platinum containing Zeolites

Various groups have investigated the use of Pt containing zeolites for the catalytic reduction of NO_x by C₂+ hydrocarbons under lean burn conditions. Kharas et. al. [33] reported that the activity of Pt containing zeolites was found to increase with Pt loading in the support material. The temperature of maximum activity was observed to be 473K. Iwamoto [34] also studied the comparative performance of Pt-ZSM-5, Cu-ZSM-5, and Fe - Modernite, for reduction of NO_x using ethylene as a reductant. They found that Pt-ZSM-5 was more effective than the other two zeolites at temperatures below 500 K. Another important observation was that, the catalytic activity of Pt-ZSM-5 was not affected by adding 8.5 % water vapour, whereas the other two catalysts were completely deactivated. The long term stability of platinum catalyst was confirmed in simulated and actual diesel engine exhaust gases containing excess O₂ and water vapour. Major disadvantage of Pt-ZSM-5 catalyst is a substantial amount

of N_2O is formed, which itself is a pollutant. Pt-ZSM catalyst offer very good result with higher hydrocarbons C_2+ and was found to be more thermally stable than other types of 'metal zeolites'. However, little work has been done on this catalyst using methane as a reductant.

3.3.2 SCR of NO_x on supported noble metal oxide catalyst

Extensive work has also been done on supported noble metal catalysts (supported on γAl_2O_3 , SiO_2). Noble metal based catalysts were found to be active at the lowest temperatures and are relatively unaffected by the presence of water vapour or sulphur dioxide (SO_2) in the inlet gases. However it was found that these catalysts have one major disadvantage, which is the fact that conversion of NO to N_2 occurs in parallel with N_2O , which itself is a potential pollutant. Amiridis [35] and Burch [36] reviewed the extensive work done on supported noble metal catalysts. Hamada et al. [37] were the first to study platinum supported on γ -alumina for the reduction of NO. They used propane / propylene under excess O_2 for NO reduction. Hamada [37] also compared the activity of supported Pd and Rh catalysts and reported that Pt- Al_2O_3 is an active catalyst at low temperatures. Alumina supported Pd and Rh were found be less effective than Pt in the same environment. The temperature of maximum NO conversion was lower for supported Pt catalyst than Rh and Ru respectively, the order of temperature is 523 K, 573 K, 573 K. With propene as a reductant, Rh is moderately active for the formation of N_2 , at the upper end of temperature 300 °C. There is not much N_2O formed with Rh catalyst, which is consistent with the properties of Rh under stoichiometric conditions. Alumina supported Rh was found to be more active than Rh/ SiO_2 [37]. Hamada [37] stated that Rh/ SiO_2 is less active towards N_2 and more active for N_2O formation, whereas Rh/ Al_2O_3 is more active towards N_2 and less active for N_2O formation. Ru is good at

lower temperatures but was not found to give better result at higher temperatures. Pd is also as good a catalyst as Pt and Rh.

Engler [38] examined NO reduction in the diesel exhaust using a Pt catalyst. They used a variety of experimental conditions and tried various hydrocarbons as a reductant. The hydrocarbons were methane, ethane, propane, pentane hexadecane, oct-1-ene, methanol, ethanol, propanol, 1-butanol and toluene through various xylenes to 1-methylnaphthalene. The main findings can be summarized as follows: Linear paraffinic hydrocarbons are active for NO reduction only at higher carbon numbers. ($n > 4$ in $C_n H_{2n+2}$) the increasing effectiveness with increasing carbon number becomes smaller. Branched paraffins like 2,2,4 trimethyl pentene are less effective than linear paraffins. However both linear and branched paraffinic hydrocarbon compounds are more effective NO_x reductant than butane or propane on the supported platinum catalyst. Olefinic compounds are more effective NO_x reductant than paraffinic compounds and show high activity at low temperatures. Ethene is equally active as 1-Octene and show NO_x conversion of 50 % at 225 °C. Alcohols are also found to be effective NO_x reductant by Engler's group. NO conversion of around 70 % was obtained with 1-propanol and 1-butanol, 40 % for ethanol but almost zero for methanol. Aromatic compounds show moderate NO_x conversions with xylenes being better in effectiveness than toluene.

Burch [36, 39] also investigated NO_x reduction on various supported platinum group metal catalysts. They studied the effect of Pt loading and dispersion on the activity using propene as a reductant. They reported that, for a catalyst with 2 % Pt loading, reaction starts below 200 °C and peaks at 250 °C, whereas with 0.1 % Pt loaded catalyst there is not detectable conversion below 250 °C, and the peak is at about 350-370 °C. The increase in NO reduction activity with Pt loading was not only due to increase in the metal area, but was also found to depend on size

of the Pt particles. Larger particles had higher reduction surface for NO_x reduction. This group suggested that dissociative adsorption of NO is rate limiting and competes with oxygen dissociative adsorption for the active reduced platinum sites. While the NO adsorption is favoured at lower temperatures, O₂ adsorption is favoured at higher temperatures. That explains the higher activity of platinum catalysts at lower temperatures and formation of N₂O in parallel with NO reduction at the same temperature. The result of Burch [36,39] suggests that reduction of NO by hydrocarbons is structure sensitive and that the presence of metallic atom ensembles of a minimum size is required for the reaction to proceed at a significant rate. Another good finding for SCR of NO_x using supported noble metal catalyst was reported by [42]. They reported that Pd deposited on ZrO₂ was an effective catalyst for the SCR of NO_x with methane, in the presence of 0.5 % NO, 1 % CH₄, and 2.5 % O₂. A 0.3 wt % Pd-SO₄-ZrO₂ catalyst produced 60 % conversion of NO to N₂ at 500 °C and at GHSV of 20000 h⁻¹.

To summarize briefly, Pt has been found to be the most active and the most resistive catalyst in the presence of H₂O and SO₂. Rh/ Al₂O₃ was found to be most selective towards the N₂ formation than N₂O [13]. At the temperature of maximum NO conversion a selectivity of about 30% towards N₂ was obtained with Pt-Al₂O₃ as compared to 90% with Rh-Al₂O₃. Replacing alumina with silica as support was found to significantly decrease the activity of Pt catalysts.

3.3.3 Future challenges for development of supported noble metal catalysts for SCR of NO_x

The limitation for the commercial application of Pt-based lean NO_x catalysts is the narrow temperature range over which they are active. A broader temperature window is required if these catalysts are to be applied in practice for automotive engine operation. Nevertheless, these

catalysts appear as of today to be a most promising material for lean NO_x reduction using on-board hydrocarbons, mainly due to their good hydrothermal stability. In addition to broader temperature window of operation a commercially viable Pt-based catalyst would also require decreased selectivity for N₂O formation. It must be suggested here that instead of using a variety of hydrocarbons as NO reductant, a more practical approach would be to use methane (CH₄) as reductant, as advantages of using methane are eliminating mainly 1) mixing any hydrocarbon with the engine fuel may affect the engine combustion efficiency and 2) separate on board storage for the reductant.

3.4 Work of other researchers on metal catalysts using different hydrocarbons for SCR of NO_x

Kikuchi and Yogo [40] worked on Gallium ion exchanged zeolites for reduction of NO using propane as a reductant. They compared the performance of Cu-ZSM-5, and Ga-ZSM-5 for the same reaction condition in a lean environment. They found that propane was almost completely oxidised on Cu-ZSM-5 above 400 °C. This was due to high activity of this catalyst for propane oxidation, which limited the amount of NO reduced to N₂ by propane in lean conditions. Ga-ZSM-5 was more active than both the other catalysts above 500 °C. They observed only 20% conversion of NO to N₂ with CU-ZSM-5 when propane concentration was lowered form 1000 ppm to 333 ppm in the lean feed. However 67% conversion was observed on Ga-ZSM-5 under same conditions. This study excluded the effect of water vapour. The same group later reported that methane and ethane are also efficient for SCR of NO_x over Ga-ZSM-5. The activity of Ga-H-ZSM-5 however was more influenced by water vapour than Co-ZSM-5 zeolites.

The kinetics of NO_x decomposition and NO reduction by CH₄, with and without presence of oxygen over the Rare Earth Oxides (REO) like La₂O₃

and Sr_2O_3 was studied by Vannice et al. [41]. They found that activity of rare earth oxide catalysts for NO reduction continuously increases with temperature unlike zeolites. They reported that the presence of oxygen increases the rate of NO reduction by CH_4 because adsorbed NO_2 is more reactive with CH_4 than NO and forms a methyl radical more rapidly. The rate of reaction between two adsorbed molecules is slower than that between an adsorbed NO molecule and adsorbed CH_4 molecule. While the reaction between adsorbed NO_2 species and adsorbed CH_4 molecule is more rapid than either of the previous reaction. Their study, however, did not consider the effect of water vapour and was carried out at 650 °C.

3.5 Basic Metal Oxide Catalysts

Zhang et. al. [41, 43] were the first to study the effect of non-zeolitic catalyst for SCR of NO_x with methane [43]. They postulated the oxidative coupling of methane. SCR catalyst would be active for this reaction due to their ability to activate CH_4 to produce methyl (CH_3) radicals. For example MgO and Li doped MgO reduce NO to N_2 between 500 °C and 680 °C. at redox ratio (ratio of oxidising species to reducing species) of up to 2.8 and a space velocity of 3000 h^{-1} . They reported the conversion of NO to N_2 of around 11 % to 20 % in presence of around 2 % to 5 % O_2 , which is not very attractive for lean burn exhaust with 7 to 10 % oxygen.

Zhang also measured the CH_4 selectivities of SCR of NO_x over basic metal oxides at a redox ratio of 1.1. He ranked catalyst in terms of selectivity as follows. $\text{Lu}_2\text{O}_3 > \text{La}_2\text{O}_3 > \text{Tm}_2\text{O}_3 \approx \text{Sm}_2\text{O}_3 > \text{Nd}_2\text{O}_3 > \text{CeO}_2$ However, Fokema and Ying [44] reported that the selectivities of Sc_2O_3 and Y_2O_3 are similar and significantly greater than La_2O_3

3.6 NO_x Adsorber (NO_x Storage) catalysts

NO_x adsorber catalyst is a technology used for the SCR in the lean exhaust. First proposed by Toyota in mid 1990s, NSR (NO_x storage and reduction) involves the oxidative adsorption of NO_x on alkali earth oxide, (Barium Oxide, BaO) forming a surface nitrate. The nitrate is then reduced by periodic rich operation of the lean burn engine, which increases the level of HC in the exhaust to promote the reduction. Engelhard Corp. proposed an NSR system of two sequential reactors for use in diesel vehicles. Some researches like Ladommatos et al. [66] proposed recycling the adsorbed NO_x to the engine where it is decomposed. Bongger et. al. [46] used simulated engine exhaust to measure the performance of various catalysts. They concluded that the catalyst stores NO_x as a surface metal nitrate BaNO₃. They also determined that the catalyst was fully regenerable under rich conditions and NO_x conversion up to 94 % were obtained using 30 s rich and 30 s lean cycles. Takahashi et al. [47] worked with supported Pt/BaO catalyst. They found that NO is oxidized to NO₂ on the Pt sites and then stored as surface nitrate on adjacent Ba sites. During the rich phase NO_x is released from Ba sites and reduced on the adjacent Pt sites. Fridell et al. [48] observed that the storage has strong dependency on temperature, with a maximum storage observed around 380 °C. They also confirmed the findings of Takahashi et al. [47] that a correlation exists between higher oxygen concentration and higher NO_x storage capacity. Various researchers [63, 64, 65] discussed the effects of temperature, CO, CO₂ on the storage and adsorption capacity of NO_x on the BaO, BaCO₃ catalysts. It was however a common observation that for a lean burn engine intermittent rich engine operation will be required, to release and reduce stored NO_x from the catalyst sites. A suitable reductant injection (mainly HC) is essential. Ongoing research on NSR catalyst may make this

technology feasible for the lean combustion NO_x emission to be below the stipulated regulation.

3.7 Direction for future research

From the research work done so far, we can conclude some major requirements. The catalytic material must have good hydro-thermal stability under prolonged operating condition of lean exhaust with broad temperature window. The hydrocarbon of choice ideally would be the one which is the fuel for lean burn engine by itself, i.e. the onboard fuel. It is found by almost all the researchers that the presence of H_2O inhibits the catalyst activity and the presence of oxygen is required for SCR of NO_x by the HC. Hence the need for a stable catalyst which would perform in the so called “adverse” condition of lean exhaust i.e. Oxygen rich and wet exhaust in a broader temperature window, from 300 to 800 °C. As an aid in understanding the system, computer models are required for the case of SCR with injected hydrocarbon. Hence the first goal of this work will be to establish a model for the system that can be used to describe lean SCR. The methodology is discussed in Chapters 4 and 5.

Chapter 4

Modelling a monolith reactor for NO_x reduction

A major objective of this work was to develop and validate a global model for the SCR of NO_x. To achieve this objective it was necessary to have a monolith reactor model and a method of optimizing kinetic parameters in proposed models. This chapter describes the methods for modelling of a monolith reactor, including details of mathematics, solution of model equations and model validation. The first section gives an overview of the model selection process, which is followed by a mathematical description of the 1D single channel model (SCM). Solution methodology and the optimization method are then presented, and finally model validation for some CO oxidation light-off curves is described.

4.1 Modelling the monolith reactor

The goal of modelling is to determine how a system will behave under a set of operating conditions without having to perform the experiment [21]. Modelling allows investigation of scenarios which might be too dangerous or too costly to perform even at the laboratory scale [21]. For example testing of a catalyst under varying conditions of flow and pollutants concentration at different temperatures can be very time consuming. As an alternative to the performance testing of catalysts for the actual exhaust environment, reactor models can be developed to scale up and measure the performance of the catalyst. A good model can predict the actual and expected performance of catalyst for the real operating conditions. To be successful, such a model must be a transient one, in which all of the rate processes occurring in the catalytic reactor are correctly described. These include rates of reactions, rates of heat generation, as well as intra and inter phase heat and mass transfer occurring in the catalyst.

4.1.1 Single channel monolith reactor model

The most commonly used catalytic converter has a monolith type substrate. The monolith consists of many parallel passageways (cells) through which the exhaust gas flows. A diagram of honeycomb types monolith channels is shown in Figure 2.2, Chapter 2. Other type of channel shape include: circular, hexagonal, rectangular, and trapezoidal. Figure 4.1 shows a monolith type support for automotive exhaust applications.

The monolith converter consists of the three regions namely, open flow region, a porous catalytic layer and a substrate. A cell is typically 1.0 to 2.0 mm wide. The catalytic layer is approximately 0.010 to 0.150 mm thick. The substrate thickness ranges from 0.025 to 0.050 mm. A typical converter contains thousands of cells. After an initial length in which the exhaust gas velocity profile develops, the gas flows in laminar flow through each cell. The Reynolds numbers is of the order of 10 to 100. The reactants in the fluid diffuse to the wall and into the catalytic layer, where the reaction occurs; heat is generated due to the exothermic reactions. The reaction products diffuse back to the fluid phase and are carried to the outlet of the converter. If all the channels in the monolith

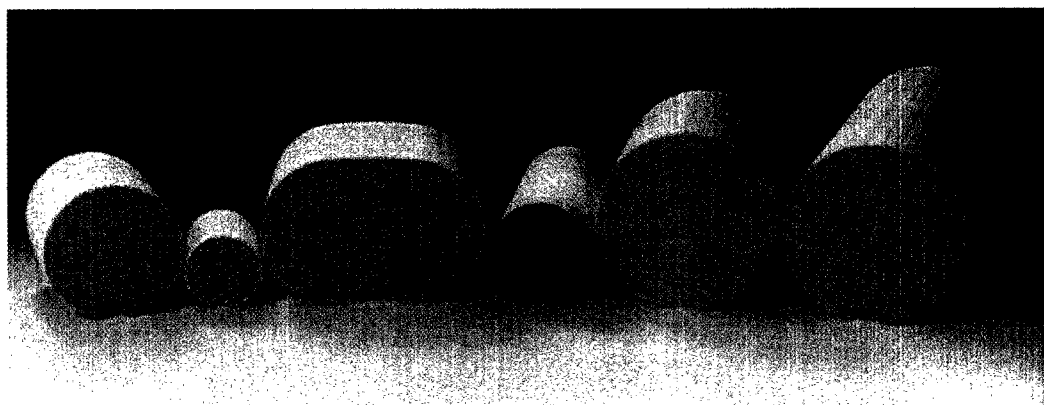


Figure 4.1 Different shapes of monoliths for automotive exhaust applications

(Fig : Courtesy of Dr. Johan Heiszwolf, Delft University of technology, The Netherlands)

are assumed to behave the same, a single channel monolith model (SCM) can be considered to be representative of the entire reactor [21]. This assumption requires that the velocity distribution is uniform among the channels, the catalyst is equally distributed among all the channels and there is no radial heat loss. If these assumptions are not met channel interactions may be added to the model and the single channel solutions from all of the channels added to build a multi channel model [21].

4.1.2 Model Dimensionality

To develop an appropriate model, decisions concerning the number of space dimensions must be made. A one dimensional (1D) model is the simplest and easiest to understand. A major advantage is that it uses significantly less computational time than two dimensional (2D) or three dimensional (3D) models. The 1D model ignores radial and angular velocity, temperature and concentration gradients and considers only axial variations. The temperature and concentration in the fluid phase are taken as the mixing cup values. This averaging of the radial values creates a discontinuity at the wall, which is accounted for by the use of heat and mass transfer coefficients.

A 2D model requires the representation of the monolith channels as right cylinders with symmetry about the axis and of the same hydraulic diameter as the channels. The hydraulic diameter is defined as the ratio of the inside perimeter divided by the cross sectional area for one channel. The gas phase temperature and concentration gradient are considered in the radial as well as axial directions. The 2D model can capture the velocity profile in the channel, including the developing flow at the inlet. The steady state model requires the solution of mole and energy balance as well as the momentum balance equations for the fluid phase. A 2D model requires more computational time than the 1D model.

A 3D model would be the most realistic model, especially for non-circular cross section passages. A 3D model will take into account variations in gas phase concentrations, temperature and velocity in the axial, radial and angular directions. A 3D model is more complex to solve and may be prohibitive to use due to its requirement of computational power and memory. It may also not be justified to use in terms of accuracy as error involved in assumptions (especially the simplified kinetic model) may be greater than the error in assuming a 1D model.

4.1.3 Choosing the Model

The challenge in selecting a suitable model is to determine the least sophisticated model that will do what is required [21]. The ideal approach is to derive a mechanistically simple and meaningful model. In the case of automobile exhaust, for realistic conditions on the road and with cold start, multiple steady state and transient operation of the engine is bound to occur. A 1D model would be a preferred choice due to its simplicity and less computational time requirement. Moreover, a 1D model can provide close agreement to 2D or 3D model [22]. The comparison between 1D and 2D model by [61, 62] for a simple experimental data showed close agreement between the results from 1D and 2D model. They showed that in terms of catalyst light off point and conversion of CO for an automobile engine exhaust, the difference between 1D and 2D model results is equivalent to less than 2 °C difference in inlet gas temperature [61]. A 1D model would be a preferred choice because it requires about 1/10th of computational time than a 2D model for a same mesh size. This time is critical if the model is to be run as part of a parameter optimization program. A 3D model can take around 8 to 10 hours for a single iteration of a simple parameter optimization problem. 1D model is comparatively a faster model and we need a fast model for the parameter optimization problem.

As mentioned above, a 1D model ignores radial and angular gradients in temperature, concentration and velocity, and considers only axial variations. There are two choices for incorporating the catalytic reaction into the heat and mole balance equations:

- i) The wall temperature and concentrations are assumed to be the same as the fluid, and the reaction rate is directly incorporated into the mole and energy balance equations. This is known as *Pseudo-homogeneous model*.
- ii) The gas solid interface at the wall is assumed to be a discontinuity and separate mole and energy balance equations are written for the solid phase. These equations are coupled to the fluid equations through mass and heat transfer coefficients. This type model is known as *heterogeneous model*.

In this work the heterogeneous model was used. A simplifying assumption often made in 1D model is that the fluid flows through the reactor in piston or plug flow, that is, there is no diffusion in axial direction of flow. The resulting model is called the *plug flow model*. Alternatively, some axial dispersion may be included. There are two methods commonly used for modelling tubular type reactors with axial dispersion. These are the dispersed plug flow model (dispersion equation) and the tanks-in-series model (TIS). Both methods were used in this work, and are briefly described in the following.

4.2 Axial dispersion model

The axial dispersion model has been widely used for both laminar and turbulent flow. In turbulent flow, it is assumed that the axial mixing caused by random velocity fluctuations follow Fick's law, but rather than molecular diffusion coefficient a new quantity called the dispersion coefficient is defined. The dispersion is superimposed on to the bulk flow

term giving the advection dispersion equation. For the gas phase the equation is:

$$D_I C_f \frac{d^2 Y_{j,f}}{dz^2} - C_f u_m \frac{dY_{j,f}}{dz} + \frac{4}{D_H} k_{m,j} C_f (Y_{j,f} - Y_{j,S}) = 0 \quad (4.1)$$

Where D_I is the dispersion coefficient in m^2/s , C_f is the fluid concentration in mol/m^3 , Y_f and Y_S are mole fractions of the component in fluid and solid respectively. In turbulent flow the dispersion coefficient can be measured experimentally using tracers. In laminar flow, both axial and radial diffusion are important and an exact solution requires that a 2D equation be solved. Taylor [54] showed that in a long tube of radius R with laminar flow, the 1D approximation gave the same solution as the 2D advection-diffusion equation when the axial diffusion coefficient was replaced by a dispersion coefficient defined by:

$$D_I = D_{AB} + \frac{u_m^2 R^2}{48 D_{AB}} \quad (4.2)$$

where D_{AB} is the molecular diffusion coefficient of A in a mixture of A and B, u_m is average velocity and R is the radius of the tube. Equation (4.2) was valid provided that the following condition was met:

$$\frac{L}{R} > 0.16 \frac{u_m R}{D_{AB}} \quad (4.3)$$

The boundary conditions for Equation (4.1) typically imposed are the so-called Dankwerts condition. They are:

$$\left(-D_I \frac{dY_{j,f}}{dz} \right)_{0^+} = u_m [Y_{j,f0} - Y_{j,f}(0^+)] \quad \text{at } z=0 \quad (4.4)$$

$$\frac{dY_j}{dz} = 0 \quad \text{at } z=L \quad (4.5)$$

In Equation (4.4) the term 0^+ indicates the position at $z = 0$ but inside the reactor. The mole fraction, $Y_{j,f0}$, is the mole fraction of species j in the feed. It has been pointed out [21] that when the influence of axial dispersion is low, and there is negligible reaction near the reactor entrance, then the inlet boundary condition can be replaced by a constant (feed) concentration with no loss of accuracy. This substitution was employed in this work.

The solid phase mole balance is:

$$k_{m,j} C_f (Y_{j,f} - Y_{j,S}) = (-R_j)_s \quad (4.6)$$

The gas phase energy balance equation is:

$$\alpha_I \frac{d^2 T_f}{dz^2} - u_m \frac{dT}{dz} + \frac{4}{D_H} \frac{h}{\rho C_p} (T_S - T_f) = 0 \quad (4.7)$$

where α_I is an effective axial thermal diffusivity defined by analogy with the Taylor – Aris diffusion coefficient:

$$\alpha_I = \alpha + \frac{u_m^2 R^2}{48\alpha} \quad (4.8)$$

Here α is the thermal diffusivity. The boundary conditions used were a fixed inlet temperature and a zero flux outlet condition.

The transient solid phase energy balance is:

$$k_w \delta_w \frac{\partial^2 T_S}{\partial z^2} - h(T_S - T_f) - \sum_{i=1}^n (\Delta H_R)_i (-R_j) = \delta_w \rho_w C_{pw} \frac{\partial T_S}{\partial t} \quad (4.9)$$

Where k_w is thermal conductivity of reactor wall in W/(m·K) and δ_w is the wall cross sectional area divided by wetted perimeter [21].

$$\delta_w = \frac{A_w}{W_P} \quad (4.10)$$

Zero flux boundary conditions were imposed at each end.

Analytical solution for the PDE that describe the axial dispersion model is not possible, hence a numerical method was used. The equations are a boundary value problem (BVP). Solution of the PDE was carried out in the first instance by using the Galerkin finite element method. Pressure drop was assumed negligible for the single channel model hence solution for the momentum balance equation was not required.

4.3 Tanks in series model

In some cases the FEM solution was slow, or failed to converge, so an alternative was developed. This method required the solution of initial value problem (IVP) only. This model begins with the assumption of plug flow, and adds the required dispersion numerically.

Consider flow in the channel and reaction in the wall (in the washcoat). A plug flow mole balance for component j in the mixture is:

$$C_T \frac{dY_{j,f}}{dt} = -u_m C_T \frac{dY_{j,f}}{dz} - \frac{4}{D_H} k_m C_T (Y_{j,f} - Y_{j,S}) \quad (4.11)$$

If we assume that the change in moles on reaction is negligible (a good assumption for trace pollutants) we can simplify and express the velocity in terms of the inlet temperature:

$$\frac{dY_{j,f}}{dt} = -u_0 \frac{T}{T_0} \frac{dY_{j,f}}{dz} - \frac{4}{D_H} k_m (Y_{j,f} - Y_{j,S}) \quad (4.12)$$

Where k_m is the mass transfer coefficient in m/s and D_H is the hydraulic diameter of the channel in m. This equation is essentially the same gas phase mole balance as used previously, but minus the dispersion term. This mole balance can be discretized in the axial coordinate (space dimension) using a backward difference. This model is then essentially the tanks-in-series model. Divide the reactor length, L , into n volume elements (tanks), each of which is denoted by the superscript index k . The resulting ODE in time can be written:

$$\frac{d(Y_{j,f})^k}{dt} = -u_0 \frac{(T_f)^{k-1}}{T_0} \frac{n}{L} \left[(Y_{j,f})^k - (Y_{j,f})^{k-1} \right] - \frac{4}{D_H} k_m (Y_{j,f} - Y_{j,S})^k \quad (4.13)$$

There is one equation for each node, for each species. Note that this ordinary differential equation is an initial value problem (IVP).

The solid phase mole balance is:

$$C_{T,S} \frac{dY_{j,S}}{dt} = \left(\frac{4D_H}{D_{WC}^2 - D_H^2} \right) k_m C_{T,f} (Y_{j,f} - Y_{j,S}) + R_j \quad (4.14)$$

where R_j is the total rate of production in mol/(m³s), based on washcoat volume. D_{WC} is the outside diameter of the channel including the washcoat, that is, the diameter of the channel plus twice the washcoat thickness. Equation (4.14) can be rearranged to give the explicit form:

$$\frac{dY_{j,S}}{dt} = \frac{4D_H}{D_{WC}^2 - D_H^2} k_m \frac{T_S}{T_f} (Y_{j,f} - Y_{j,S}) + \frac{1}{C_{T,S}} R_j \quad (4.15)$$

This equation is written at each node. For the adsorbed species, there is no transfer with the bulk gas phase, and the equation is written:

$$\frac{d\theta_j}{dt} = R_j \quad (4.16)$$

The number of nodes required in the axial direction can be estimated from the axial Peclet number by analogy with the tanks-in-series (TIS) model. In effect, we now add sufficient numerical dispersion to the model to account for the physical dispersion. The amount of numerical dispersion is controlled by fixing the number of tanks. The Taylor-Aries axial dispersion coefficient is calculated as before, from Equation (4.2). The axial Peclet number is defined as:

$$\left(\frac{D_{a,\text{eff}}}{u_m L} \right) = \frac{1}{Pe} \quad (4.17)$$

The number of nodes, (tanks) n , is related to the Peclet number by:

$$\frac{1}{n} = \frac{2}{Pe} - \frac{2}{Pe^2} [1 - \exp(-Pe)] \quad (4.18)$$

Typically, for the monolith reactors used in this study the Peclet number was of the order of 50 to 100, so 25 to 50 nodes were used.

The energy balance is also written for fluid and solid phases. The governing PDE for the fluid is:

$$\bar{C}_{P,f} C_T \frac{dT_f}{dt} = -u_m C_T \bar{C}_{P,f} \frac{dT_f}{dz} - \frac{4}{D_H} h(T_f - T_S) \quad (4.19)$$

It is important to note the correct units for the heat capacity. In explicit form, the equation is:

$$\frac{dT_f}{dt} = -u_0 \frac{T_f}{T_0} \frac{dT_f}{dz} - \frac{4}{\bar{C}_{P,f} C_T D_H} h(T_f - T_S) \quad (4.20)$$

The equation is then discretized along the axial direction using a backward difference scheme:

$$\frac{d(T_f)^k}{dt} = -u_0 \frac{(T_f)^{k-1}}{T_0} \frac{n}{L} \left[(T_f)^k - (T_f)^{k-1} \right] - \frac{4}{\bar{C}_{P,f} C_T D_H} h(T_f - T_S)^k \quad (4.21)$$

The solid phase is computed as an average of the washcoat (where the reaction occurs) and the substrate, which is included to achieve the correct thermal mass. We ignore the axial conduction in the solid phase to preserve the ODE nature of the problem.

$$\frac{dT_S}{dt} = \frac{[D_{WC}^2 - D_H^2] \sum_{j=1}^m (-\Delta H_j^0) R_j}{[D_S^2 - D_H^2] \bar{C}_{P,W} \rho_S} + \frac{4D_H}{[D_S^2 - D_H^2]} \frac{h(T_f - T_S)}{\bar{C}_{P,W} \rho_W} \quad (4.22)$$

The equation is again evaluated at each node. The solid heat capacity is a weighted average of the substrate and washcoat values.

The tanks in series model consists of a series of initial value problems. These were solved using a public domain software package for the solution of such problems, described shortly.

4.4 Software for solution of SCM

As discussed in the foregoing, two solution methods were adopted in this work. For the solution of the BVP (axial dispersion model) the finite element method was used. A software package developed previously for the simulation of single channel monolith reactors was adapted for this work. This software is called Mono1D. The basic flow diagram of this program is shown in Figure 4.2. The primary modifications required to the code were the addition of the appropriate kinetic models to the code.

The tanks in series model was solved using the ODE solver DVODE. This software is part of a software family called SUNDIALS, SUite of Nonlinear Differential / ALgebraic equations Solver. DVODE is a solver for stiff and non-stiff initial value problems. In this work an interface was written to Mono1D so that the same input and output data files were generated.

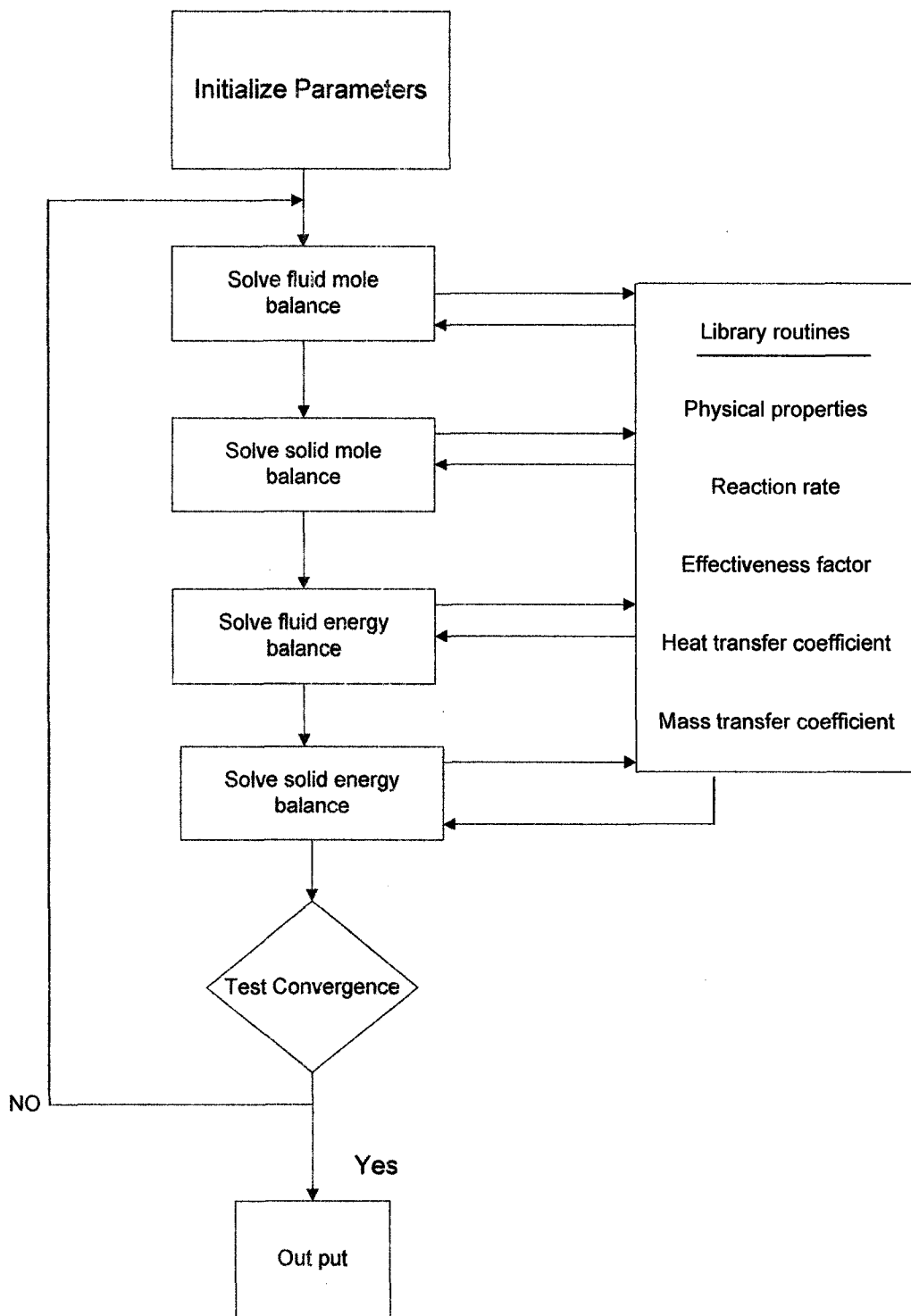


Figure 4.2 Solution scheme for 1D model

4.5 Generalized Pattern Search (GPS) Optimizer

A principal objective of this work was to find a global kinetic model for the SCR of NO_x . An additional requirement was therefore to have an efficient optimizer so that fitting of experimental data would be possible. The generalized pattern search (GPS) algorithm was selected because of its demonstrated success in fitting parameters to light-off curves. The GPS method is advantageous because it is a gradient free method that can easily be coupled to a “black-box” simulator.

The GPS searches a pre-defined parameter space in an efficient way in an effort to find a parameter set that minimizes the objective function. Typically, the objective function depends on the difference between the predicted results and the experimental results. Pattern search algorithms are designed as derivative free search method for unconstrained minimization of smooth functions [28]. These methods are useful, when the derivatives are not available or expensive to evaluate with sufficient precision [51].

In this work, the predicted results were provided by Mono1D, using either the finite element method or DVODE. The GPS solver used was available in the MATLAB optimization toolbox. A computing framework was written in MATLAB, which called the simulator and GPS optimizer, and passed the appropriate data between the two.

4.6 Testing and validation of software

The testing and validation of the solution software, including Mono1D, DVODE and the GPS algorithm was carried out using some literature data. Published work on the catalytic combustion of CO [51] in which the transient light-off was reported under a variety of conditions was used as the test data.

In [51] a set of experiments on the light-off of CO in a monolith reactor

with a Pt catalyst was reported. A GPS algorithm was used to find the best fit set of parameters in a kinetic model. In the light-off experiments, the feed temperature was increased at 50°C/min. from an initial temperature of 50 °C, while continuously monitoring the outlet concentration of CO, and hence its conversion.

The classical rate expression for the oxidation of CO used in the catalytic converter community is based on the model proposed by Voltz et. al. [53]:

$$(-r_{\text{CO}}) = \frac{A_w \exp\left(\frac{-E_w}{R_g T}\right) Y_{\text{CO}} Y_{\text{O}_2}}{\left(1 + A_A \exp\left(\frac{E_A}{R_g T}\right) Y_{\text{CO}}\right)^2} \quad \frac{\text{mol}}{\text{m}^2 \text{s}} \quad (4.23)$$

This model was used in [51], and was used at this step for validation purposes. In [51] three sets of experimental data were reported. The experiments had a space velocity of 25000 h⁻¹, and the ratio of oxygen and CO was varied, with excess, stoichiometric, and deficient oxygen for CO respectively. An additional six sets of data were available, with the same oxygen and CO concentrations but with GHSV of 50 000 h⁻¹ and 100 000 h⁻¹. In this work these additional data were also modelled. The experimental inlet gas composition (CO and O₂) is given in Table 4.1. The balance of the composition was nitrogen. In all cases the total flowrate to the reactor was the same. Changes in GHSV were made by changing the size of the reactor.

The first three results presented are a repeat of the results presented in [51]. Figures 4.3, 4.4 and 4.5 present the results for GHSV 25 000 h⁻¹. It can be seen that a reasonable match is attained between the experimental and predicted results. The optimal parameter values given by the GPS optimizer are shown Table 4.2 following all of the graphs. The results are essentially the same as reported in [51] which gives confidence in the implantation of the software

Table 4.1 – Inlet concentrations (mole %) in the feed gas and GHSV for the nine experiments used to test the optimiser.

Run	6474	6476	6478	6481	6483	6485	6488	6490	6492
% CO	0.477	0.94	1.44	0.48	0.945	1.45	0.49	0.96	1.45
% O ₂	0.535	0.528	0.576	0.565	0.532	0.578	0.536	0.536	0.564
GHSV h ⁻¹ ×10 ⁻³	25	25	25	50	50	50	100	100	100

Figures 4.6 to 4.11 show the results for the additional six experiments at higher space velocities. Again, it is observed that there is a reasonable match between experiment and prediction.

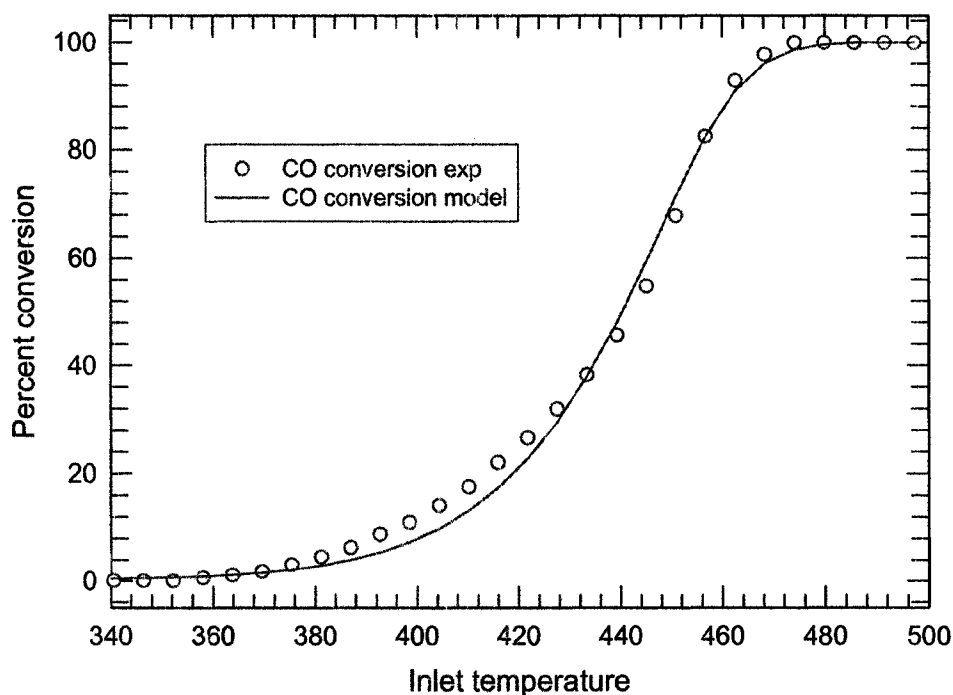


Figure 4.3 Experimental and predicted light-off curves for run 6474. GHSV 25000 h⁻¹ with excess oxygen.

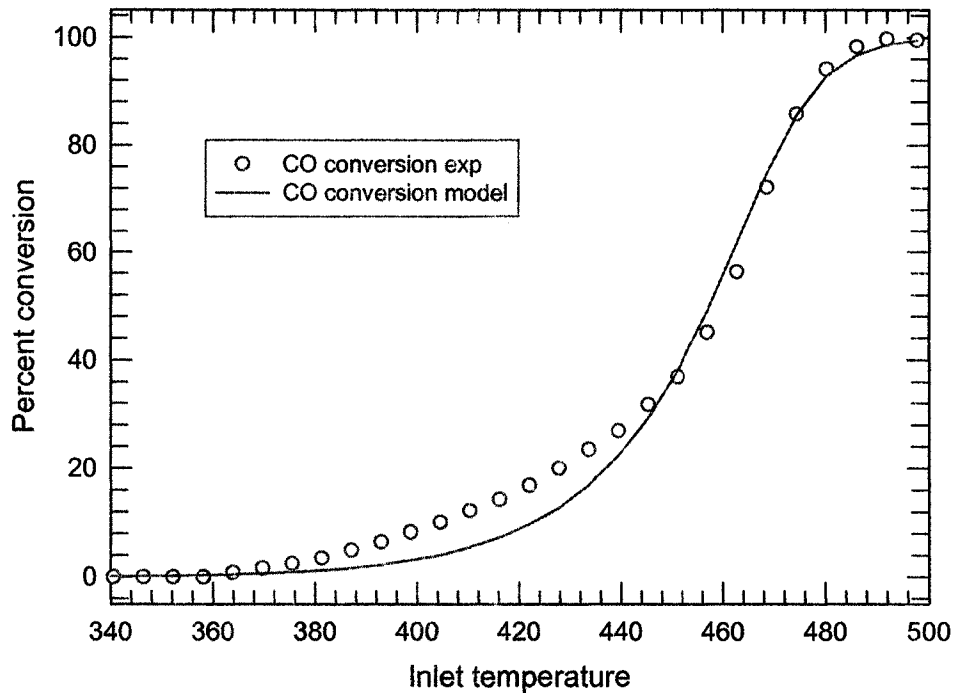


Figure 4.4 Experimental and predicted light-off curves for run 6476. GHSV 25000 h⁻¹ with stoichiometric oxygen.

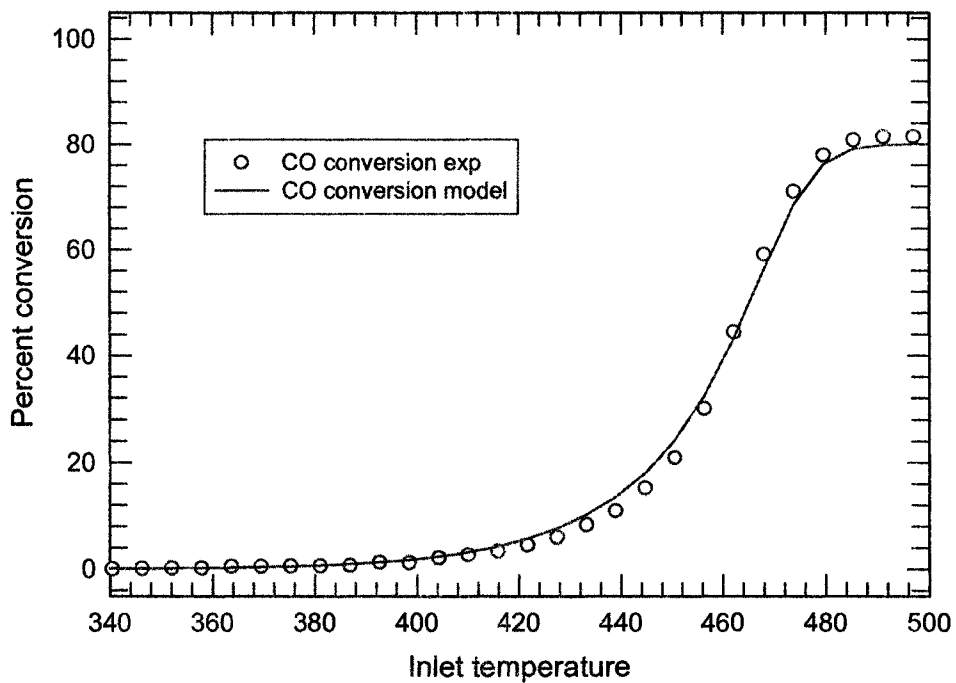


Figure 4.5 Experimental and predicted light-off curves for run 6478. GHSV 25000 h⁻¹ with excess CO.

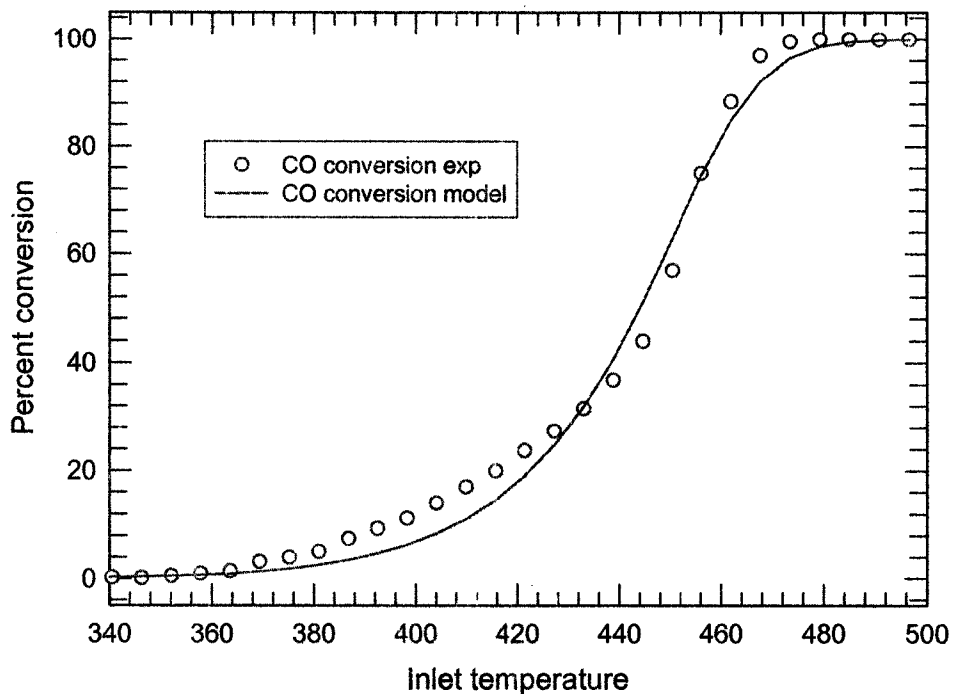


Figure 4.6 Experimental and predicted light-off curves for run 6481. GHSV 50000 h⁻¹ with excess oxygen.

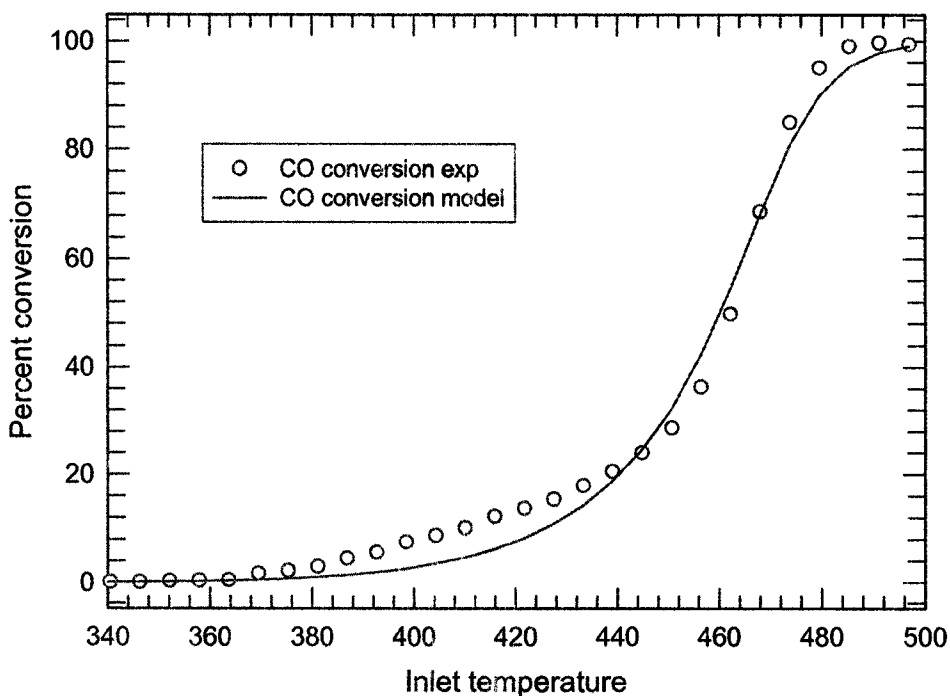


Figure 4.7 Experimental and predicted light-off curves for run 6483. GHSV 50000 h⁻¹ with stoichiometric oxygen.

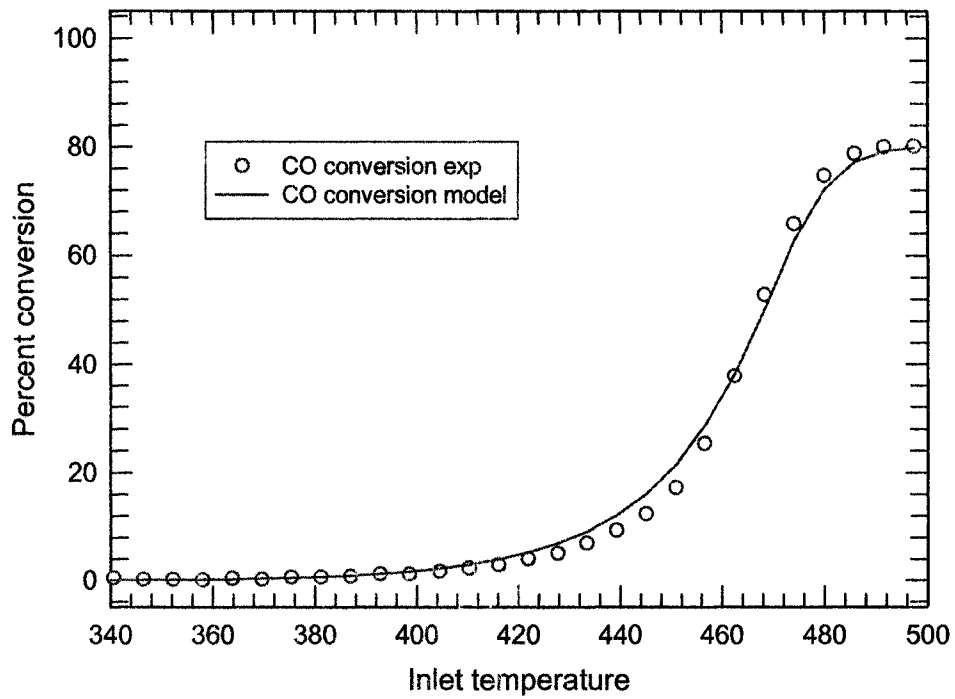


Figure 4.8 Experimental and predicted light-off curves for run 6485. GHSV 50000 h⁻¹ with excess CO.

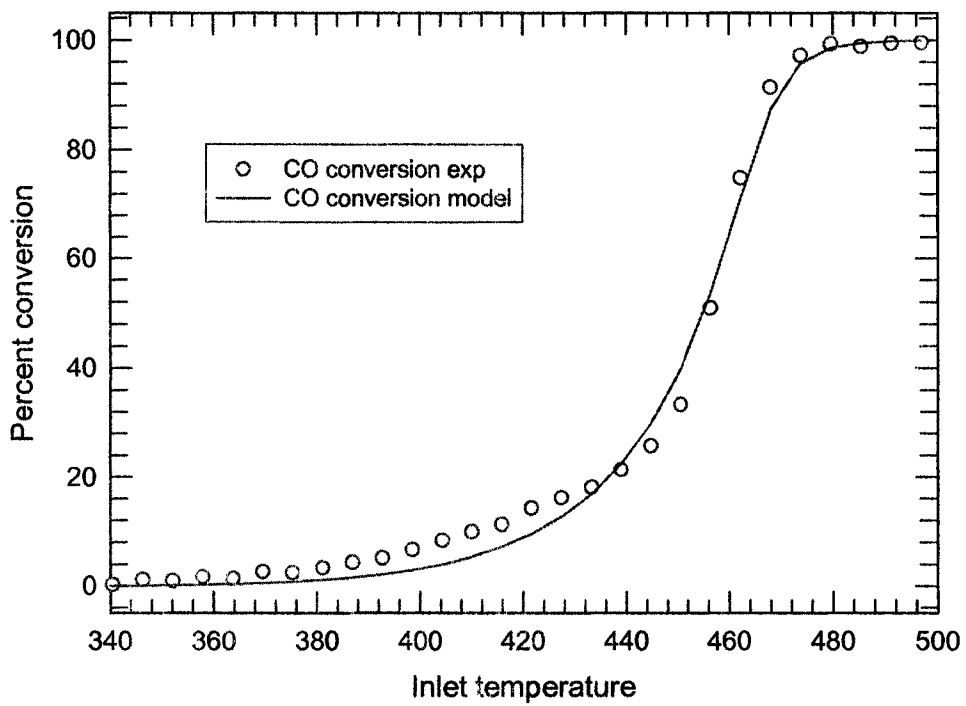


Figure 4.9 Experimental and predicted light-off curves for run 6488. GHSV 100000 h⁻¹ with excess oxygen.

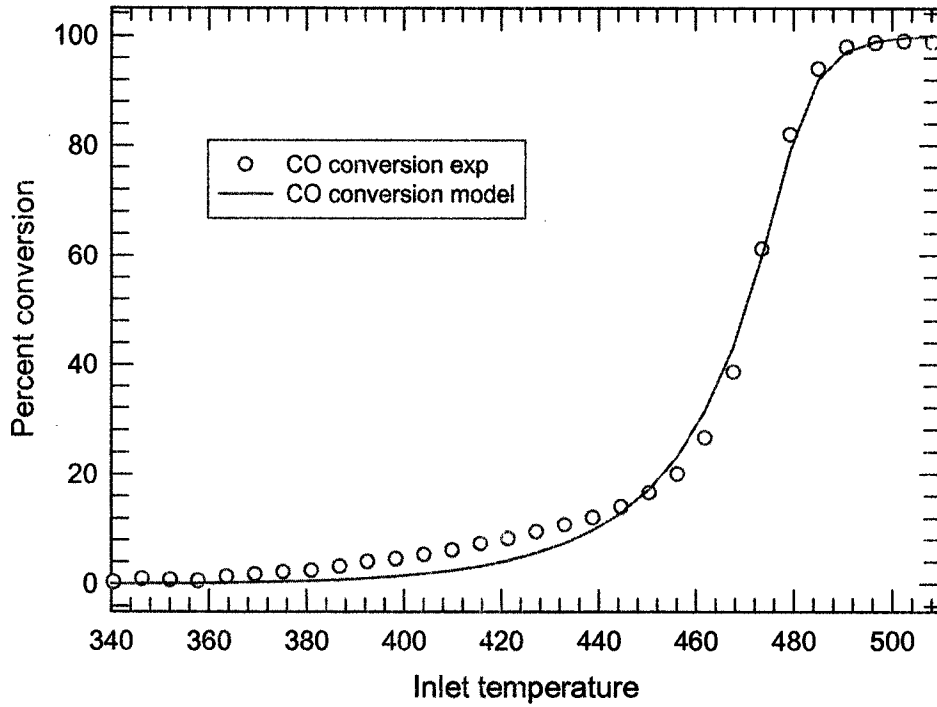


Figure 4.10 Experimental and predicted light-off curves for run 6490. GHSV 100000 h⁻¹ with stoichiometric oxygen.

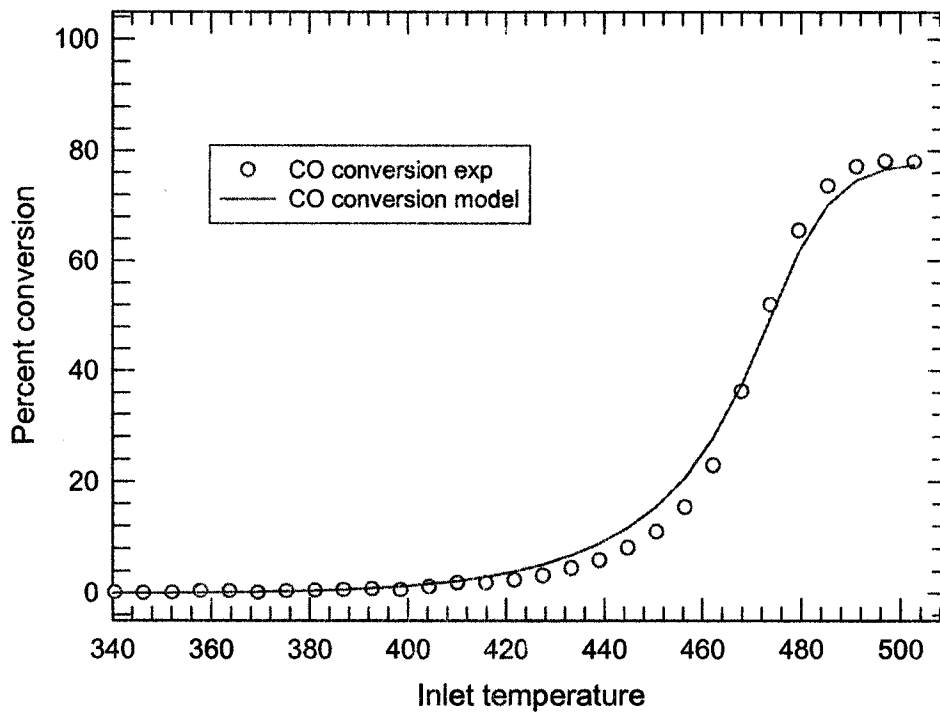


Figure 4.11 Experimental and predicted light-off curves for run 6492. GHSV 100000 h⁻¹ with excess CO.

Table 4.2 - Optimal parameters obtained for each of the CO light-off curves.

Run number	A_w	E_w	A_A	E_A
6474	9.67E+008	59667	92	997
6476	1.02E+009	59624	123	991
6478	1.95E+009	59624	160	1671
6481	9.56E+008	59561	98	1033
6483	1.22E+009	59667	131	1180
6485	1.42E+009	59667	133	1379
6488	3.54E+009	59667	214	3075
6490	4.11E+009	59667	200	3106
6492	2.26E+009	59667	157	1559

4.7 Summary

This chapter has discussed the development and validation of a single channel monolith reactor model and its coupling to the MATLAB GPS optimizer. Based on the results of the validation exercises, it was concluded that the changes implemented into the software, and its coupling to the optimizer was performed correctly. In the next chapter, the application of this software to some experimental data is described.

Chapter 5

Model Development for SCR of NO Using Hydrocarbons

This chapter describes the development of global kinetic model for the SCR of NO by hydrocarbons. Validation is performed using literature data and new experimental data.

5.1 Literature model for hydrocarbon SCR

As noted in Chapter 3, there has been much work done on SCR catalysts for hydrocarbons. For the SCR of NO_x present in the exhaust from a lean burn diesel engine, the paper by Ansell et al. [52] is a significant work. Although their work contains some flaws (as will be discussed presently), it none the less represents a good starting point for the development of a global kinetics models for the prediction of light-off performance of SCR catalysts. In the following the work is briefly summarized.

Ansell et al. [52] performed a series of steady state and transient experiments for the reaction of both synthetic exhaust gas mixtures as well as real exhaust from a diesel engine. They used a monolith supported Pt catalyst and concluded that transient experiments were required to determine the kinetics. They coupled their experiments to a single channel model of the monolith reactor to develop their kinetic models. They also used some mechanistic information as a guide in selecting the form of the model.

Engine emission data were obtained using 2.5 L TDI engine run without exhaust gas recirculation (EGR). Propene (C₃H₆) was injected into the engine exhaust pipe, upstream of the catalyst, to boost the HC/NO ratio. Extra hydrocarbon is required because the HC levels emitted from diesel engines are not high enough to effect substantial NO conversion.

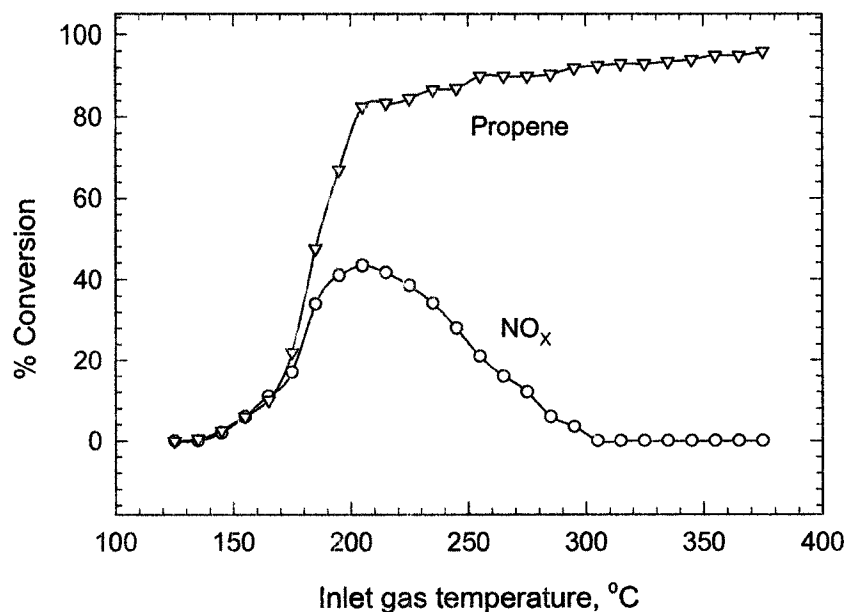
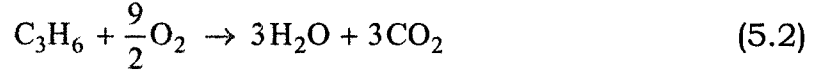
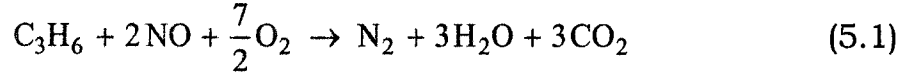


Figure 5.1 – Experimental conversion curves for propene and NO_x from Ansell [52].

The concentration of propene, CO, NO, and CO₂ were monitored. The gas hourly space velocity (GHSV) was 22 000 h⁻¹. The feed gas was heated at the rate of 5 °C/min from 120 °C to 400 °C. The experiments were repeated with different inlet gas composition, but at constant HC/NO ratio. Figure 5.1 shows a typical plot of experimental conversions of NO_x and propene.

In all of their experiments, the reactor feed was a mixture of N₂, O₂, CO, NO and C₃H₆. In some experiments (including those that used real exhaust gas), H₂O and CO₂ were also present. Because there was an excess of oxygen in the reactor feed, oxidation of both CO and hydrocarbons occurs easily. However, the reduction of NO under oxidising conditions is difficult. There is a competition between the hydrocarbon oxidation by NO and oxygen. The competing pathways for propene conversion under oxidising conditions can be represented by the following global reactions:



The lean NO application requires high catalyst selectivity towards reaction (5.1). The rate expressions that they proposed for propene and NO_x conversion are:

$$(-R_{\text{C}_3\text{H}_6}) = A_{\text{C}_3\text{H}_6} \exp\left(-\frac{E_{\text{C}_3\text{H}_6}}{R_g T}\right) \frac{C_{\text{C}_3\text{H}_6} C_{\text{O}_2}}{(1 + X C_{\text{C}_3\text{H}_6})(1 + Y C_{\text{NO}})} \quad (5.3)$$

$$(-R_{\text{NO}}) = (-R_{\text{C}_3\text{H}_6}) \frac{k_{\text{NO}}}{\left(1 + K_{\text{NO}} \exp\left(-\frac{E_{\text{O}_2}}{R_g T}\right) C_{\text{O}_2}\right)} \frac{C_{\text{NO}}}{(1 + Z C_{\text{NO}})} \quad (5.4)$$

The rate expressions were derived using LHHW principles, and assume that adsorption of propene and NO inhibit the rate. The mechanistic study as well as experimental observation strongly implied that the rate of NO reduction depends on the rate of propene oxidation. It was also observed that at higher catalyst temperatures O₂ competes with NO for catalyst sites, which favours HC oxidation. This caused a decline in NO conversion to N₂. An exponential temperature dependent term for the adsorption of O₂ was included in the denominator of Equation (5.4). This exponential temperature dependent term increases the surface coverage of O₂ at high temperature, and acts to decrease the NO conversion by HC at higher temperature. Rather, NO is oxidised to NO₂. They used the model [52] to predict the performance for different conditions and some correlation between experimental and predicted values was obtained.

Ansell [52] did not present any experimental parameter values in their publication. As a first exercise, therefore, the Ansell rate model was programmed into the Mono1d monolith reactor simulator and an effort was made to optimize a set of their experimental results. The parameter

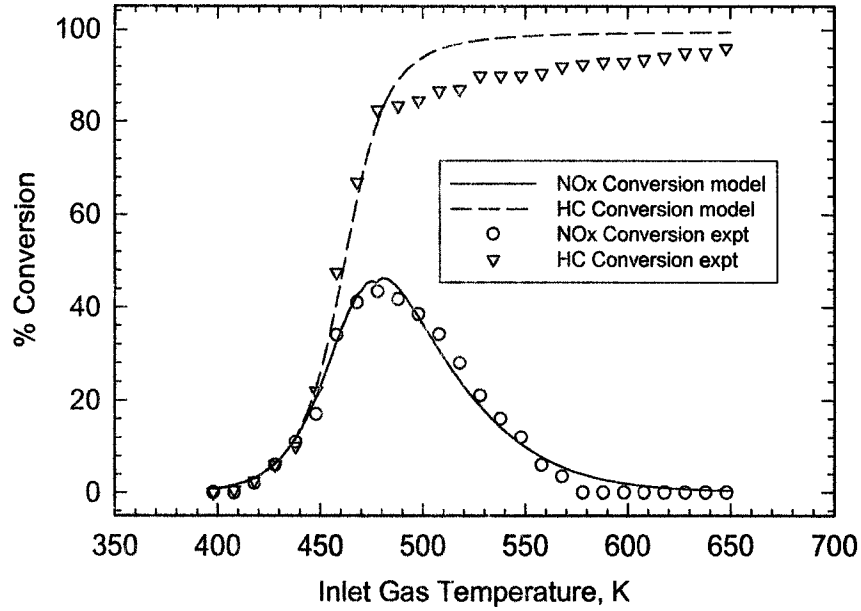


Figure 5.2 – Comparison of predicted curves to experiment for the data of Ansell [52].

optimization routine described in Chapter 4 (MATLAB GPS algorithm) was used to determine the best fit parameters in the rate expression for the reduction of NO_x. The finite element solver was used.

Figure 5.2 shows a comparison of the experimental results obtained by [52] and the model results in this investigation. Considering the likely experimental error, the model provides an acceptable fit to the data. The optimal rate expressions were:

$$(-R_{C_3H_6}) = 1.8 \times 10^{13} \exp\left(\frac{-98780}{R_g T}\right) \frac{C_{C_3H_6} C_{O_2}}{(1 + 51 C_{C_3H_6})(1 + 120 C_{NO})} \quad (5.5)$$

$$(-R_{NO}) = (-R_{C_3H_6}) \frac{1667}{\left(1 + 6.41 \times 10^{10} \exp\left(\frac{-100700}{R_g T}\right) C_{O_2}\right)} \frac{C_{NO}}{(1 + 1076 C_{NO})} \quad (5.6)$$

These results can be viewed as both providing a validation for the computational technique and the model proposed by Ansell.

5.2 Modelling of engine exhaust from a CNG engine

After performing the comparison with the literature data, an effort was made to model some data obtained using a real engine exhaust from an engine that used compressed natural gas (CNG) as a fuel. As noted earlier, CNG is proposed as a cleaner fuel alternative for diesel engines. The exhaust gas from CNG engines is relatively clean compared to diesel engine exhaust, owing to absence of particulate emission and negligible SO_2 / SO_3 . Natural gas engines usually operate in a lean combustion mode (Air to fuel ratio between 14.7 to 22) hence CO is found in trace amounts due to abundance of oxygen. CO_2 and H_2O along with CH_4 is observed in the exhaust of CNG engines. Today, the SI stoichiometric natural gas engine operation is gaining popularity compared to the lean combustion natural gas engine. This is mainly due to difficulty observed in reducing the NO in lean exhaust, containing excess oxygen. The temperature of lean CNG engine exhaust gases is relatively lower than SI engine and ranges from 150 to 900 °C.

5.2.1 Experimental results

Experimental engine emission data (courtesy of Alternative Fuel Systems, Calgary) were obtained using a turbo-charged six cylinder Navistar engine of $7.6 \times 10^{-3} \text{ m}^3$ displacement. The engine was installed in an eddy current dynamometer test bed. Engine speed was controlled using a digital dynamometer controller and the engine torque was controlled manually. The digital dynamometer controller was set in the RPM (engine speed) mode. For a desired engine operating condition, the engine was first set to the desired engine speed using the dynamometer controller, and then adjusted to give the desired engine torque manually.

The catalyst (of which the composition is unknown) was supported on a Cordierite (ceramic) monolith substrate which was cylindrical in shape, with a diameter 10.5 inch and a length of 6 inches. The monolith was

installed in the metal reactor, and was partitioned so that each half of the cylinder was a separate reactor; that is, the gas flowed down through one half of the cylinder and then returned through the other half. Figure 5.3 experimental set up illustrates the device used for the investigation. The composition of the engine exhaust was determined before and after the catalyst. The components measured were O₂, CO₂, CO, NO_x and HC.

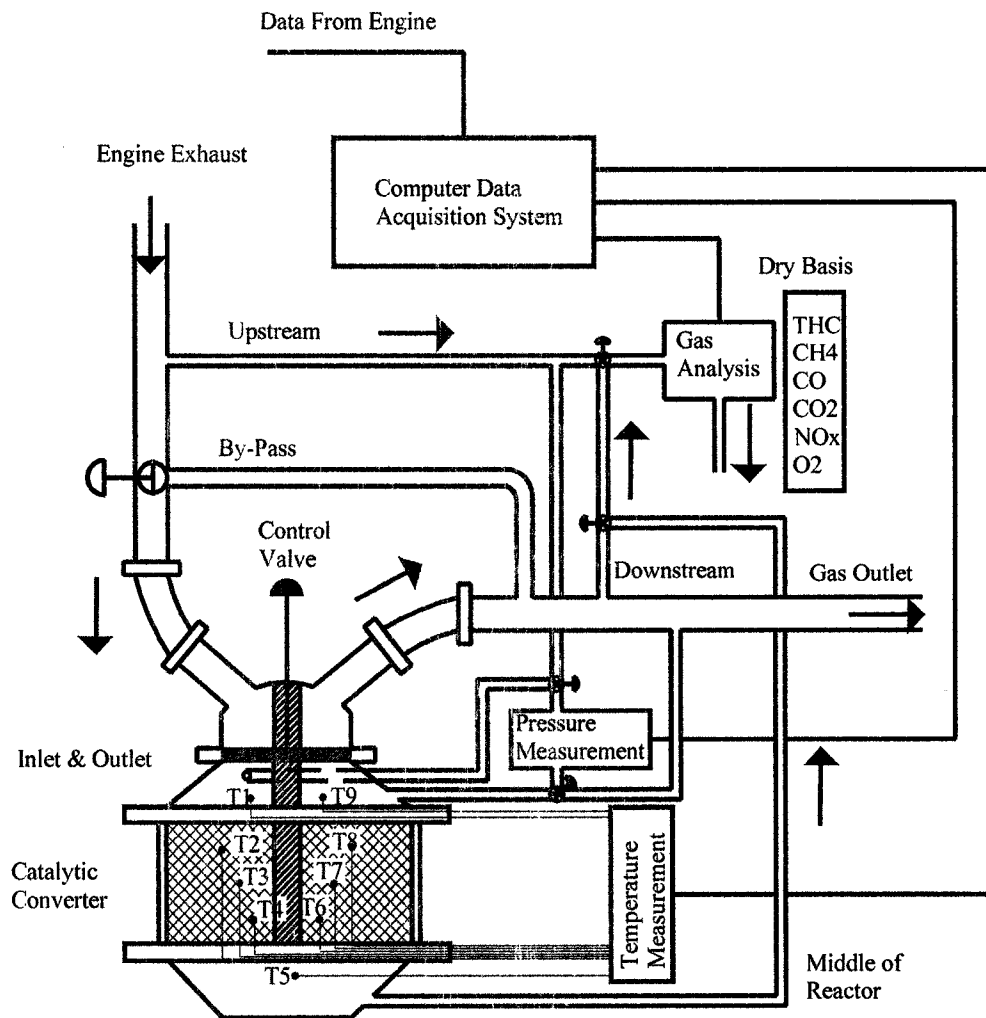


Figure 5.3 – Experimental catalytic converter system used by AFS to measure the SCR activity of their catalyst.

The fresh catalyst has a very high activity, however, it loses its activity over time, as shown in Figure 5.4. These data were obtained with HC/NO_x ratio of about 6. It took about ten hours of operation to stabilize the catalyst. The NO reduction efficiency depended on the HC/NO ratio, as shown in Figure 5.5. In this case, the engine was run at 1500 rpm and 300 Nm torque. The engine exhaust temperature was 520 °C and the composition was 1459 ppm NO_x, 426 ppm HC, 1900 ppm CO, 4.3 % oxygen and 10 % CO₂, with the balance nitrogen (measurements on a dry basis). Without propane injection, the HC/NO ratio was about 0.29 and NO reduction efficiency was about 4 %. The HC/NO ratio was raised by adding propane to the exhaust gas, which gave higher NO reduction

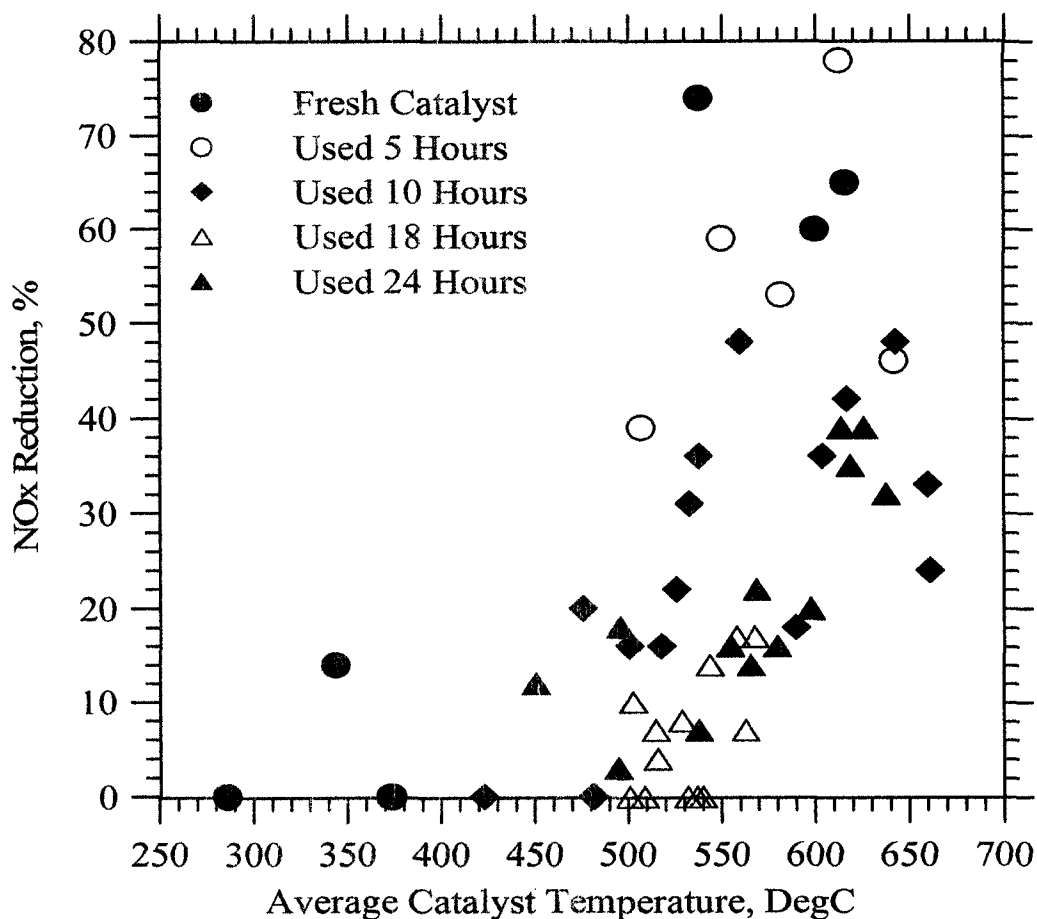


Figure 5.4 – Catalyst activity with age. The activity tends to stabilize after some time. Graph courtesy of AFS.

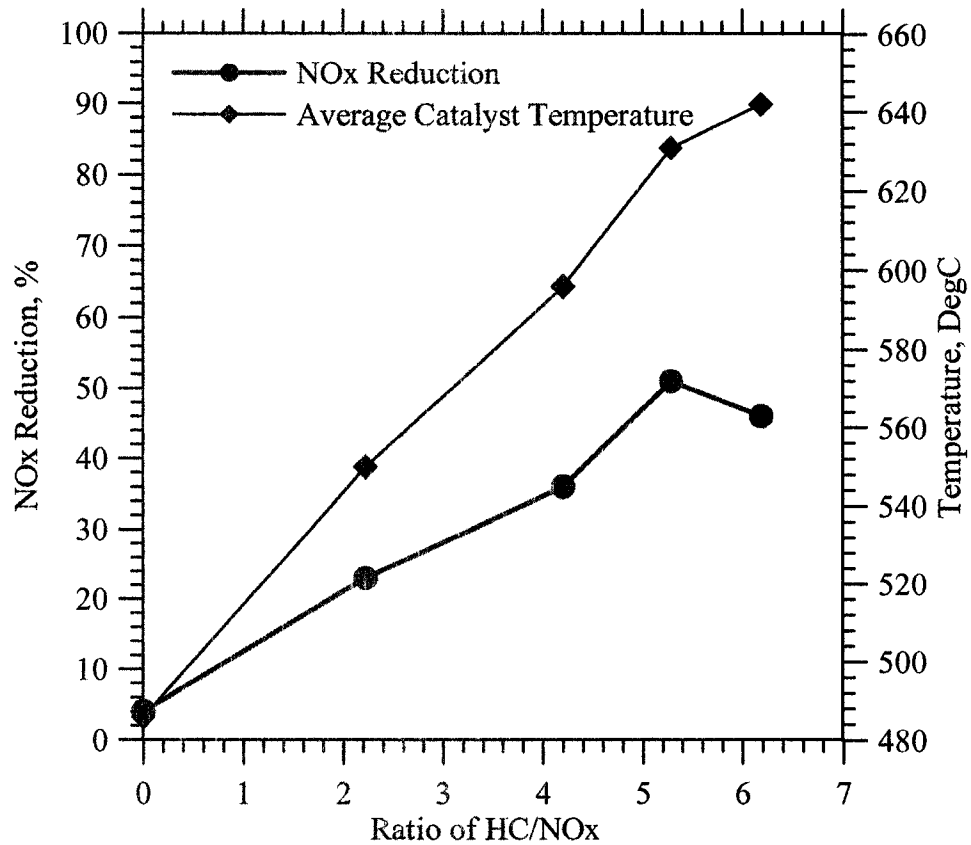


Figure 5.5 - Effect of HC/NO ratio on the NO conversion and reactor temperature. Graph courtesy of AFS.

efficiency and higher catalyst temperature. When the HC/NO ratio was raised to about 5.28, the NO_x reduction efficiency increased to 51 %. A further increase of HC/NO ratio caused the NO reduction efficiency to drop. This showed that the catalyst required a HC/NO ratio about 6 for the proper NO reduction efficiency with low fuel penalty. This result was consistent with the findings from Eranen et al. [59].

5.2.2 Modelling results

An attempt was made to model the results using the Ansell model [52], with the reaction stoichiometry and enthalpy of reaction modified to reflect the change in hydrocarbon from propene to propane. Otherwise, the modelling approach was the same as used in modelling of the data

from [52]. There were a total of 37 steady state experiments with different operating conditions of feed concentration and temperature. In the first instance, the kinetic parameters were optimised using all of these data. Preliminary results indicated that it was not possible to fit the proposed kinetic model to the data within an acceptable degree of error. Regardless of the parameters chosen, a significant fraction of the data had a large difference between prediction and experiment.

For the best result, about thirteen of the experiments were well predicted by the model. All of these experiments showed fairly high conversions of propane and NO. An optimization exercise was performed on these points alone. The comparison between the predictions and the experiments is shown in Figure 5.6, along with the 10 % error bounds. If these parameters were then used for the entire data set, the graphs shown in Figure 5.7 were obtained. It is seen that the agreement is not very good.

The reasons for the discrepancy can be related to either experimental error or a lack of suitability of the model. Discussions with the personnel responsible for the data did indicate a certain uncertainty in the data. Furthermore, some of the parameters required for the model were not known. At this point it was decided that these data were not be a reliable test for the model, and alternative experimental data were sought.

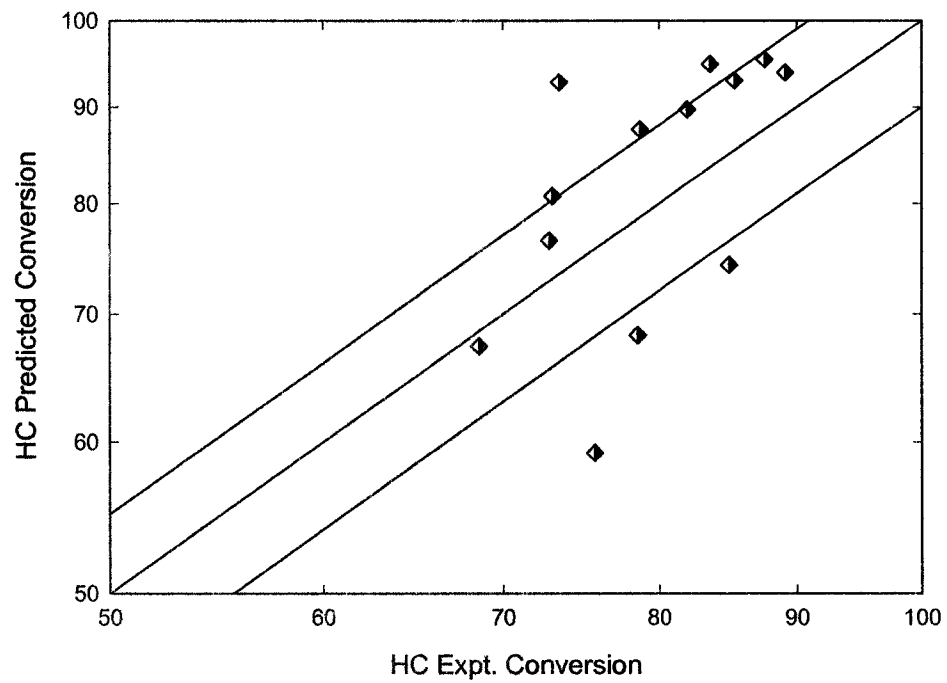
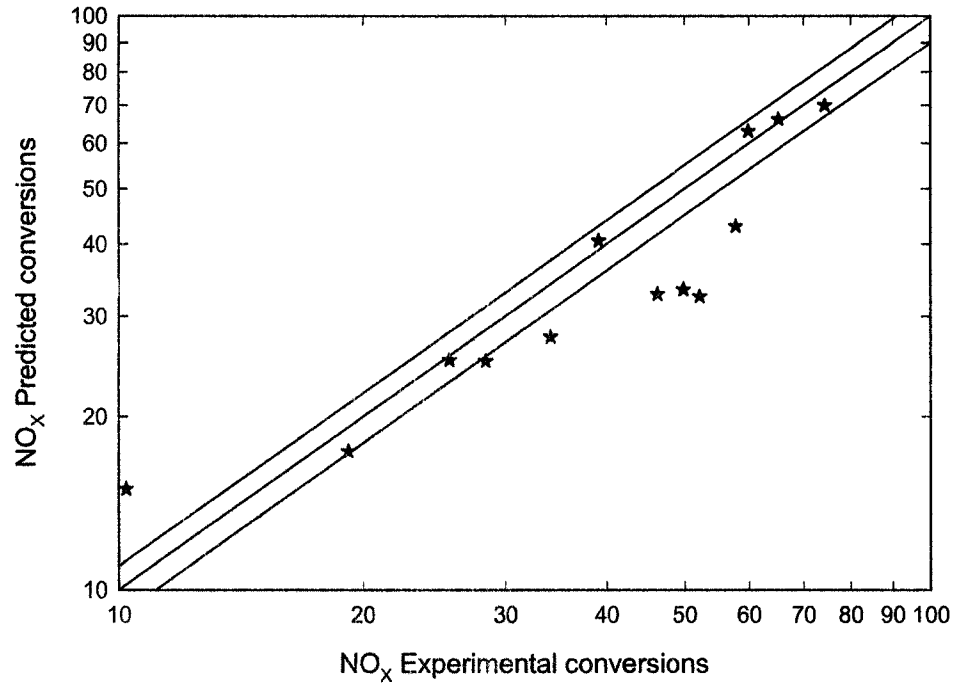


Figure 5.6 – Comparison of predicted and experimental data points for 13 experiments used in the optimisation. NO_x conversion is shown at the top and hydrocarbon conversion in the bottom.

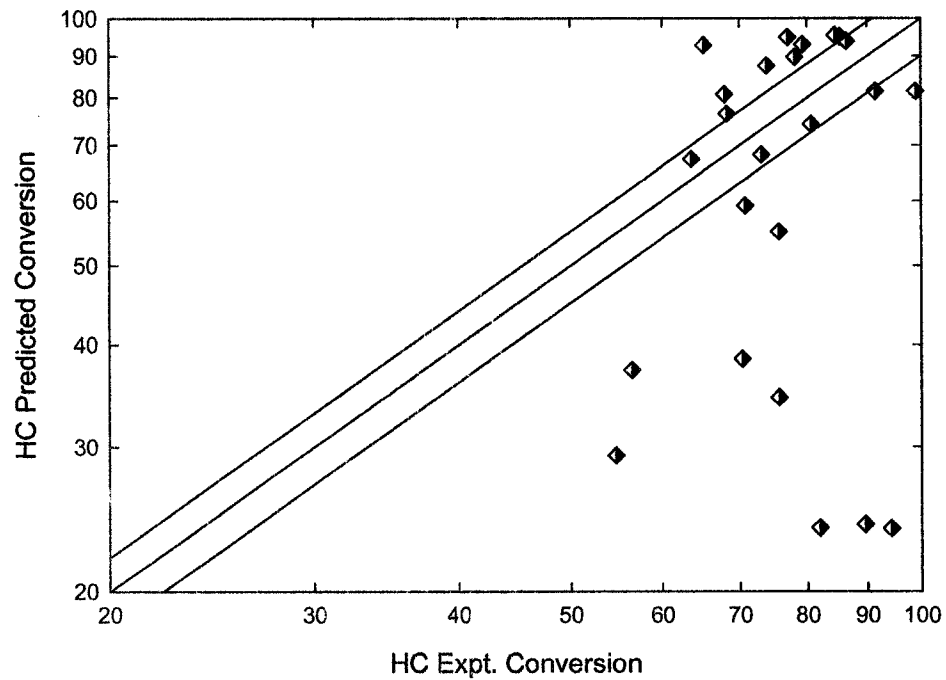
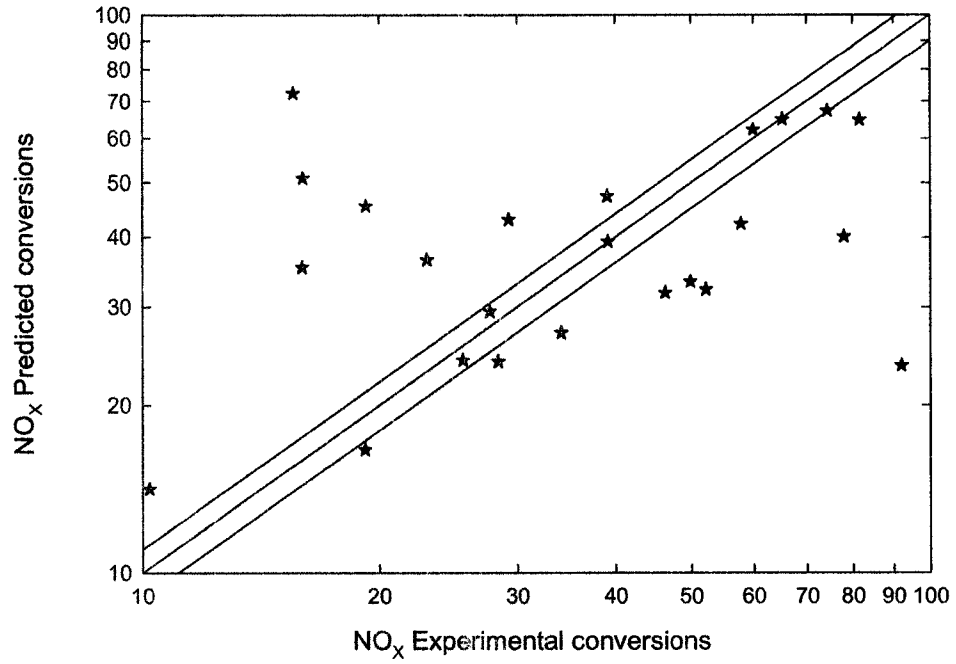


Figure 5.7 – Comparison of predicted and experimental data points for 24 experiments, with parameters from the 13 point optimization. NO_x conversion is shown at the top and hydrocarbon conversion in the bottom.

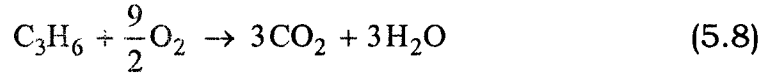
5.3 Experiments with a synthesis gas mixture

The experimental results provided by AFS proved to be unsatisfactory, as noted above. Therefore the next step was to model some data based on synthesis gas mixtures. These data were provided by Umicore AG, Hanau Germany. The data consisted of a set of light-off curves for the mixtures of CO, propene, H₂ and NO, with the balance being N₂, O₂, H₂O and CO₂. The experiments are discussed in detail shortly; however, before proceeding it is necessary to examine further the model proposed by Ansell [52].

5.3.1 Model development

It was noted earlier that the model of Ansell [52] provides a good starting point. However, there are some drawbacks to this model. For example, there is no term in this model for the oxidation of CO, in spite of the fact that they used CO in their feed. It is well known that CO will inhibit the light-off of hydrocarbons, because CO is strongly adsorbed on the surface. Clearly the model must be extended to account for this effect. CO is present in the exhaust of all IC engines that use HC as a fuel.

For oxidation catalysts in the automotive catalytic converter industry, probably the most widely used global kinetic model for oxidation is the one based on the work of Voltz et al. [53]. They studied the kinetics of carbon monoxide and propene oxidation on a platinum-alumina catalyst at 200 °C to 375 °C. They used synthetic gas mixture which represented the exhaust from an internal combustion engine. Their global kinetic models were based on LHHW principles, and included inhibition terms for CO, hydrocarbons and NO. They suggested that the rates of oxidation increases with increasing the oxygen concentration, whereas it is inhibited by increasing either CO, propene or NO. The global reactions for the oxidation of CO and propene are:



The rate of oxidation of CO expressed in terms of mole fraction, Y , is given by:

$$(-R_{\text{CO}}) = \frac{k_1 Y_{\text{CO}} Y_{\text{O}_2}}{T(1 + K_1 Y_{\text{CO}} + K_2 Y_{\text{C}_3\text{H}_6})^2 \left(1 + K_3 (Y_{\text{CO}} Y_{\text{C}_3\text{H}_6})^2\right) (1 + K_4 Y_{\text{NO}})} \quad (5.9)$$

The rate of oxidation of propene is given by:

$$(-R_{\text{C}_3\text{H}_6}) = \frac{k_2 Y_{\text{C}_3\text{H}_6} Y_{\text{O}_2}}{T(1 + K_1 Y_{\text{CO}} + K_2 Y_{\text{C}_3\text{H}_6})^2 \left(1 + K_3 (Y_{\text{CO}} Y_{\text{C}_3\text{H}_6})^2\right) (1 + K_4 Y_{\text{NO}})} \quad (5.10)$$

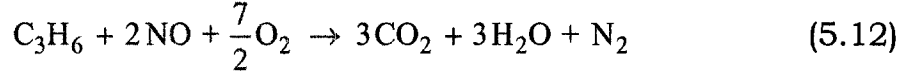
Hydrogen is present in engine exhaust gas. Models for the oxidation of H_2 are scarce because of the difficulty of measuring hydrogen concentrations. Typically, the rate of oxidation of hydrogen in the presence of CO is taken as equal to the rate of oxidation of CO, with the concentration of CO replaced by the concentration of H_2 . The reaction rate is thus:

$$(-R_{\text{H}_2}) = \frac{k_1 Y_{\text{H}_2} Y_{\text{O}_2}}{T(1 + K_1 Y_{\text{CO}} + K_2 Y_{\text{C}_3\text{H}_6})^2 \left(1 + K_3 (Y_{\text{CO}} Y_{\text{C}_3\text{H}_6})^2\right) (1 + K_4 Y_{\text{NO}})} \quad (5.11)$$

Hydrogen is very reactive over a diesel oxidation catalyst. In the absence of CO, it will oxidise at room temperature. However, in the presence of CO, it does not react until the CO starts to react. As shown by Salomons et al. [63], the CO starts to react first, then the hydrogen will suddenly convert, with the 50 % conversion point (light-off) occurring at essentially the same time as the CO. Therefore the assumption of equating the rate models and parameters appears to be a good one. Because these

oxidation models are widely used in the automotive converter industry, and have some success, these oxidation models were selected as the basis for the global kinetic models in this work.

The reduction of NO by propene is given by the overall reaction:



To model the reduction reaction, a similar equation to that used by Ansell et al. [52] was adopted. Thus the rate is:

$$(-R_{\text{NO}}) = (-R_{\text{C}_3\text{H}_6}) \frac{K_{\text{NO}}}{(1 + K_5 Y_{\text{O}_2})} \frac{Y_{\text{NO}}}{(1 + Z Y_{\text{NO}})} \quad (5.13)$$

Note that the oxidation rate for propene used in Equation (5.13) is taken from Equation (5.10). Most of the parameters are temperature dependent. Thus the constants are specified with the following nomenclature:

$$\begin{aligned} k_1 &= A_1 \exp\left(\frac{-E_1}{R_g} \left[\frac{1}{T} - \frac{1}{450}\right]\right) & k_2 &= A_2 \exp\left(\frac{-E_2}{R_g} \left[\frac{1}{T} - \frac{1}{450}\right]\right) \\ K_1 &= A_{A1} \exp\left(\frac{H_1}{R_g} \left[\frac{1}{T} - \frac{1}{450}\right]\right) & K_2 &= A_{A2} \exp\left(\frac{H_2}{R_g} \left[\frac{1}{T} - \frac{1}{450}\right]\right) \\ K_3 &= A_{A3} \exp\left(\frac{H_3}{R_g} \left[\frac{1}{T} - \frac{1}{450}\right]\right) & K_4 &= A_{A4} \exp\left(\frac{-H_4}{R_g} \left[\frac{1}{T} - \frac{1}{450}\right]\right) \\ K_5 &= A_{A5} \exp\left(\frac{-H_5}{R_g} \left[\frac{1}{T} - \frac{1}{450}\right]\right) \end{aligned}$$

The parameters K_{NO} and Z were not dependant on temperature. The global kinetic model thus developed contained 16 adjustable parameters. The reference temperature of 450 K was introduced into the Arrhenius terms to reduce the search space for the pre-exponential factor when running the optimizer.

5.3.2 Experimental methods for the synthetic exhaust data

Nine experimental results were obtained by Umicore, plus one repeat experiment. These experiments consisted of light-off curves obtained by slowly raising the feed temperature to the reactor. The reactor was 76.2 mm long, and 25.4 mm in diameter, ceramic monolith with 400 cells per square inch (CPSI) and hexagonal channels. The test data from Umicore are shown in Table 5.1. Four results were obtained with only CO, H₂ and NO in the feed. The CO concentration varied from 100 ppm to 3000 ppm, with the NO concentration constant at 150 ppm. The H₂ concentration was always one third of the CO concentration. Four results were obtained with the same conditions but with 350 ppm of propene in the feed. These eight experiments were performed at a GHSV of 50 000 h⁻¹. An additional experiment was performed at a GHSV of 25 000 h⁻¹. All runs had 10 % water, 10 % carbon dioxide, 10 % oxygen, with the balance nitrogen. There was also a repeat of Experiment 3.

Table 5.1 – Summary of inlet gas compositions for the experimental data provided by Umicore.

Run	GHSV [1/h]	CO [ppm]	H ₂ [ppm]	Propene [ppm]	NO _x [ppm]
1	50 000	100	33	350	150
2	50 000	300	100	350	150
3	50 000	1000	333	350	150
4	50 000	3000	1000	350	150
5	50 000	100	33	0	150
6	50 000	300	100	0	150
7	50 000	1000	333	0	150
8	50 000	3000	1000	0	150
9	25 000	1000	333	350	150

5.3.3 Simulation results for the synthetic exhaust data

The modelling approach for this work was carried out in the same manner as previously, using the tanks-in-series model with the solver based on the DVODE software. This model was found to give faster execution times for the simulations, especially where higher temperatures were used. The objective was to determine if the proposed model was suitable for the data provided. To be useful, a single set of parameters should be able to fit all of the data within the experimental error of the system. We note that there are 16 adjustable parameters, and that in the first instance only a vague idea of the parameter range is known. The optimal strategy appeared to be to start with the experiments in which hydrocarbons were not present, and attempt to fix the parameters for the CO oxidation. Because all of the CO oxidation experiments contained NO, the inhibition term of NO was retained. Thus, for experiments 5 to 8 the appropriate rate equation reduces to:

$$(-R_{\text{CO}}) = \frac{k_1 Y_{\text{CO}} Y_{\text{O}_2}}{T(1 + K_1 Y_{\text{CO}})^2 (1 + K_4 Y_{\text{NO}})} \quad (5.14)$$

The optimizer was run for each of experiments 5 to 8, attempting to optimize the fit for each curve. The optimiser was also run with an attempt to optimise all four curves simultaneously using a single set of parameters. One statistical problem with these data is that there were no experiments run without NO present. It is therefore not possible to optimise for the value of K_4 when each CO light-off experiment was treated separately. When all CO curve were simultaneously optimised, the influence of K_4 is felt through an additional temperature dependence.

Many optimisation runs were performed, using both the GPS optimiser and manual tuning. These runs were done to investigate the range of parameters that had to be explored. Although the expected range of some of the parameters are known reasonably well, others are not. For

example, experience has shown that the activation energy for the oxidation of CO could be expected to be in the range from around 60 000 to 100 000 J/(mol K). The first result shown is for the final best set of parameters obtained for the CO alone runs when all curves were optimised simultaneously. The results are shown in Figure 5.8.

The parameter values obtained for the simultaneous optimisation were:

$$k_1 = 1.55 \times 10^{11} \exp\left(\frac{-66\,306}{R_g} \left[\frac{1}{T} - \frac{1}{450}\right]\right) \quad \frac{\text{mol}}{\text{m}^3\text{s}} \quad (5.15)$$

$$K_1 = 2.46 \times 10^4 \exp\left(\frac{7777}{R_g} \left[\frac{1}{T} - \frac{1}{450}\right]\right) \quad \text{dimensionless} \quad (5.16)$$

$$K_4 = 2.45 \times 10^4 \exp\left(\frac{-42\,120}{R_g} \left[\frac{1}{T} - \frac{1}{450}\right]\right) \quad \text{dimensionless} \quad (5.17)$$

Figure 5.9 shows the best fit curves when each experiment was optimised individually. In this case, the parameter A_{A4} and H_4 were held constant at the values found previously. The best fit parameters for the four curves are given in Table 5.2.

Table 5.2 – Best fit parameters for the CO light-off curves represented by experiments 5 to 8. The plots are shown in Figure 5.9

Run	A_1 $\frac{\text{mol}}{\text{m}^3\text{s}}$	E_1 $\frac{\text{J}}{\text{mol}}$	A_{A1}	H_1 $\frac{\text{J}}{\text{mol}}$
5	1.979×10^{11}	72635	13637	10703
6	4.933×10^{10}	95150	5110	11259
7	1.937×10^{11}	76859	26210	9647
8	1.880×10^{11}	84671	26062	10405

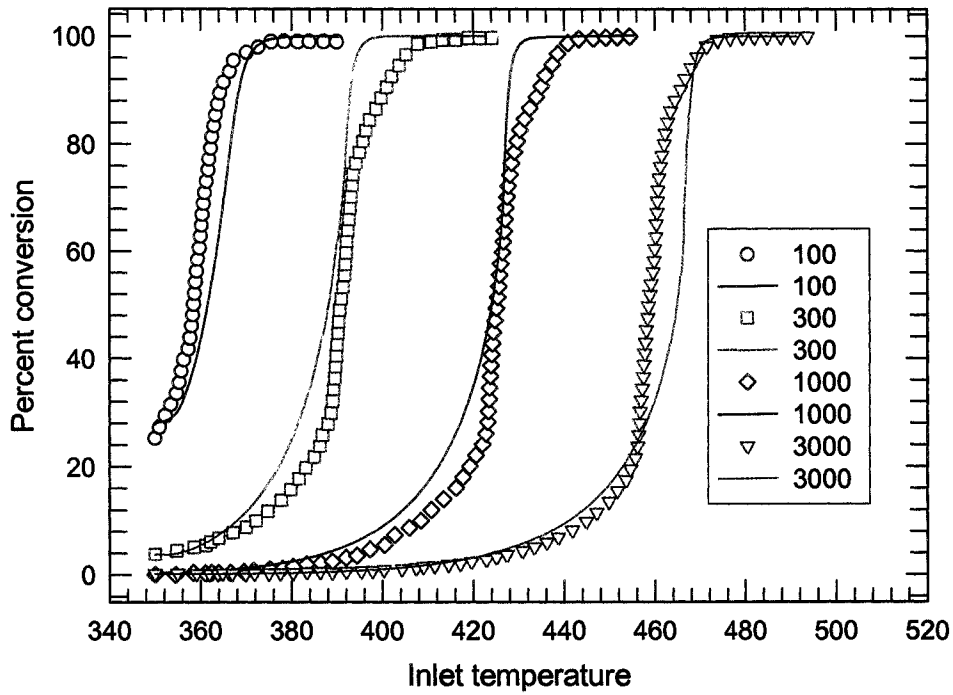


Figure 5.8 – Comparison of the simulation and experimental results obtained when all four of the CO light-off curves were optimised simultaneously.

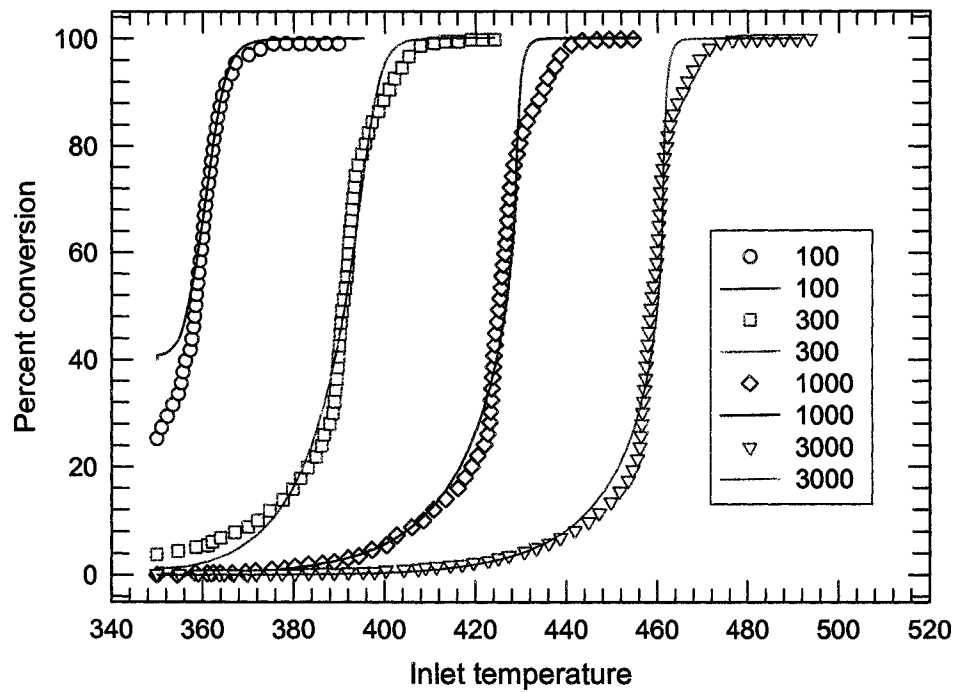


Figure 5.9 – Comparison of the simulation and experimental results obtained when all four of the CO light-off curves were optimised individually.

The model appears to give a reasonable representation of the light-off curves, and the agreement over a broad range of concentration is encouraging. Typically, reports on the use of the Voltz model report results over narrow concentration range only. Experience with the experimental apparatus used in this investigation suggests that the fits are within the range of experimental error. This aspect should be explored by performing repeat runs at each set of conditions. Unfortunately these data were not available. Furthermore, it was not possible to differentiate separately the effects of NO concentration on the CO oxidation. It is suggested that in a future investigation runs with and without NO be performed, and at different levels of NO concentration.

The next modelling attempt was addressed at Experiments 1 – 4. Variable concentrations of CO were used at fixed concentrations of propene and NO. In the first instance, the optimiser was run on each experiment using a fairly broad range of parameters. All 16 parameters were allowed to vary. A certain amount of trial and error was required to be certain that the proposed parameter range was correct. Figure 5.10 to 5.13 show the comparison of the prediction to the experiments for experiments 1 to 4. The parameter values are given in Table 5.3.

Figures 5.10 to 5.13 show that the form of the model is able to provide a reasonable agreement with the experiments. There is, however, a wide variation in the values of the parameters. The next step was to take the optimal values of the parameters found in the CO and NO curves (experiments 5 to 8), and fix these values in the optimiser. These parameters were A_1 , E_1 , A_{A1} , H_1 , A_{A4} and H_4 . The optimiser was re-run allowing variation in the remaining parameters. The fit between the experiment and model was not as good (which is expected). There was variation among the ten remaining parameters. However, it was observed that some of the parameters did not have a large effect on the solution, provide that they were of the right order of magnitude. These parameters

were fixed, and then the remaining parameters were allowed to vary whilst simultaneously optimising all of the curves. The fixed parameters were A_{45} , H_5 , K_{NO} , Z , and E_2 . The results are shown in Figures 5.14 to 5.17. The parameters are also given in Table 5.3. Note that some values are rounded.

Table 5.3 – Best fit parameter values for runs 1 to 4. The parameter values that fit best each run when optimised individually, and the values that gave the overall best fit when all curves were optimised simultaneously, are given.

Parameter	Run 1	Run 2	Run 3	Run 4	All runs
A_1	1.02×10^{10}	2.98×10^{10}	8.0×10^9	1.9×10^{11}	1.55×10^{11}
E_1	62354	94559	62300	69263	66306
A_2	5.04×10^8	1.293×10^8	8.04×10^8	4.95×10^9	2.0×10^9
E_2	84925	117287	84920	119492	85000
A_{A1}	3044	9674	3044	26725	24622
H_1	664	526	664	7158	7777
A_{A2}	8368	7262	8368	15523	20000
H_2	236	215	236	417	18500
A_{A3}	1.22×10^5	2122	1219	2031	2.0×10^{11}
H_3	9428	8072	9428	8010	18500
A_{A4}	2231	22550	2231	27730	24511
H_4	25842	48168	25842	24463	42120
A_{A5}	0.2624	0.4951	0.262	0.4991	0.2624
H_5	85282	81376	85282	76794	85000
K_{NO}	9948	14476	9948	12852	10 000
Z	14000	25914	19128	26879	20 000

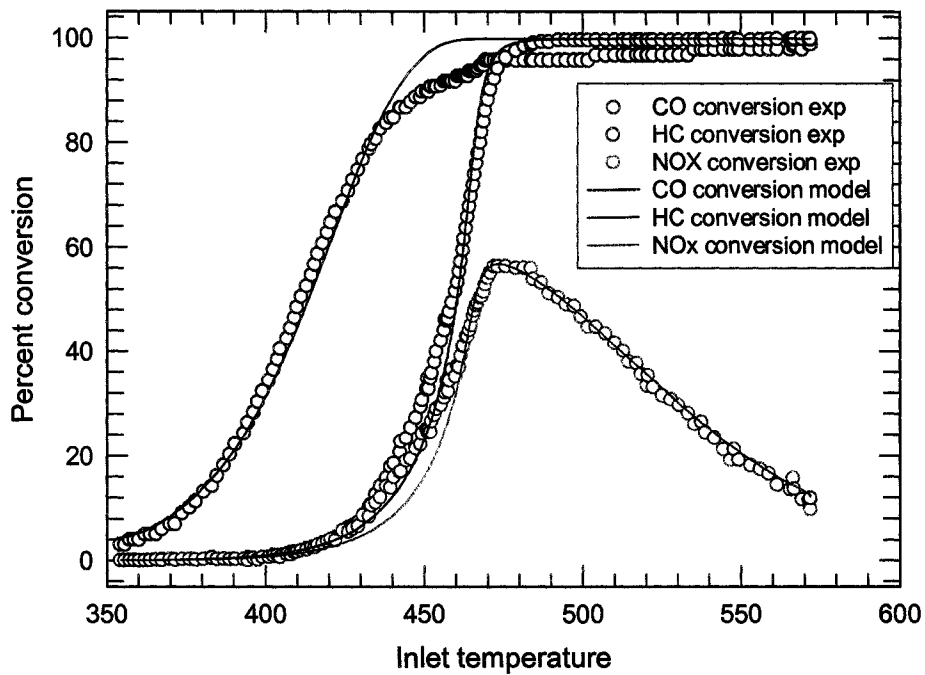


Figure 5.10 – Simulated and experimental conversions for inlet concentrations of 100 ppm CO, 350 ppm propene and 150 ppm NO. GHSV 50 000 h⁻¹.

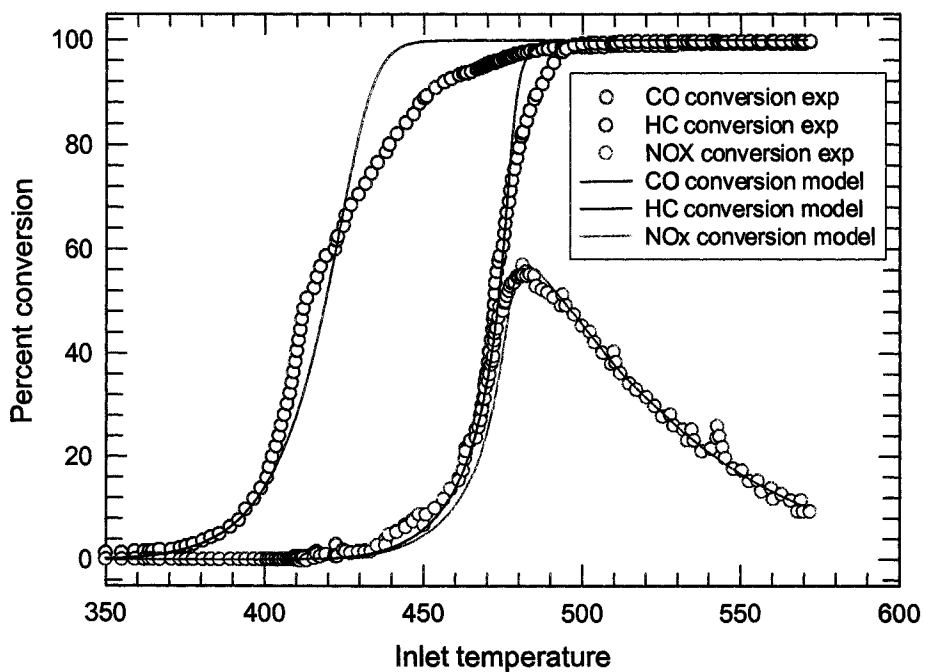


Figure 5.11 – Simulated and experimental conversions for inlet concentrations of 300 ppm CO, 350 ppm propene and 150 ppm NO. GHSV 50 000 h⁻¹.

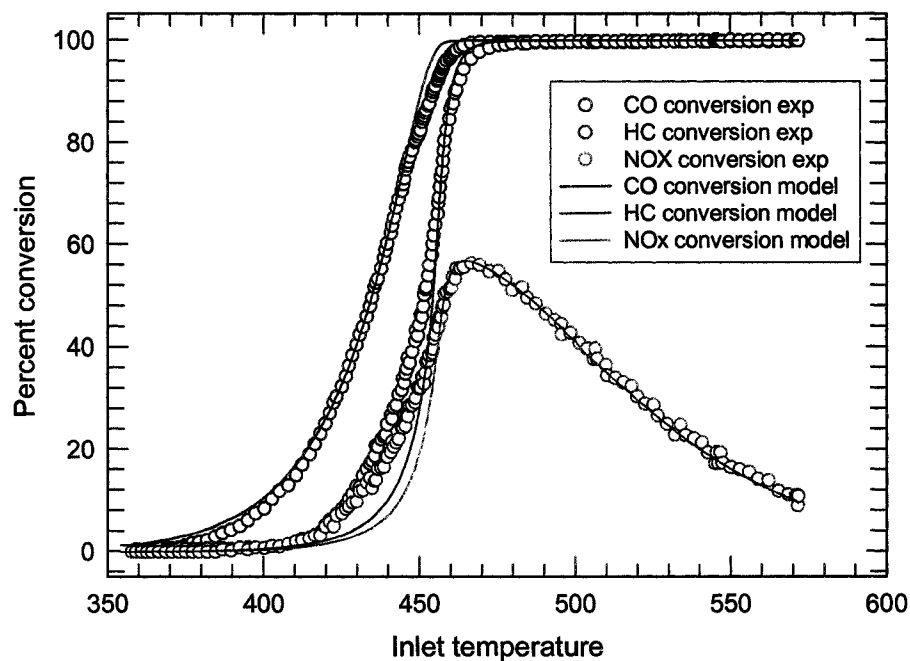


Figure 5.12 – Simulated and experimental conversions for inlet concentrations of 1000 ppm CO, 350 ppm propene and 150 ppm NO. GHSV 50 000 h⁻¹.

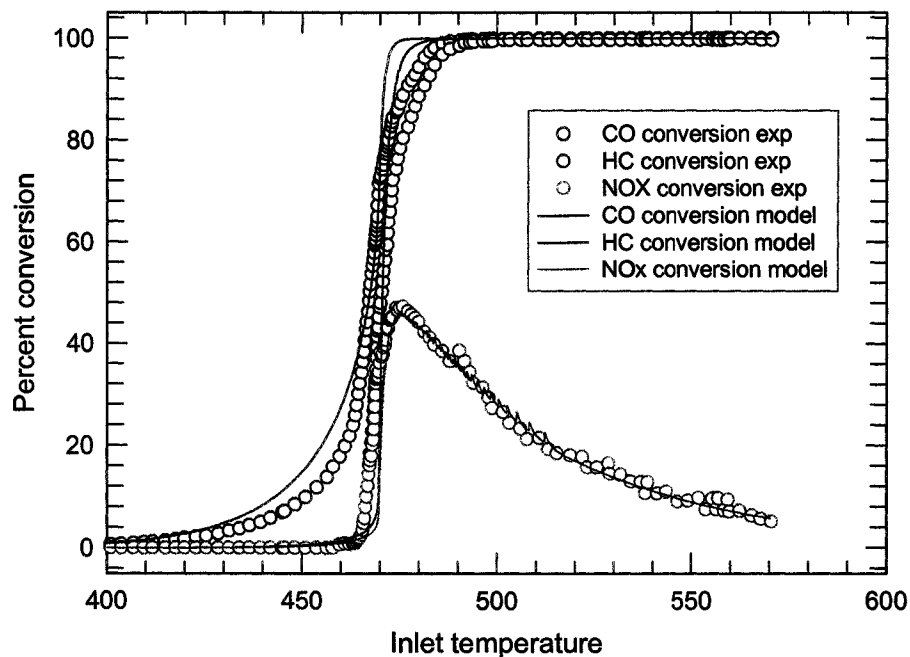


Figure 5.13 – Simulated and experimental conversions for inlet concentrations of 3000 ppm CO, 350 ppm propene and 150 ppm NO. GHSV 50 000 h⁻¹.

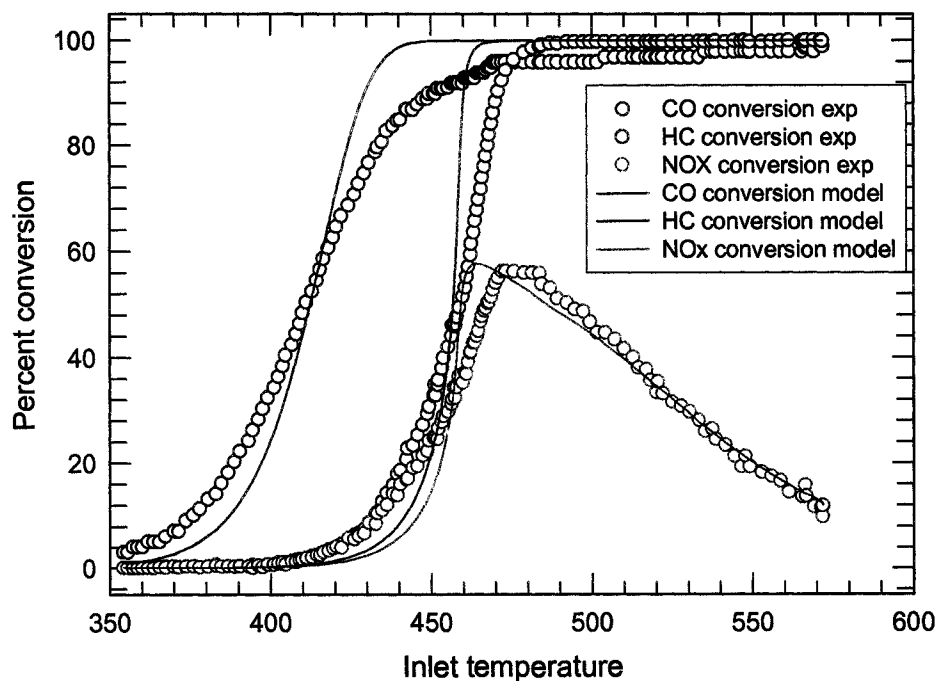


Figure 5.14 – Simulated and experimental conversions for inlet concentrations of 100 ppm CO, 350 ppm propene and 150 ppm NO. Common parameters. GHSV 50 000 h⁻¹.

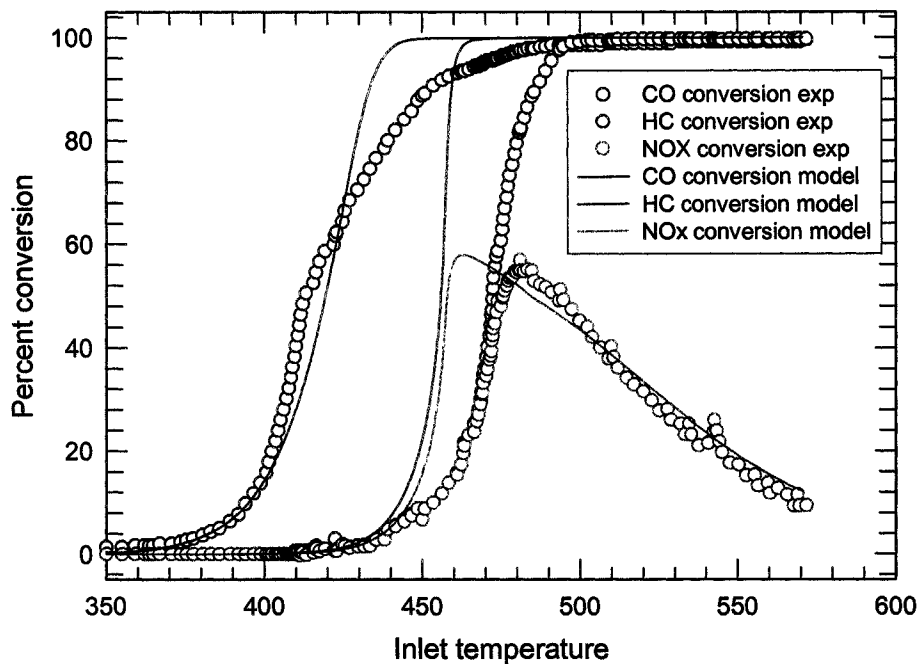


Figure 5.15 – Simulated and experimental conversions for inlet concentrations of 300 ppm CO, 350 ppm propene and 150 ppm NO. Common parameters. GHSV 50 000 h⁻¹.

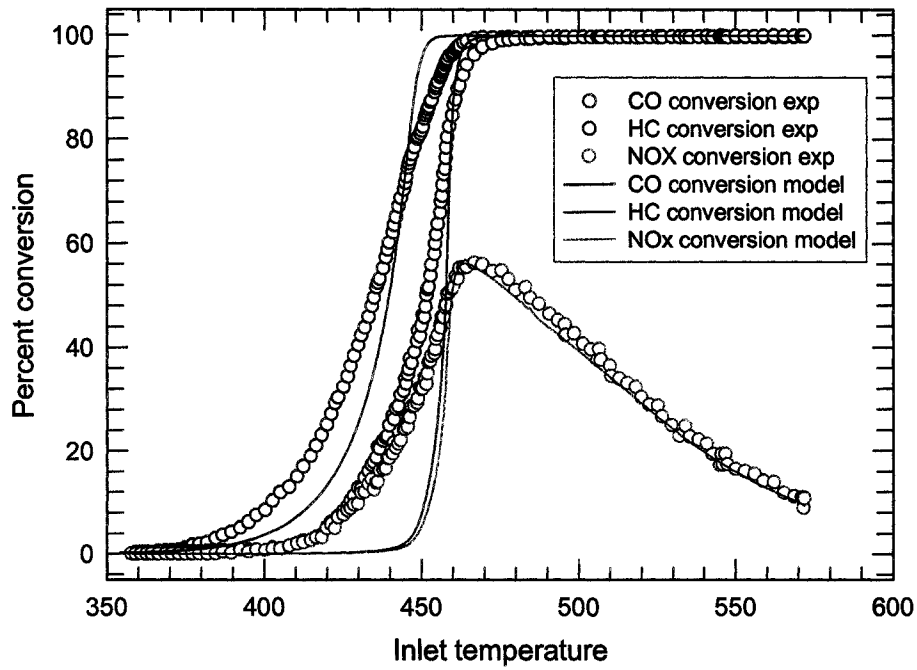


Figure 5.16 – Simulated and experimental conversions for inlet concentrations of 1000 ppm CO, 350 ppm propene and 150 ppm NO. Common parameters. GHSV 50 000 h⁻¹.

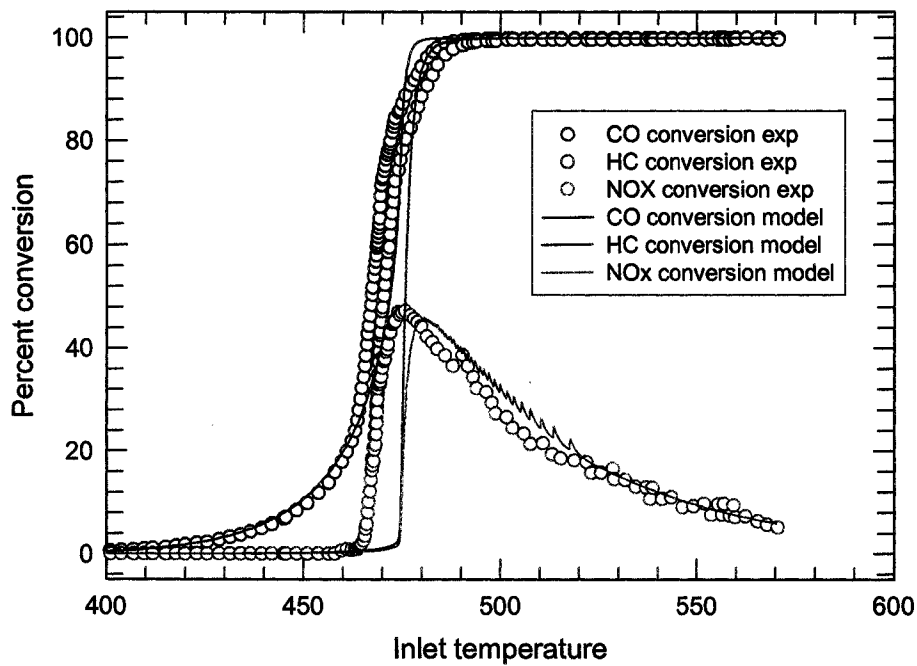


Figure 5.17 – Simulated and experimental conversions for inlet concentrations of 3000 ppm CO, 350 ppm propene and 150 ppm NO. Common parameters. GHSV 50 000 h⁻¹.

It can be observed that generally the model is able to reproduce the experiments well when all parameters are allowed to vary. This is probably not a good test of the model, owing to the large number of parameters. However, it does show that at least mathematically the form of the model is acceptable. When a common set of parameters was used, the fits were not as good, which is expected. Generally speaking, the position of the CO light-off is well captured, but the propene and NO curves tend to be delayed. The exception is experiment 2 (300 ppm CO) where these curves rise early. However, the experimental result from experiment 2 is a bit suspect. At this low CO concentration, the CO has essentially all reacted before the propene ignites, and therefore one would expect the experimental light-off would occur at around 450 K, as in Experiment 1. However, it occurs even later than in experiment 3, which is inconsistent.

The next set of results shown uses the parameters found by the optimizer to simulate two additional experiments. The first is experiment 9, which had the same inlet gas composition as Experiment 3, but at a GHSV of 25 000 h⁻¹. Both the common set of parameters was used and the optimal parameters found in experiment 3. The graphs are shown in Figures 5.18 and 5.19 respectively. It is seen that with the common parameters, the CO oxidation is captured well, but the conversion of propene and NO is delayed. When the parameters from Experiment 3 were used, the reverse was observed, That is, the propene and NO conversions were well predicted, but the CO light-off was early.

The final result shows the simulation of a repeat of Experiment 3 using the best fit parameters from Experiment 3 (Figure 5.20) and the common parameter set (Figure 5.21). The fit is fairly reasonable. This experiment gives an idea of the reproducibility of the experiments.

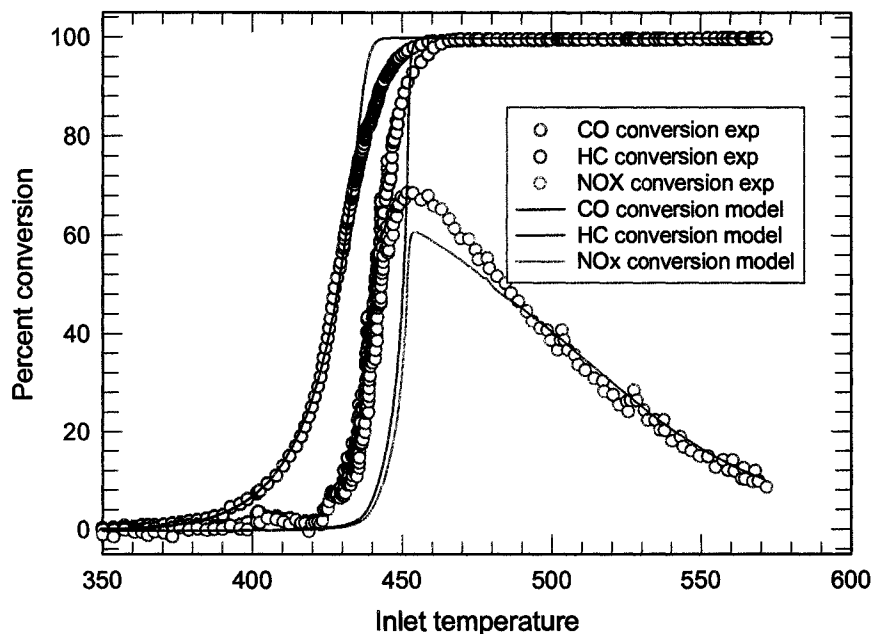


Figure 5.18 – Simulated and experimental conversions for inlet concentrations of 1000 ppm CO, 350 ppm propene and 150 ppm NO. Common parameters. GHSV 25 000 h⁻¹.

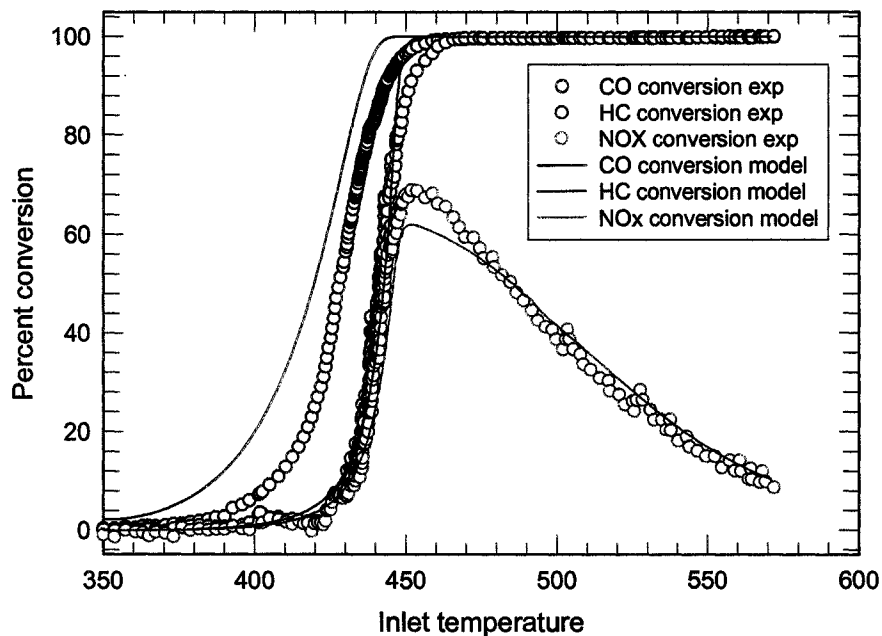


Figure 5.19 – Simulated and experimental conversions for inlet concentrations of 1000 ppm CO, 350 ppm propene and 150 ppm NO. Parameters from experiment 3. GHSV 25 000 h⁻¹.

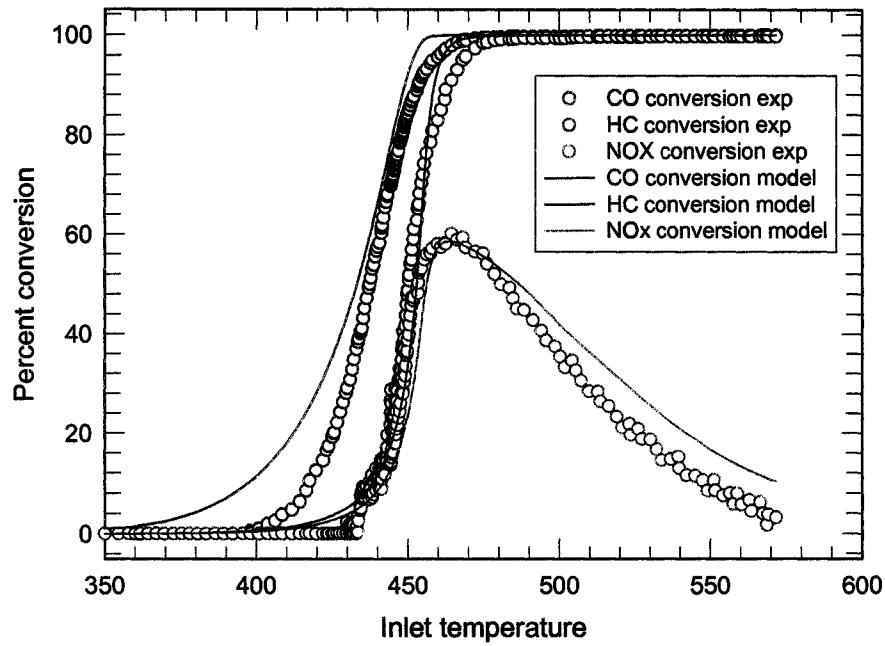


Figure 5.20 – Simulated and experimental conversions for inlet concentrations of 1000 ppm CO, 350 ppm propene and 150 ppm NO. Parameters from experiment 3. GHSV 50 000 h⁻¹.

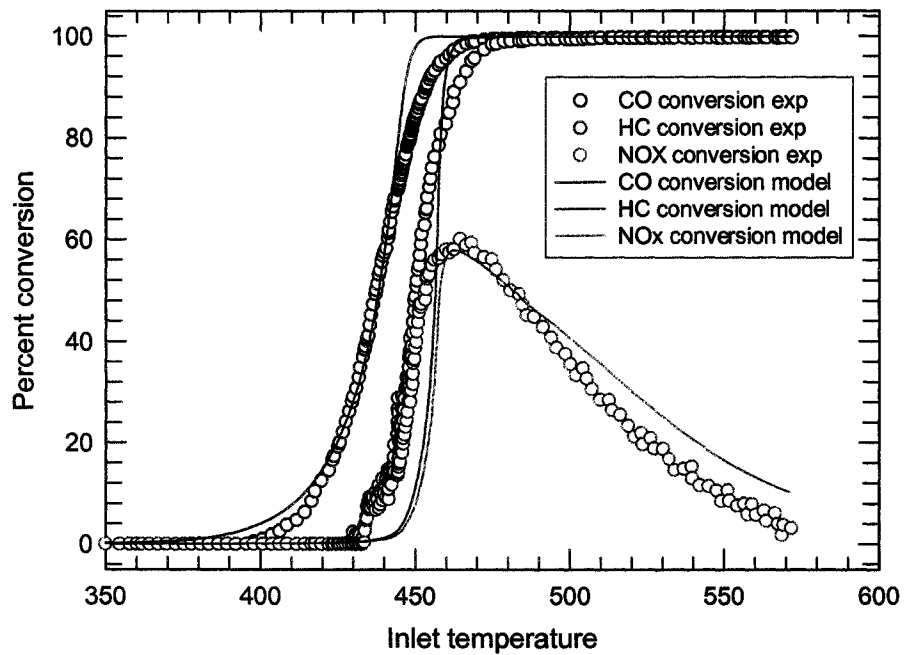


Figure 5.21 – Simulated and experimental conversions for inlet concentrations of 1000 ppm CO, 350 ppm propene and 150 ppm NO. Common parameters. GHSV 50 000 h⁻¹.

5.4 Summary

One of the key objectives of this modelling exercise was to develop a kinetic model which will describe the oxidation of CO, HC and selective catalytic reduction of NO in real engine exhaust in the lean atmosphere. Based on the simulation results of the experiments by Umicore AG, it would appear that a global kinetic model of the proposed form, combining elements of Voltz and Ansell models, offers promise. The proposed model should probably be tested over a broader range of experimental conditions. It would be a good idea, for example, to have a broader range of concentrations of hydrocarbon and NO. It is not necessary to have an extremely broad range, but the range should cover that of interest for the lean combustion engine.

Chapter 6

Testing of NO_x Absorber Catalyst on CNG Engine

The NO_x absorber catalyst is designed to enable the reduction of NO_x from the exhaust of a lean burn engine. The engine is normally run in the lean mode, and the NO_x produced is stored in the catalyst. The converter is then periodically regenerated by the injection of hydrocarbon into the exhaust, either from a separate supply or by temporarily running the engine in the rich mode to produce HC in the exhaust. In this chapter, a series of experiments with a NO_x absorber catalyst placed in the exhaust of a compressed natural gas (CNG) engine is described. The intention was to gain some preliminary information on the performance of these catalysts on a CNG engine. Engine performance was measured using four parameters: exhaust temperature, NO_x emission, HC emission and mass flow of air and fuel needed at various crank angles with wide open throttle at three different engine speeds (900, 1100, and 1250 RPM). The performance of the catalyst was monitored under steady state (saturated catalyst) conditions, and with hydrogen injected upstream of the catalyst. Hydrogen is considered the most reactive species for catalyst regeneration.

The experimental system is described in Section 6.1. Experimental strategy is discussed in Section 6.2. The engine performance with the graphs is presented in Section 6.3. The catalyst performance is described in Section 6.4.

6.1 Experimental system and procedure

(a) Engine

The engine was a Waukesha CFR, which is a single cylinder, four stroke, water cooled, spark ignition fuel research engine. Table 6.1 gives the engine specifications. Figure 6.1 shows a schematic of the system, and Table 6.2 gives the component names for the items shown in Figure 6.1.

(b) Intake system

The intake system was designed to incorporate the accurate and continuous measurement of air mass flow rate, fuel mass flow rate and the equivalence ratio. On the upstream side of the air intake a filter was installed to eliminate air borne contaminants. A pulsation barrel was installed in the air line to avoid air flow fluctuations. A 12.7 mm butterfly valve was incorporated in the air supply line as an intake throttling device. Mass flow meters were installed to measure the mass flow rate of air and fuel. The equivalence ratio measurement was programmed into the Labview software using these mass flow rates.

Table 6.1 : CNG lean burn test engine specifications

Displacement (cc)	612
Bore (mm)	82.6
Stroke(mm)	114.3
Compression ratio	11.5
Combustion chamber	Disc cylinder head, flat top piston
Intake valve (mm)	31.8
Exhaust valve (mm)	31.8
Crank Angles	
Maximum Brake Torque	340 °
Advance combustion	333 °
Retarded combustion	350 °
RPM selected for tests	900, 1100, 1250
Combustion	Lean with equivalence ratio : 1.2 to 1.3

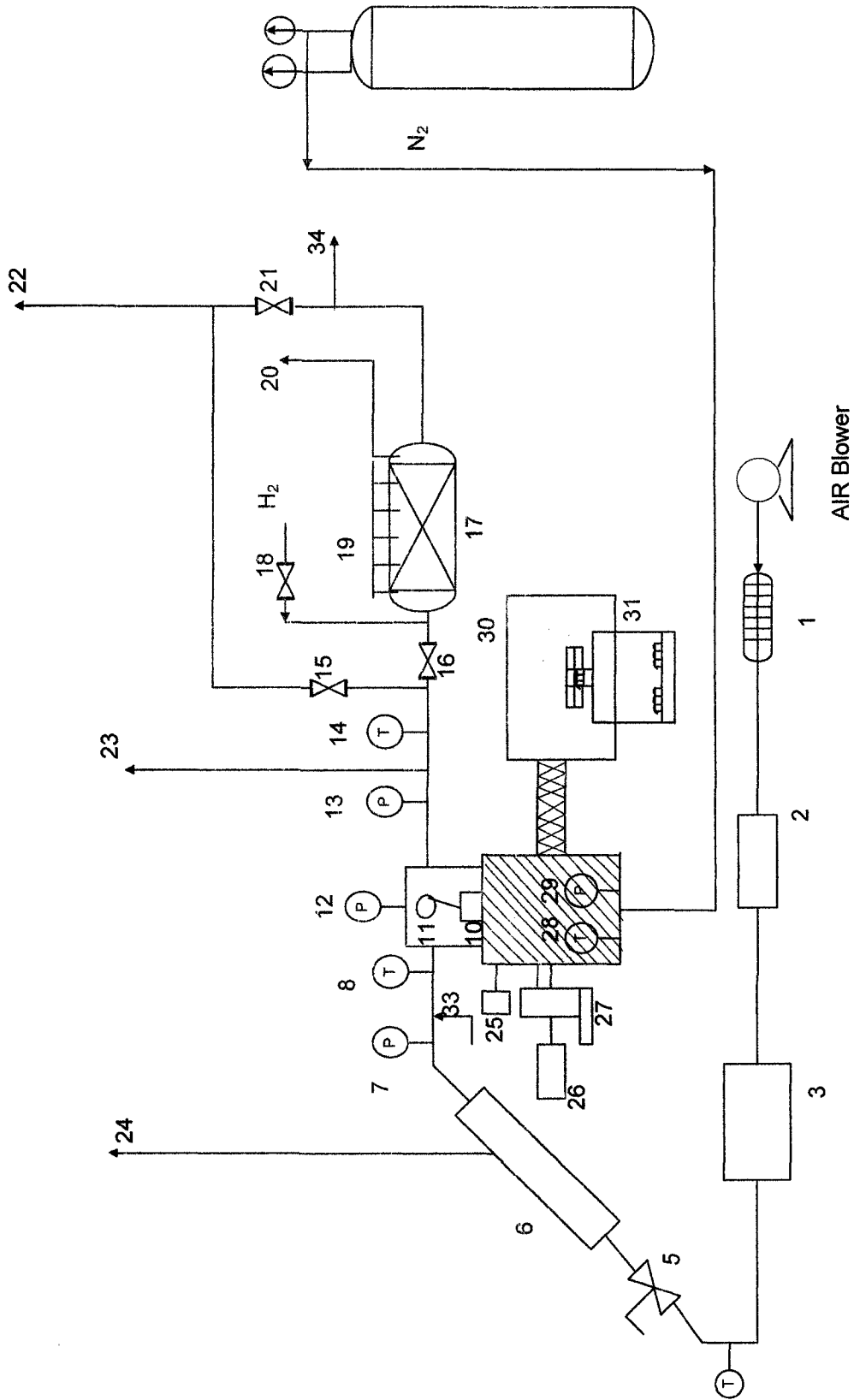


Figure 6.1 Engine schematic arrangement (Refer to table 6.2 for item description)

Table 6.2 Engine System Schematic Label Descriptions

Label	Description
1	Intake air filter
2	Intake air mass flow meter
3	Intake pulsation barrel
4	Intake air thermocouple
5	Intake throttle valve
6	Intake plenum
7	Intake pressure transducer
8	Intake mixture thermocouple
9	Engine
10	Ignition Coil
11	Spark Plug
12	Cylinder pressure transducer
13	Exhaust pressure transducer
14	Exhaust thermocouple
15	Catalytic converter bypass valve (Gate valve)
16	Catalytic converter isolation valve (Gate valve)
17	Catalytic converter
18	Hydrogen Injection
19	Thermocouples for catalytic reactor temperature
20	Thermocouple connection to the data acquisition System
21	Catalytic converter isolation valve (Gate valve)
22	Exhaust to atmosphere
23	Exhaust gas sample to analyzer
24	Intake air for A/F ratio measurement
25	Camshaft hall effect sensor
26	Crank shaft rotary encoder
27	Variable reluctance crank shaft sensor
28	Oil sump thermocouple
29	Oil pressure gauge
30	DC motor dynamometer
31	Dynamometer force transducer
32	N2 for crank case purging
33	Fuel (CNG) injection
34	Downstream of catalytic converter gas sample to analyzer

(c) Fuelling and H₂ injection system

Figure 6.2 and Table 6.3 give the details of the CNG supply and H₂ injection system. The fuelling system was designed to allow computer control and measurement of the CNG flow to the engine as well as injected hydrogen gas flow to the catalytic reactor respectively. Both H₂ and CNG were taken from pressurized cylinders. Industrial grade H₂ was obtained from Praxair while the natural gas cylinder was filled from high pressure domestic natural gas supply. The pressure of both H₂ and natural gas were regulated using pressure regulators mounted on cylinders, prior to use. To prevent unintended flow, each gas was routed through normally closed solenoid shut-off valves. Prior to engine operation the entire fuel system was purged with N₂ to maintain oxygen levels below the flammability limits for natural gas.

Table 6.3 Fuelling and H₂ injection system schematic label descriptions

Label	Description
1	H ₂ Cylinder
2	Two stage H ₂ pressure regulator
3	H ₂ Solenoid Shut-off valve
4	H ₂ Pressure gauge
5	H ₂ Thermocouple
6	H ₂ Thermal mass flow meter
7	H ₂ Plenum
8	H ₂ Ball shut off valve
9	H ₂ Injection to reactor
10	Natural gas fuel tank
11	Natural gas pressure regulator
12	Natural gas solenoid shut off valve
13	Natural gas pressure gauge
14	Natural gas thermocouple
15	Natural gas thermal mass flow meter
16	Natural gas plenum
17	Natural gas ball shut off valve
18	Natural gas to engine

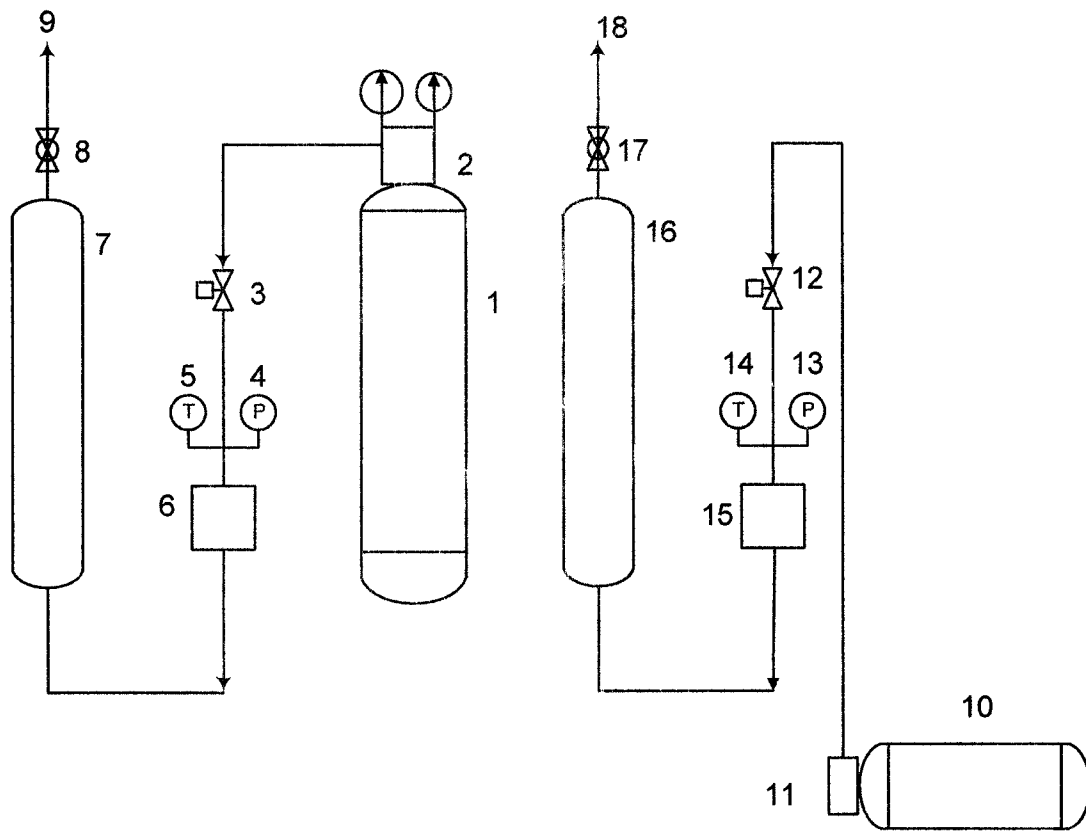


Figure 6.2 Engine fuelling and Hydrogen injection system
See Table 6.3 for number description

(d) Torque measurement

The power output of the engine was absorbed by an eddy current dynamometer. To measure the brake torque of the engine, an Eaton model 3168 load cell [60] was used to measure the force generated at a measured distance from the centreline of the dynamometer. However torque was measured only for Maximum Brake Torque (MBT) spark timing, which represents the crank angle of 340° .

(e) Emissions measurement before and after catalytic reactor

The gas analysis system was designed to determine gas composition based on samples of exhaust gas taken at the upstream and downstream of the reactor. There was a selector switch provided to switch between upstream and down stream gas sample. Gas samples were routed to the emissions analyzer via 6 mm stainless steel and Teflon tubing. To desiccate the samples prior to reaching the emission analyzers, they were routed through spiral tube exchangers filled with cold water which is an arrangement to avoid bubbling. Any condensed water was captured in glass beakers. A diaphragm type vacuum pump was used to transport the gas samples to the gas analyzers. A chemiluminescent detector (CLD) [60] was used to measure the concentration of NO_x ($\text{NO} + \text{NO}_2$) in the gas samples. Total hydrocarbon (THC) emissions were measured with a flame ionization detector (FID). Both CO and CO_2 concentrations in the gas samples were measured using a non-dispersive infra red (NDIR) analyzer. NO_x , THC and CO were measured in ppmv, CO_2 and O_2 were measured in vol % or mol %. Prior to start of experiments the gas analyzers were calibrated using mixtures of bottled calibration gases. H_2 injection rate was measured using a hydrogen gas mass flow meter.

(f) Temperature measurement

Engine exhaust temperature was measured using resistance temperature detector (RTD) in the gas exhaust pipe just after the engine. Nine thermocouples were inserted at various locations in the NO_x absorber reactor, which were in turn directly connected to the computer through the data acquisition system. The temperature and gas composition readings were recorded in the computer lab view output at the interval of 3 seconds. One cycle of 3 minutes consisted of around 100 readings.

(g) Labview data acquisition system

The data acquisition system consisted of two separate sub-systems: a Labview system which was used to record data and a MTS CAS which was used to measure engine cylinder pressure data. Both Lab view and MTS CAS systems were interfaced to a computer for display and storage of the experimental result. Table 6.4 shows a summary for a typical engine exhaust measurement.

Table 6.4 Engine performance, NO and THC

Torque, Nm	Speed, rpm	Spark Timing MBT	NO conc., ppm	THC, ppm
5.00	900	340	636	1962
4.80	1100	340	817	1700
4.70	1250	340	938	2169
	Speed, rpm	Spark Timing ADVC	NO conc., ppm	THC, ppm
	900	333	702	1775
	1100	333	1200	1657
	1250	333	1757	2058
	Speed, rpm	Spark Timing RTDC	NO conc., ppm	THC, ppm
	900	350	132	1954
	1100	350	176	1607
	1250	350	232	1743

(h) Engine start up procedure

At the start of the engine run the barometric pressure was measured with a mercury barometer and used to update the Labview and MTS CAS programs. The humidity of the air within the engine lab was also measured and recorded using a wet sling psychrometer at the beginning of each experiment cycle. This was updated in the Labview program because humidity affects properties of the intake mixture. The calibration bottle gases were supplied to each of the emissions analyzers and analyzers were then allowed to warm up for one hour before doing the calibration. Another 30 min warm up was needed for FID analyzers [60]. After the instruments are warmed up, the CFR engine was run with eddy current dynamometer. Fuel gas supply is started to the engine. The exhaust fan and air intake blower started simultaneously. The natural gas fuel injector pulse width set to an approximate value and spark timing is adjusted to get the CFR engine to run. Once running the eddy current dynamometer was set to absorb power from the engine and control the engine speed to the desired value. The fuel air ratio was set to lean ($\lambda = 1.2$ to 1.3)

(i) Catalytic reactor

The NO_x absorber catalyst was supplied by Umicore AG. A 1.5 inch diameter core six inches long was cut from a full size unit. The catalyst was a commercial catalyst normally used for diesel engines. The catalyst used a standard 400 CPSI ceramic monolith support with catalyst washcoat. The cell shape was square. The reactor was placed in a steel housing, which was flanged at each end for easy attachment into the exhaust system. A bypass valve allowed the exhaust to flow around the catalyst if desired. Reactor temperature was also monitored continuously using five thermocouples inserted into the channels.

6.2 Experimentation strategy for NO_x absorber catalyst and engine performance

The experimental strategy was designed to achieve two objectives. The first was to determine the emission characteristics of the engine for CNG lean combustion at different RPM and varied spark timings. The second was to evaluate the performance of the catalyst using hydrogen as a reductant.

The engine was allowed to run at wide open throttle continuously for around 30 minutes. The equivalence ratio set to favour the lean combustion of CNG within the engine. NO_x, THC, CO and CO₂ as well as exhaust gas temperatures were measured at points upstream and downstream of the catalytic reactor. The NO_x absorber catalyst was allowed to absorb the NO_x. H₂ was injected after certain amount of time at a rate of between 1.0 to 2.0 mg/sec (Approximately 3000 to 6000 ppmw basis) to generate a rich atmosphere needed for regeneration of the catalyst. The same experiments were repeated for three different spark timings (340, 333, and 350 °) and three different speeds (900, 1100, and 1250 rpm). The same experiments were also repeated with idle running of engine i.e. with throttle open 1/4th. It was decided to measure engine performance with respect to exhaust temperatures, NO emissions, THC emissions, and mass flow rate of intake mixture.(air + fuel) at different RPM.

6.3 Engine performance in SI lean combustion using CNG

Figures 6.3 to 6.6 show the engine performance at 900, 1100 and 1250 RPM for crank angle of 340 333 and 350 degrees. The maximum brake torque (MBT) conditions are indicated by 340° crank angle, whereas 350° represents ignition before the TDC and 333° represents ignition after the TDC. The same sets of plot were repeated with the engine torque

measurement, but were done only for the crank angle of 340 ° (MBT condition). These results are shown in Figures 6.7 to 6.10. The following observations were made. In Figures 6.5 and 6.9 the lowest THC emissions from engine were observed at 1100 rpm. In Figure 6.3 the lowest average exhaust temperatures from the engine was observed at a crank angle of 333°, which was around 400 to 420 °C, whereas the highest average exhaust gas temperature of 500 °C is observed at 1100 rpm and 350° crank angle. It was interesting to note the drop in exhaust temperature at 1250 rpm and the same crank angle of 350°. Another interesting fact was also observed from the plots in Figure 6.5 and 6.9, which are rpm with THC (Total hydrocarbon) and torque with THC, respectively. Engine THC emissions were observed to be the lowest at 1100 rpm, at all three crank angles from 333 to 350 degrees. This may indicate that the engine performance with respect to the THC emissions and the exhaust temperature is better at 1100 rpm and crank angle of 340 degrees than 900 and 1250 rpm. NO emissions, however, increased at higher engine rpm and higher torque as seen from Figures 6.4 and 6.8 respectively for all the three spark timings.

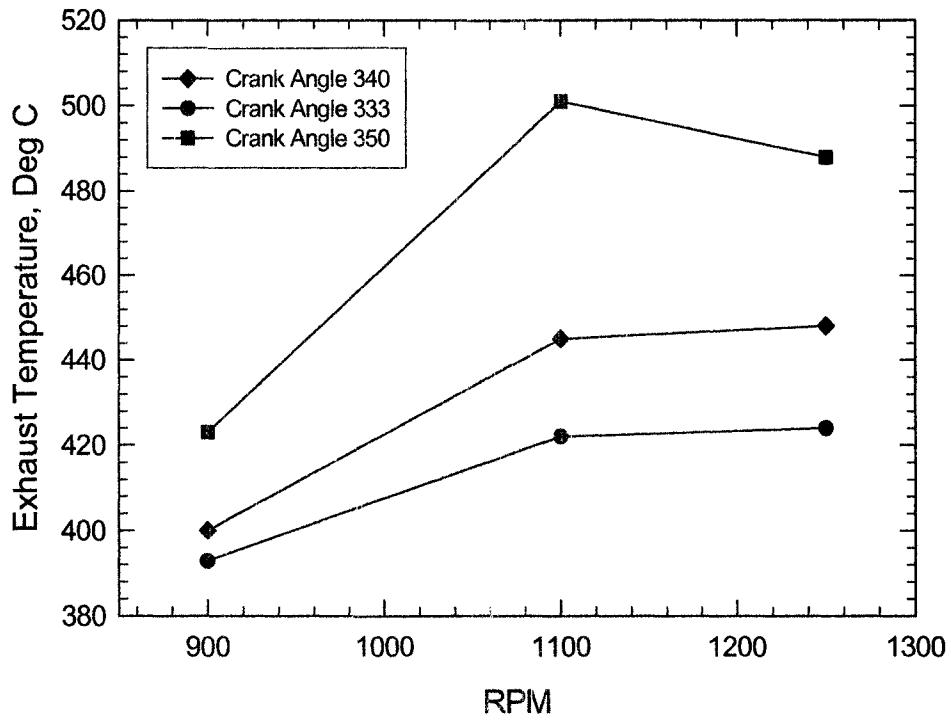


Figure 6.3 – Effect of engine speed on the exhaust gas temperature.

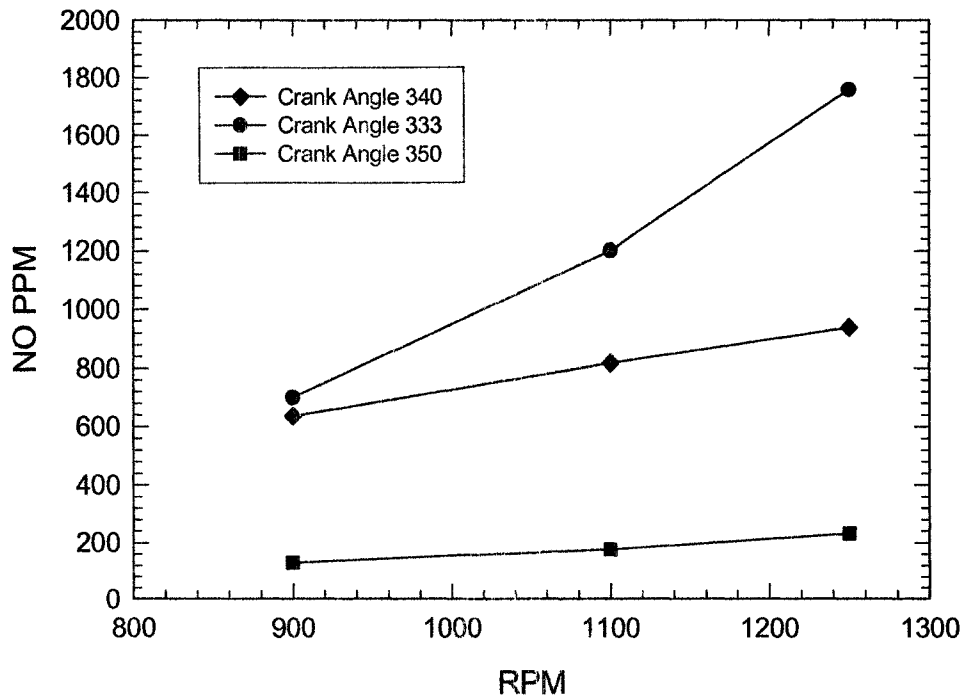


Figure 6.4 - Effect of engine speed on the NO exhaust concentration.

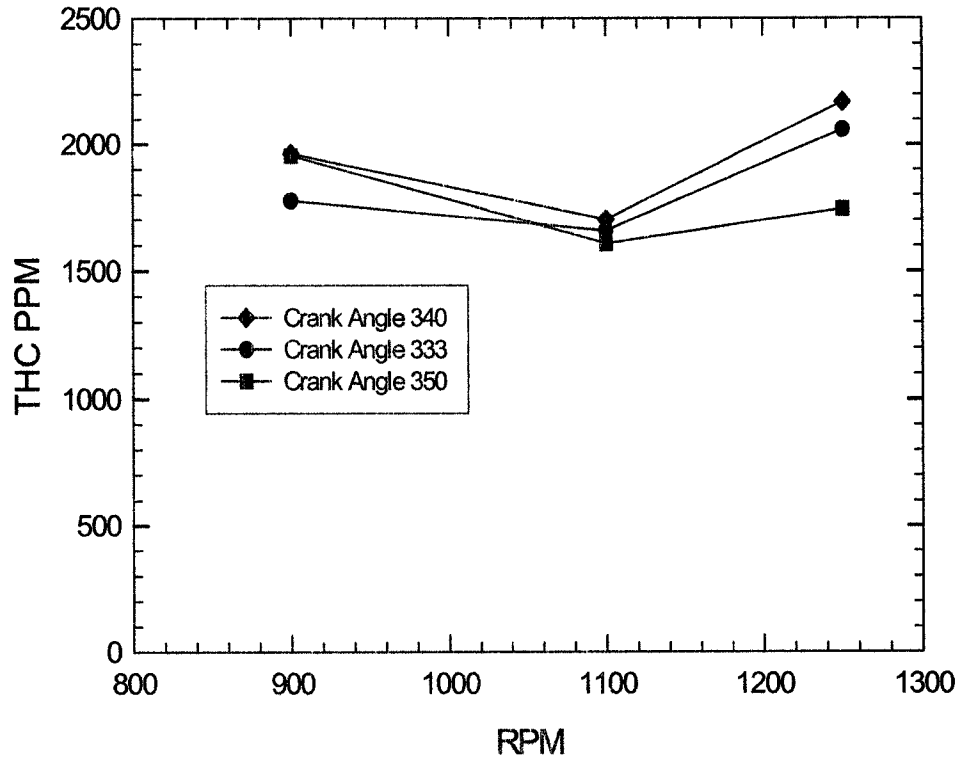


Figure 6.5 – Effect of engine speed on the hydrocarbon emission.

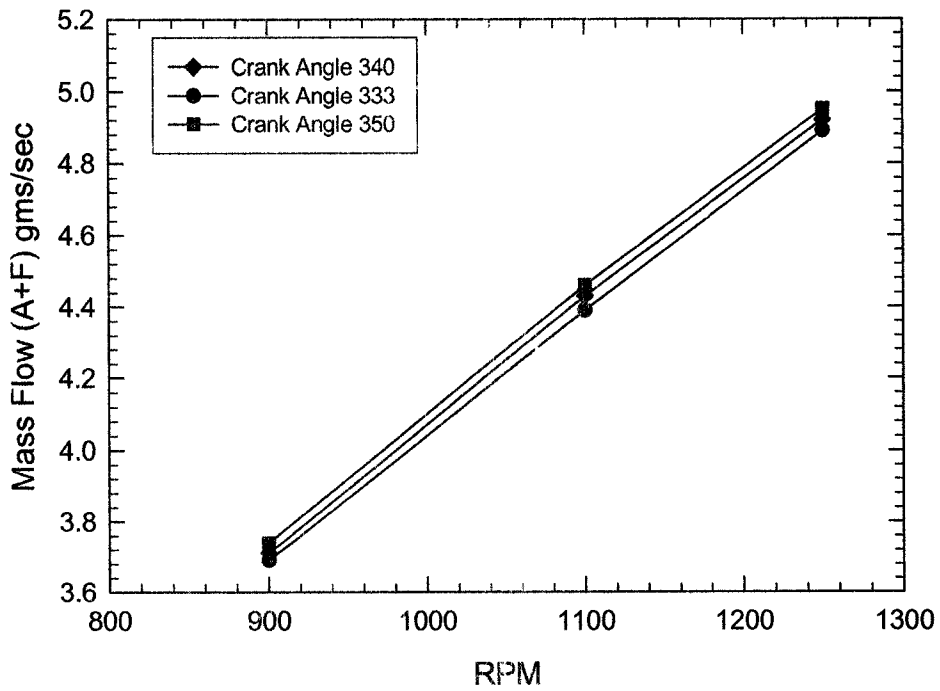


Figure 6.6 – Effect of engine speed on the mass flowrate of engine feed.

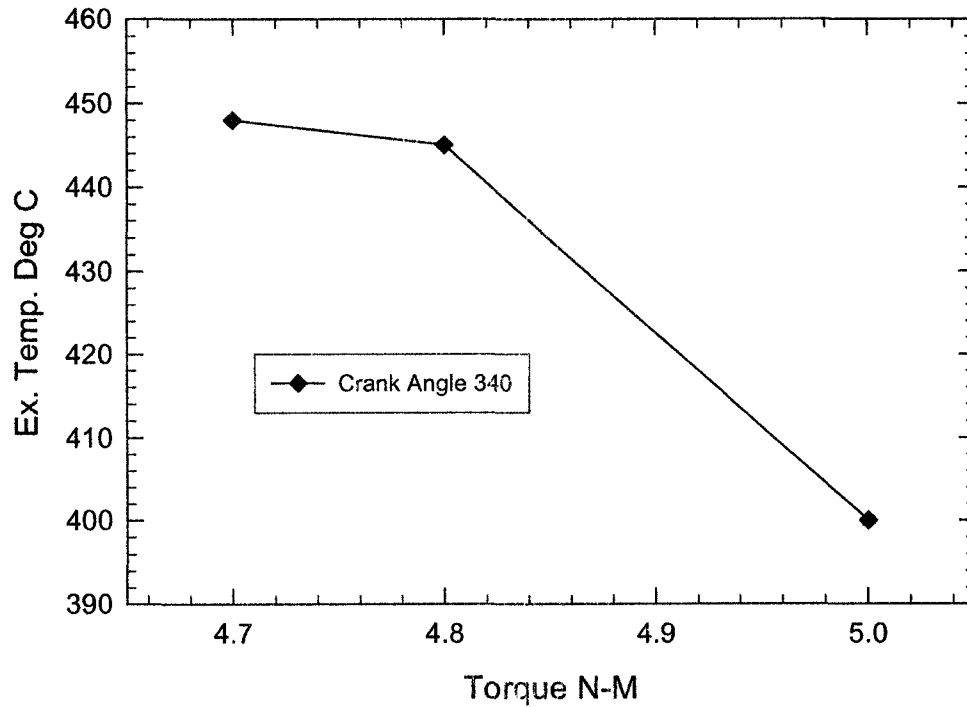


Figure 6.7 – Effect of torque on the exhaust gas temperature.

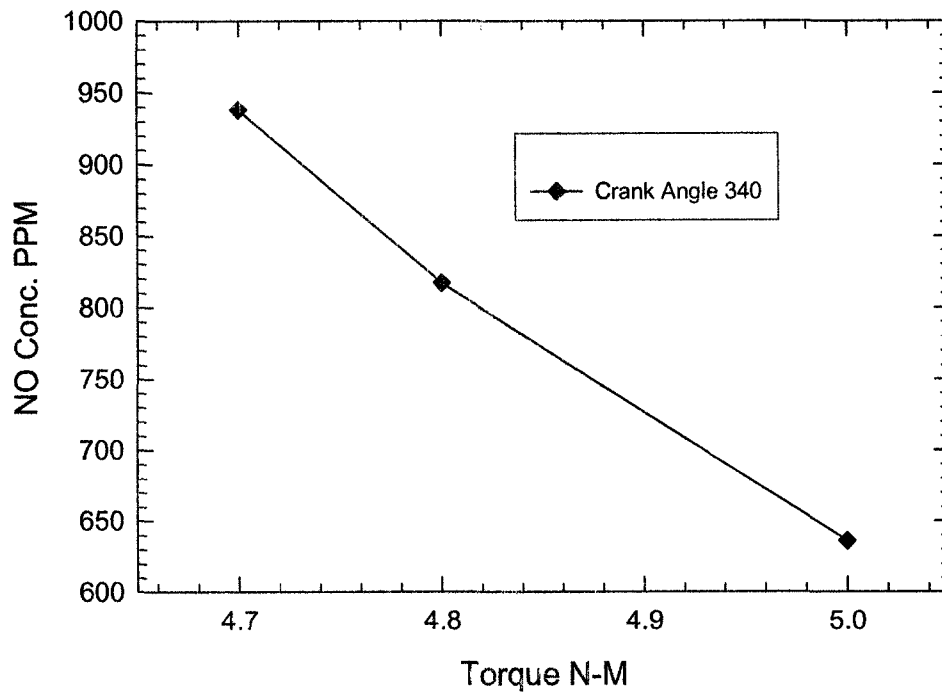


Figure 6.8 - Effect of torque on the NO exhaust concentration.

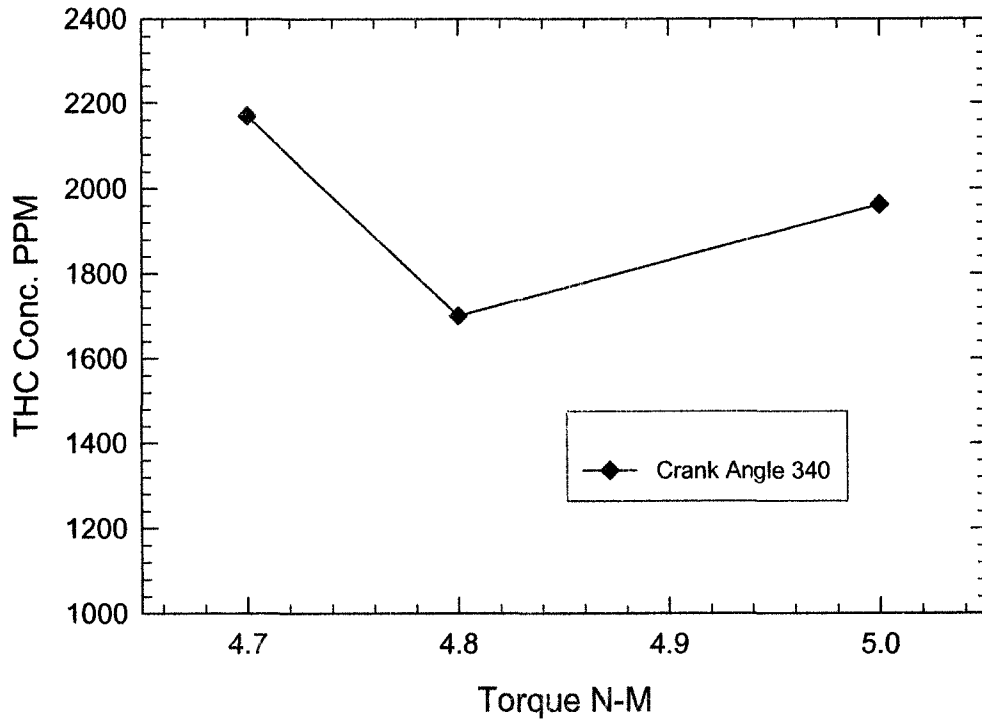


Figure 6.9 – Effect of engine speed on the hydrocarbon emission.

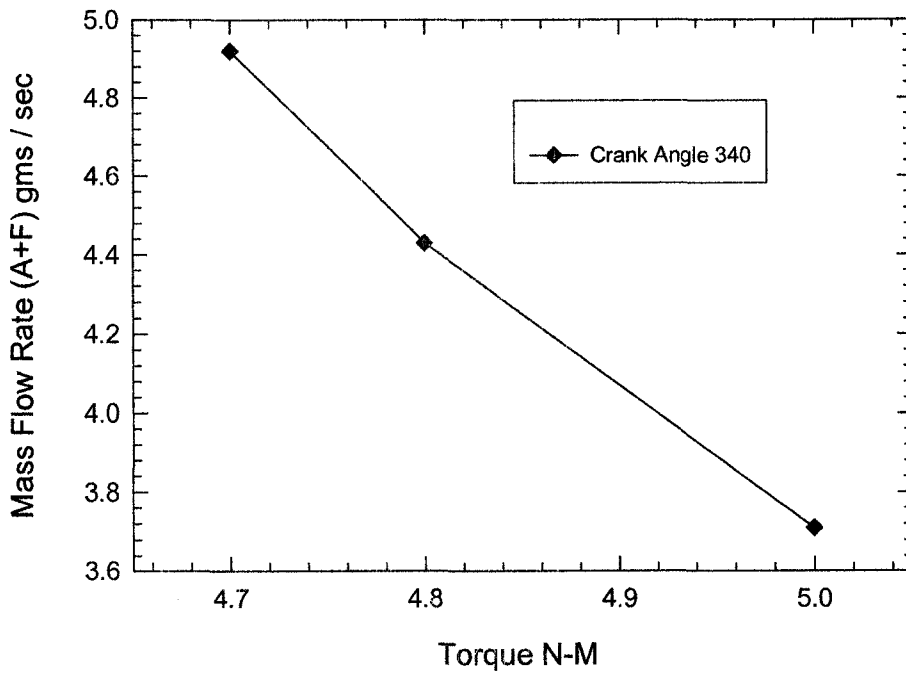


Figure 6.10 – Effect of engine speed on the mass flowrate of engine feed.

6.4 Performance of the NO_x absorber catalyst

The performance of the NO_x absorber catalyst was measured for all engine operating conditions. The overall trend is essentially same for all cases, and one engine condition (1250 rpm, MBT, wide open throttle) was selected for presentation of results. The performance of the catalyst is divided into four parts. These correspond to the steady state values achieved with and without hydrogen injection, and the transient performance that corresponded to the transition between these steady states.

Figure 6.11 shows the NO_x emissions upstream and downstream of the reactor. It is seen that the catalyst achieves a reasonable reduction of NO_x even without the addition of hydrogen. Engine exhaust contains around 1000 ppm. The standard steady state conversion is around 75 % to 250 ppm. At approximately 4000 ppmv hydrogen injection, the NO_x in the reactor effluent drops by around 50 ppm to 200 ppm

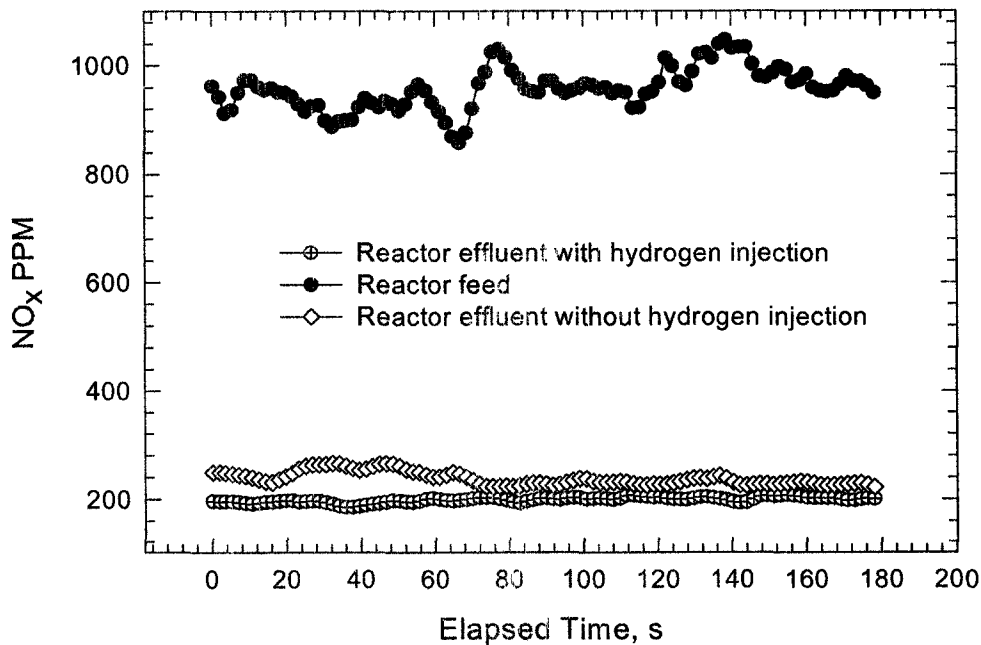


Figure 6.11 – Steady state NO_x emissions upstream and downstream of the reactor, with and without hydrogen injection.

Figure 6.12 shows the transient NO_x conversion when the hydrogen was switched in and out of the reactor feed. With hydrogen addition, the NO_x concentration gradually drops from around 250 ppm to 197 ppm in 180 seconds. It takes about the same time reverse itself when hydrogen was switched off.

Figure 6.13 and 6.14 shows the catalyst performance with respect to total hydrocarbon (THC) conversion. Figure 6.13 shows the THC in the reactor feed and effluent with and without H_2 injection. These curves are at steady state. The hydrogen injected was about 4000 ppmv. The engine exhaust average value of THC is close to 2200 ppm, and after the reactor without H_2 injection it is 487 ppm, for a conversion of around 77 %. After H_2 injection the THC is reduced to 414 ppm. The engine exhaust THC fluctuates, which may indicate some fluctuations in engine operation. In Figure 6.14 similar behaviour to that observed in Figure 6.12 is seen, albeit with more fluctuations.

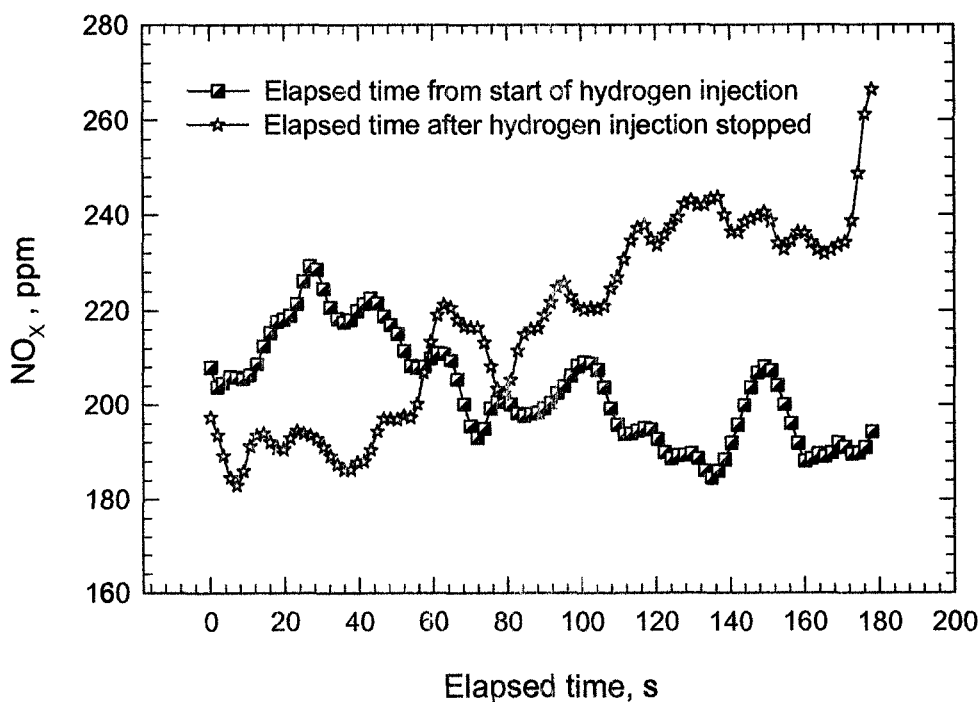


Figure 6.12 – Transient NO_x concentration in the reactor effluent, following the switch of hydrogen into and out of the reactor feed.

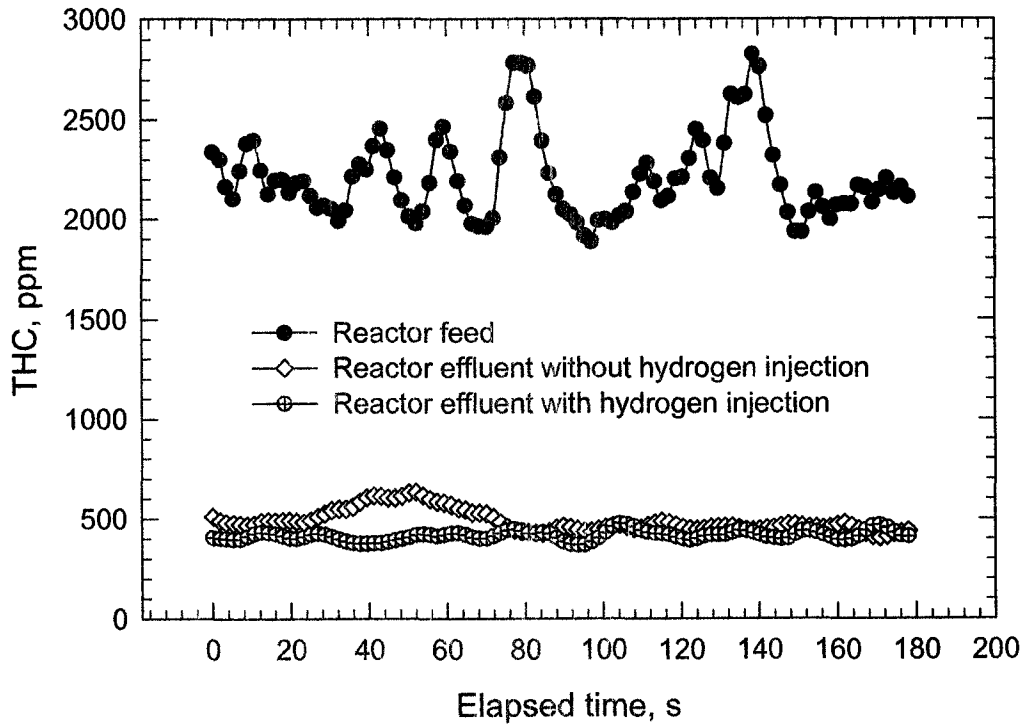


Figure 6.13 – Steady state THC emissions upstream and downstream of the reactor, with and without hydrogen injection.

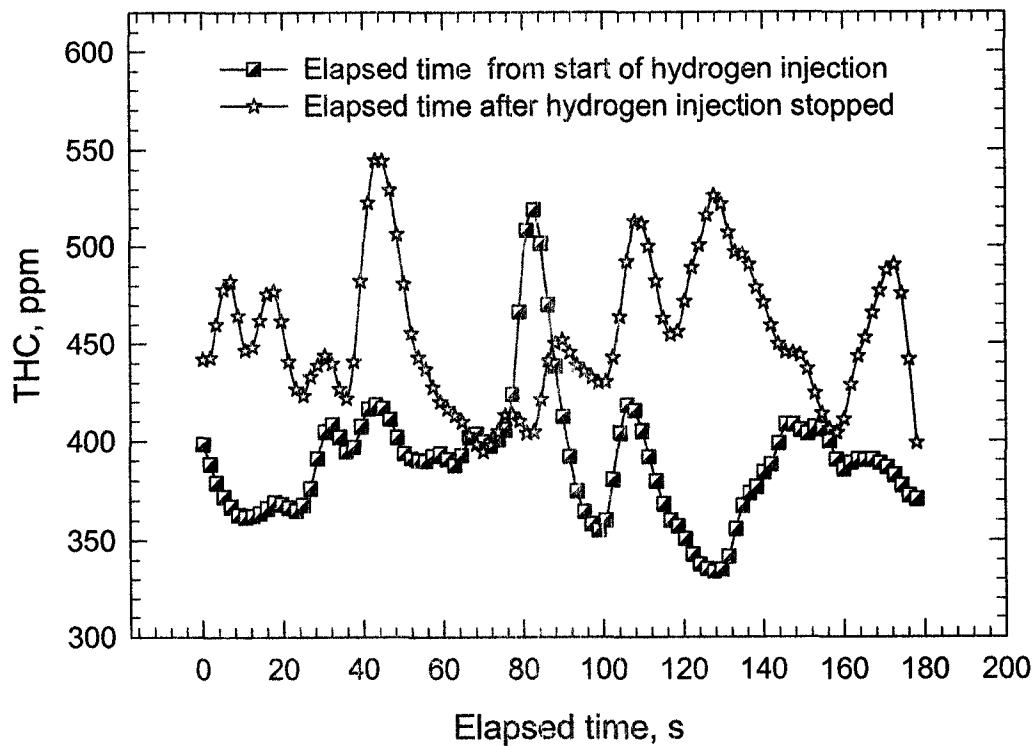


Figure 6.14 – Transient THC concentration in the reactor effluent, following the switch of hydrogen into and out of the reactor feed.

Figures 6.15 and 6.16 show the catalyst performance for CO emission for both steady state (Figure 6.15) and transient periods. The average exhaust gas CO concentration is 1260 ppm, which is reduced to about 800 ppm in the catalytic converter. With hydrogen addition, the concentration drops to about 650 ppm.

Figure 6.16 shows the transient responses observed when the hydrogen was switched in and out of the system. Similar to the performance with THC, the transition period is about 180 s.

In Figure 6.17, the maximum reactor temperature in the reactor with and without hydrogen is plotted. In figure 6.18 the transition of maximum reactor temperature when hydrogen was switched is show. The average maximum reactor temperature increases from about 330 °C to 413 °C.

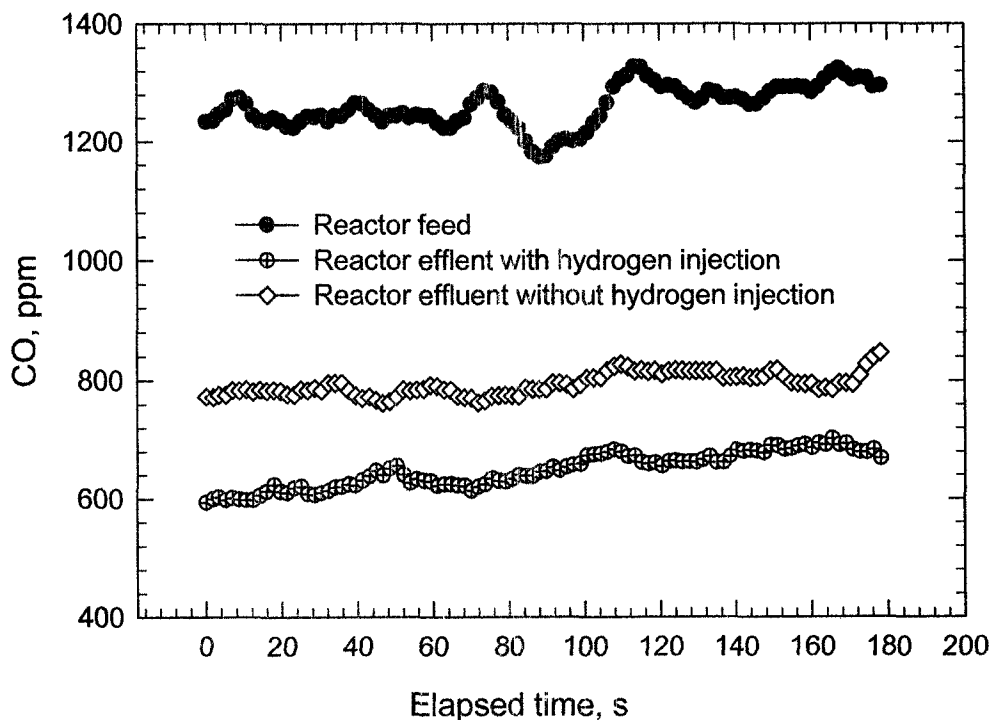


Figure 6.15 – Steady state CO emissions upstream and downstream of the reactor, with and without hydrogen injection.

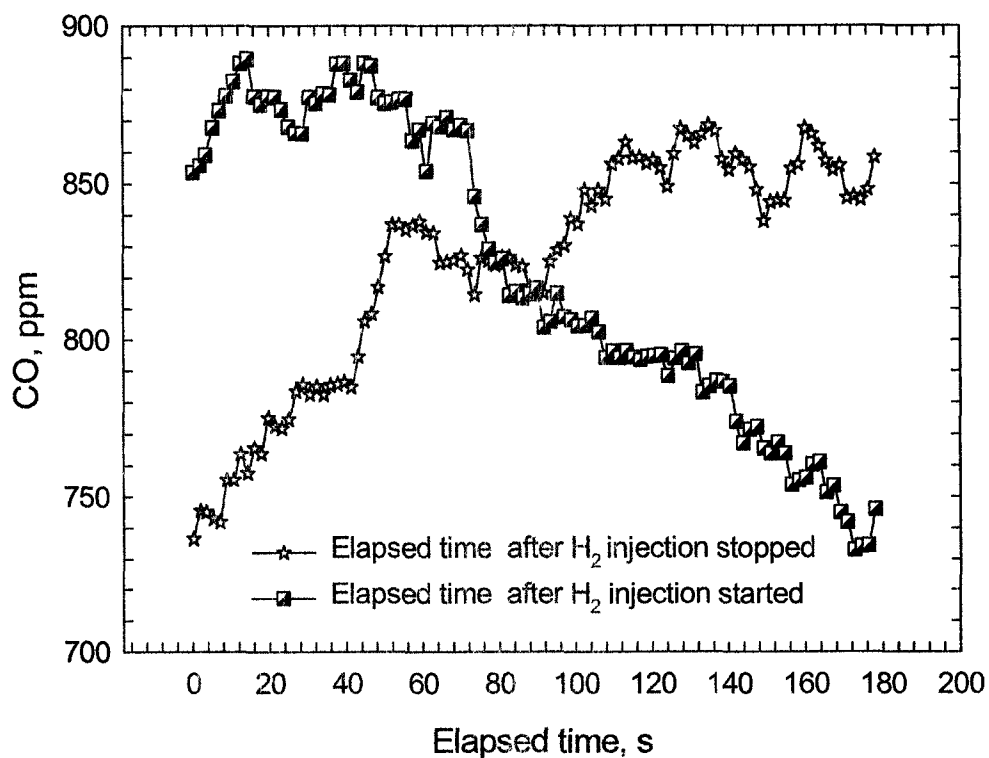


Figure 6.16 – Transient CO concentration in the reactor effluent, following the switch of hydrogen into and out of the reactor feed.

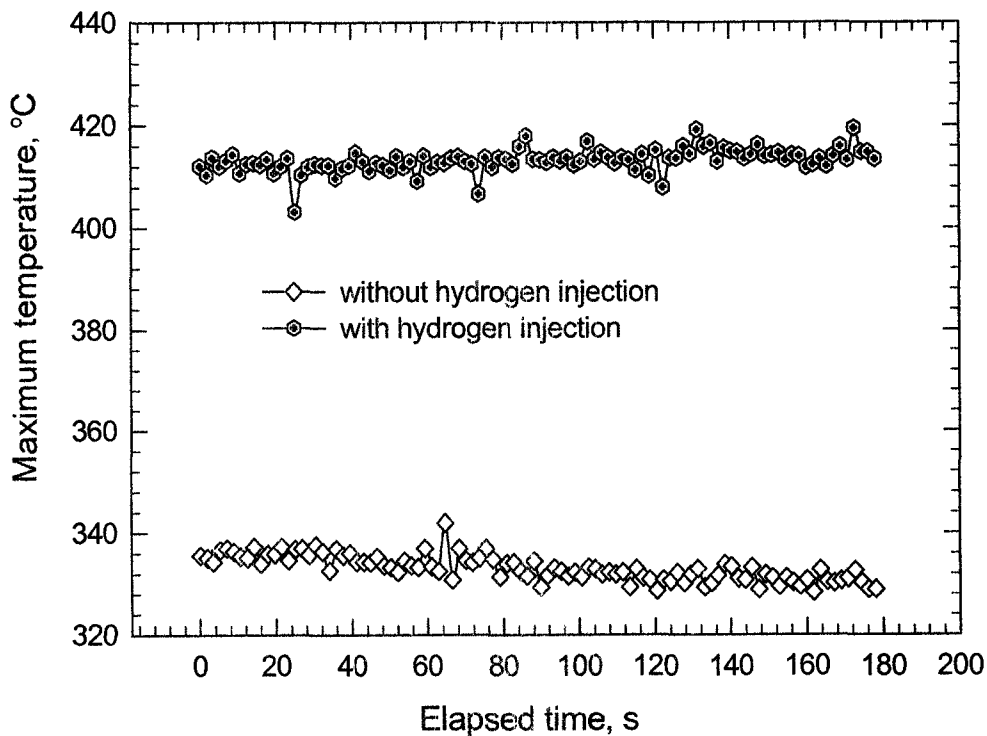


Figure 6.17 – Steady state maximum reactor temperature, with and without hydrogen injection.

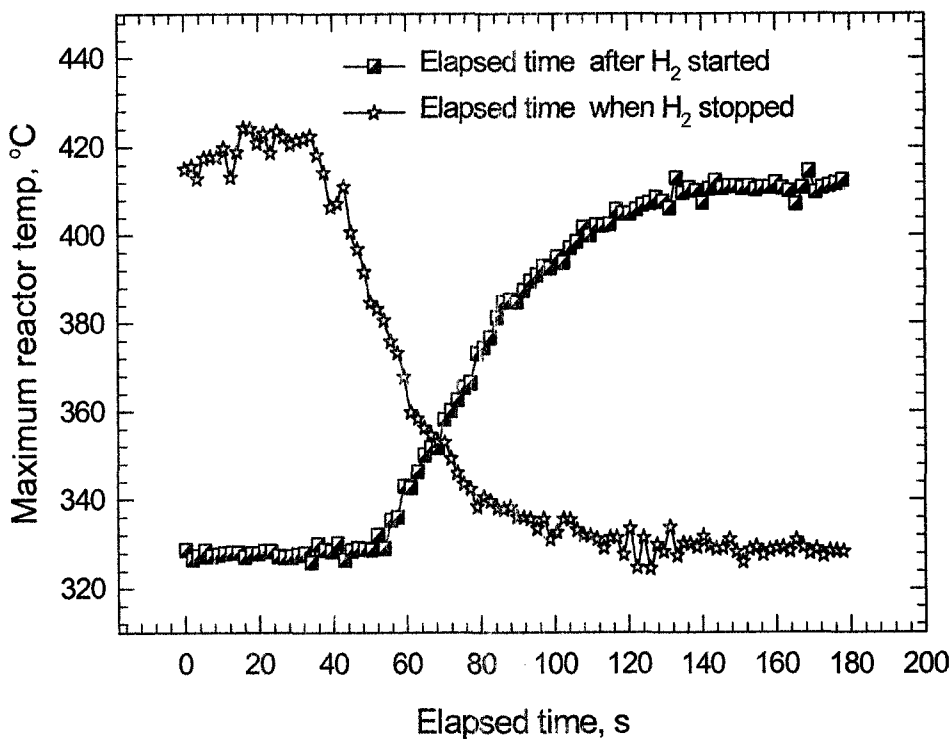


Figure 6.18 – Transient maximum reactor temperature, following the switch of hydrogen into and out of the reactor feed.

6.4 Summary of catalyst performance

The tests showed encouraging result for lean burn engine. NO_x reduction of around 75 % was observed without the H₂ injection, with around 80 % observed with H₂ injection. The additional level of reduction obtained when the hydrogen present was not large, and may be the result of the increased operating temperature present when hydrogen was present. A 37 % and 48 % reduction in CO concentration was observed for the same conditions without and with H₂ injection respectively. This level is not as high as expected, and may result due to lower exhaust gas temperature and the high space velocity. The catalyst performance for THC was similar to that of NO_x with 77 % and 81 % reduction without and with H₂ respectively. Catalyst temperature increases by 25 % when hydrogen is injected. This shows that exothermic reactions of CO and THC oxidation and simultaneous NO_x reduction occurring under rich conditions generated by H₂ injection at the upstream of reactor.

The results of this preliminary study have suggested the potential of the NO_x absorber catalyst for the lean burn engine. For further investigation, and to provide data suitable for modelling, some suggestions are made. The experiments were run at fairly high space velocity (about 85 000 h⁻¹) and a lower space velocity should be used. This may be achieved by using a larger catalytic converter. The temperature of operation was also relatively high (by about 50 K) and outside the optimal range of the catalyst. A lower temperature should be used. Finally, it is recommended that other hydrocarbons be tested as a reductant.

Chapter 7

Summary, Conclusions and Recommendations

In this work, studies of some aspects of selective catalytic reduction of NO_x in lean burn engine exhaust have been examined. Based on this work, some conclusions can be drawn and recommendations made.

The monolith reactor simulator coupled to the GPS algorithm for optimization provides a relatively simple method for parameter estimation, without a large amount of additional computation, which is often required for the gradient based methods.

From a standpoint of modelling the reactions, the global kinetic models proposed as a combination of the models of Voltz and Ansell appear to offer some promise. To explore these models further, a more rigorous program of experiments is suggested, in which the concentrations of the reactants are more widely varied. To limit the number of experiments required, a design of experiments approach may be useful. The model, although not representative of the reaction mechanism, may be useful for the prediction of performance over a limited range of conditions.

For the control of NO_x from the CNG engine, preliminary investigations have shown that there is promise in the NO absorber catalyst. The converter design can be improved, and testing with a broader range of hydrocarbon reductants is suggested. In particular, it is suggested that a larger volume of reactor be used, to represent more realistically the conditions in a real vehicle. Modelling of the data presents a challenge, and it is important to have high quality data where all of the operating conditions are well known.

REFERENCES:

- 1] *Air quality criteria for oxides of nitrogen*. Research Triangle Park, NC, US Environmental Protection Agency 1993 (EPA Report number EPA/600/8-91/049aF-cF, 3v)
- 2) *Air quality criteria for ozone and related photochemical oxidants*. Research Triangle Park, NC. US Environment Protection Agency, 1995 (EPA Report No. EPA/600/P-93/004aF-cF.3v).
- 3) *Canada's GHG Inventory – 1990 -2002*. Environment Canada GHG division, Report on Green House Gases Emission, 2004.
- 4) Emission standards Europe cars and light trucks. *Data obtained from dieselnet.com website*.
- 5) Y.A. Zeldovich, Oxidation of nitrogen in combustion, *Acta Physicochem. (USSR)*, **21**, 557-558, 1946.
- 6] J. B. Haywood, *Internal combustion engine fundamentals*: McGraw Hill publishing Co., 1988.
- 7] R. Stone, *Introduction to Internal Combustion engines – Third edition*, 1999, SAE publishing.
- 8) K. B. Schnelle, C. A. Brown, *Air pollution control technology handbook*, Ch 17.1.2. , CRC Press, 2001.
- 9] J. Van Mierlo, G. Maggetto, Ph. Lataire. Which energy source for road transport in the future ? A comparison of battery, hybrid, and fuel cell vehicles. *Energy conservation and management*, **47**, 2748-2760, 2006.
- 10] A. M. Kreso, J. H. Johnson, L. D. Gratz, S. T. Bagley and D. G. Leddy. A study of effects of EGR on heavy duty diesel emissions, *SAE paper 981422*, 1998.
- 11) John Zink Company, Burner design parameters for flue gas NO_x control. *II international conference on combustion technology, Lisbon, Portugal*, 1993.
- 12] A. Kohl and R. Nielsen. *Gas purification handbook*. Gulf publishing company, 1997.

- 13] R. Ferrel, Controlling NO_x emissions a cooler alternative, *Pollution eng.* **32** (4) 50-52, 2000.
- 14] X. Lu, W. Chen and Z. Huang, Fundamental study on the control of the HCCI combustion and emissions, *Fuel*, **84** 1074-1083 2005.
- 15] S. Soyulu, Examination of combustion characteristics and phasing strategies of natural gas HCCI engine. *Energy conservation and management*, **46**, 101-119, 2005.
- 16] G. C Koltsakis and A. M Stamatelos, Catalytic automotive exhaust after treatment. *Prog. in energy and combustion science*, **23**,1-39, 1997.
- 17] J.M Thomas and W.J. Thomas. *Principles and Practice of Heterogeneous Catalysis*, chapters **1-8**. VCH, 1997.
- 18] H.S. Gandhi and M. Shelef, Twenty-five years after introduction of automotive catalysts what next? *Catalysis Today*, **62**, (1), 25, 35-50, 2000.
- 19] J.T Kummer, Catalyst for automobile emission control, *Progress in energy and combustion science*, **6**, 177 – 199, 1980.
- 20] H.W. Jen, G.W. Graham, W Chun, R.W. McCabe, J.P. Cuif, S.E. Deutsch, and O. Touret. Characterization of model automotive exhaust catalysts: Pd on Ceria and Ceria-Zirconia supports. *Catalysis today*, **50** (2), 309-328, 1998.
- 21] R.E. Hayes and S.T. Kolaczkowski. *Introduction to catalytic combustion*, Gordon and Breach science publishers 1997.
- 22] B. Liu, R. E. Hayes, M.D. Checkel, M. Zheng and E. Mirosh. Reversing flow catalytic converter for a natural gas / diesel dual fuel engine. *Chemical engineering science* 56, 2641-2658, 2001.
- 23] H.C Yao and Y.F. Yu Yao, Ceria in automotive exhaust catalysts *Journal of catalysis*, **86**, 254-265, 1984.
- 24] J.W. Hightower and D.A. Van Leirsburg, *The catalytic chemistry of Nitrogen Oxides*, Plenum Press, New York, 63, 1975
- 25] W. Held, A. Konig, T. Richter and L. Puppe: *SAE Paper 900496*. 1990.

- 26] M. Iwamoto and H. Hamada, Removal of NO from exhaust gases through novel catalytic processes, *Catalysis today*, **10**, 57-67, 1991.
- 27] A.P. Walker, Mechanistic studies of SCR of NO_x over CU-ZSM-5 catalyst *Catalysis today*, **26**, 107-128, 1995.
- 28] M. Iwamoto, H. Yahiro, N. Mizuno, Removal of nitrogen monoxide through a novel catalytic process. *Journal of physical chemistry*, **96** (23), 9360-9366, 1992.
- 29] G.P Ansell, S.E. Golunski, J.W. Hayes, A. P. Walker, R. Burch and P.J. Millington, The mechanism of the lean No-x reaction over Pt-based catalysts. *Catalysis and automotive pollution control III, studies in surface science and catalysis* **96**, 577-590, 1995.
- 30] Monroe D.R., C.L. Di Maggio, D.D. Beck and F.A. Matekunas, *SAE paper 930737*, 1993.
- 31] J. N. Armor, Catalytic removal of nitrogen oxides: where are the opportunities, *Catalysis today*, **26**, 99-105 and 147 – 158, 1995.
- 32] J. N. Armor, Y. Li and P. J. Battavio, Effect of water vapour on the selective catalytic reduction of NO by methane. *Journal of catalysis* **142**, 561-571, 1993.
- 33] K.C.C. Kharas, H.J. Robota, D. J. Liu. Structure-function, properties in Cu-ZSM-5 NO decomposition and NO SCR catalysts. *Catalysis today*, **26**, 129-145, 1995
- 34] M. Iwamoto, H. Yahiro, S. Shundo, Y. Yoshihiro and N. Mizuno, Influence of sulfur-dioxide on catalytic removal of nitric-oxide over copper ion-exchanged ZSM-5 zeolite *Applied Catalysis*, 69(2) L15-L19 (1991).
- 35] M. Amiridis, T. Zhang and R. J. Farrauto, Slecetive catalytic reduction of nitric oxide by hydrocarbon. Review Article, *Applied catalysis B - Environmental*. **10**, 203-227, 1996.
- 36] R. Burch and P.J. Millington, Selective catalytic reduction of nitric oxide by hydrocarbons under lean burn conditions. *Catalysis today*, **26** (2), 185-206, 1995.
- 37] H. Hamada, Y. Kintaichi, Y.Ito, M.Tabata, Database for catalysis design. *Catalysis today*, **10** (2), 223-232, 1991.

- 38] B.H. Engler, J. Leyerer, E.S. Lox, and K. Ostgathe, Catalytic reduction of nitrogen oxides in diesel exhaust gases, catalysis and automotive pollution control series III. *Studies in surface science and catalysis*, **96**, 529-547, 1995.
- 39] R. Burch and D. Ottery, The selective catalytic reduction of nitrogen oxides by higher hydrocarbons *Applied catalysis B Environmental* **13**, 105-111, 1997.
- 40] E. Kikuchi, M.Ogura, I. Terasaki and Y. Goto Selective catalytic reduction of nitric oxide with methane on Gallium and Indium containing zeolites. *Journal of catalysis*, **161** (1), 465-470, 1996.
- 41] M.A. Vannice, A. B. Walters and X. Zhang, Kinetics of NO_x decomposition, *Journal of catalysis*, **159**, 119-126, 1996.
- 42] C. J. Loughran and D.E. Ressayco, Functionality of Pd based catalysts used in used in the reduction of nitric oxide by methane in the presence of oxygen, *Applied catalysis, B: Environmental* **7**, 113-126, 1995.
- 43] M. A. Vannice, A. B. Walters and X. Zhang, Catalytic reduction of NO by methane, *Journal of catalysis*, **146**, 568-578, 1994.
- 44] M. D. Fokema and J. Y. Ying, The selective catalytic reduction of nitric oxide with methane over non zeolitic catalysts, *Catalysis reviews*, **43** (1&2), 1-29, 2001.
- 45] R. L. Muncrief, K. S. Kabin and M. P. Harold, NO_x storage and reduction with propylene on Pt/Ba O/ Alumina, *AIChE journal*, **50**, (10), 2526-2540, 2004.
- 46] W.M. Bonger, M. Kramer, B. Krutzsch, Removal of nitrogen oxides from the exhaust of a lean burn engine. *Applied catalysis B: Environmental* , **7**, 153-171, 1995.
- 47] N. Takahashi, The new concept 3-way catalyst for automotive lean burn engine, NO_x storage and reduction catalyst. *Catalysis today*, **27**, 63-79, 1996.
- 48] E. M., Fridell, M. Skoglundh, S. Johansson, B. Westerberg, A Torncrona, G. Smelder, Investigations of NO_x storage catalysts, *Catalysis and automotive pollution control III, studies in surface science and catalysis*, **116**, 537-547, 1997.

- 49] J.T. Kummer, Catalysts for Automobile emission control, *Progresses in energy and combustion sciences*, **6**, 177-199, 1980.
- 50] B. Liu, *Experimental and modeling study of reverse flow catalytic converters for Natural gas diesel dual fuel engine pollution control*. Ph.D. thesis, University of Alberta 2000.
- 51] R. E. Hayes, F. H. Bertrand, C. Audet and S. T. Kolaczkwoski. Catalytic combustion kinetics: using a direct search algorithm to evaluate kinetic parameters from light off curves. *Canadian journal of chemical engineering*, **81**, 1192-1199, 2003.
- 52] G.P. Ansell, P.S. Bennett, J.P. Cox, J.C. Frost, P.G. Gray, A.M Jones, R. R. Rajaram, A. P. Walker, M. Litorell and G. Smedler, The development of a model capable of predicting diesel lean NO_x catalyst performance under transient conditions. *Applied catalysis B: Environmental*, **10**, 183-201, 1996.
- 53] S. E. Voltz, C. R. Morgan, D. Leiderman and S. M. Jacob, Kinetic study of carbon monoxide and propylene oxidation on platinum catalysts. *Industrial engineering chemistry, production, research and development*. **12**, 294-301, 1973.
- 54] G.I. Taylor, Dispersion of soluble matter in solvent flowing through a Tube, *Proceedings of Royal Society*, **A 219**, 186-203, 1953.
- 55] B Liu and P. Newman, Engine test bed for SCR of NO_x . using propane as a reducing agent. *Unpublished research data, Alternative fuel systems*, Calgary, AB, Canada, 2001.
- 56] Y. Sh. Matros & Grigori A. Bunimovich. Reverse flow operation in fixed bed catalytic reactors. *Catalysis Reviews – Sci – Eng*, **38** (1), 1-68 1996.
- 57] V.O., Strots, G.A., Bunimovich, Y. S. Matros, M. Zheng and E. A. Mirosh, Novel catalytic converter for natural gas powered diesel engines. *SAE paper 980194* , 1998.
- 58] K. Hanamura, R. Echigo and Zhdanok, Super adiabatic combustion in a porous medium. *International journal of heat and mass transfer*, **36**, 3201 – 3209, 1993.
- 59] K. Eranen, L. Lindfors, A. Niemi, P. Elfving and L. Cider, Influence of hydrocarbons on the SCR of NO_x over Ag/Al₂O₃-laboratory and engine tests, *SAE paper*, 2000-01-2813, 2000.

- 60] D. M. Arthur, *Using hydrogen to extend the EGR limit of SI natural gas engine*. MSc thesis, University of Alberta, 2005.
- 61] R. H. Heck, J. Wei, and J. Katzer, Mathematical modelling of monolithic catalysts, *AIChE journal*, **22**, (3), 477-483, 1976.
- 62] L. C. Young, and B. Finlayson, Mathematical models of the monolith catalytic converter; application to automobile exhaust, *AIChE journal* **22**, (2), 331-342, 1976.
- 63] S. Salomons, R.E. Hayes, A. Drochner, H. Vogel, M. Votsmeier and J. Gieshof, CO and H₂ Oxidation on a platinum monolith diesel oxidation catalyst, *Catalysis today*, in press, 2006.